Università di Pisa

Facoltà di Ingegneria

Corso di Laurea Specialistica in Ingegneria dei Veicoli Terrestri

Suspension design of a Formula Student single-seater race car

CANDIDATO
Paolo Di Sacco

RELATORE
Prof. Massimo Guiggiani

Anno Accademico 2012/2013

Alla mia famiglia, ai miei amici più cari: Michele, Francesco, Ruth,
Salvatore, Alessandro, Giovanni;
a Massimo Guiggiani e Francesco Bucchi per la loro disponibilità;
al GreenTeam Uni Stuttgart per avermi accolto e aiutato.

Contents

Abstract

This thesis proposes the design of the suspensions system of a Formula Student single-seater race car, in collaboration with the GreenTeam University of Stuttgart.

The suspension design consists of kinematic designs of both front and rear axle, inclusive of the steering system, as well as the management of the suspension's vertical motion realized by the pushrod-rocker system. Kinematic analysis design considers the heights of roll centers, the heights of longitudinal velocity centers, pitch-center heights and most of the main parameter trends, according to suspensions vertical motion and roll motion.

The values of springs, spring ratios, roll-bars, dumpers, steering system kinematic, were decided according to literature and to already available parts.

After the kinematic analysis, a multibody model of the car was created to validate vehicle dynamic, suspension kinematic and to verify vehicle behavior in most common tasks, like steer-steps and constant speed slowly increasing steer angle tasks. The suspension's design is tangled by introduction of vertical load due to aerodynamics enclosures and packaging restraints.

After kinematic and dynamic validation, a mathematical model of a four-wheels steered car was created. This model has the precise purpose to consider, in a first approach, the possible benefits and improvements of vehicle performance due to four-wheel steering.

In conclusion, the structural validation of all the suspension components designed was reached, inclusive of fatigue validation and bonding between carbon fiber arms and aluminum supports.

Chapter 1

Introduction

1.1 What is Formula Student?

Formula SAE is a student design competition organized by SAE International. The competition was started in 1978 and was originally called SAE Mini Indy.

The idea behind Formula SAE is that a fictional manufacturing company has contracted a student design team to develop a small Formula-style race car. The prototype race car is to be evaluated for its potential as a production item. The target marketing group for the race car is the non-professional weekend autocross racer. Each student team designs, builds and tests a prototype based on a series of rules, whose purpose is both ensuring on-track safety (the cars are driven by the students themselves) and promoting clever problem solving. The prototype race car is judged in a number of different events.

At the beginning of the competition, the vehicle is checked for rule compliance during the Technical Inspection. Its braking ability, rollover stability and noise levels are checked before the vehicle is allowed to compete in the dynamic events (Skid pad, Autocross, Acceleration, and Endurance). Formula SAE encompasses all aspects of a business including research, design, manufacturing, testing, developing, marketing, management, and fund raising. Formula SAE takes students out of the class room and puts them in the real world.

Figure 1.1: Green Team's E0711-4 at Formula Student Germany 2013.

1.2 Goal of this report

The goal of this thesis is to design the suspensions system and the whole steering system of a single-seater Formula Student race car. The work is made in collaboration with the GreenTeam University of Stuttgart by an Erasmus exchange.

Another aim of this report is to consider the conveniences on the vehicle performances of an actuated rear axle steering system, and to set up a preliminary design of this system, to be used in future cars.

The suspensions design consist of kinematic and dynamics design of double fish bone arms as well as suspensions springs system and dumping systems:

the design is made with support of multibody simulation software, a self made mathematical model of the car, and a finite element simulation software for the structural part.

Chapter 2

Basic information

Formula student's cars are light-weight high performance Formula-style cars, GreenTeam is the second team based in Stuttgart and produces electric cars. This year a four driven system was introduced. This system consists of two rear engines with mechanical reduction, and two front engines directly connected to the wheels. The total output power is limited by FSA rules to 73.5 kw (100 hp) and is split electronically between the four wheels according to the vertical load available. Aerodynamics was also introduced this year to take to extreme dynamics' performances. Most of the car is made of carbon-fiber or light-weight alloys, like Ergal (Al 7075). State of the art productive processes, electrical and electronics components were used: all this to clarify that, for University of Stuttgart is really important to achieve the best results in these competitions and differently from other teams, funds and renowned sponsors do not lack.

2.1 List of requisites

The car has to respect some design requirements: first of all the tracks and the wheelbase are imposed by the team. The wheel base is 1530 mm long, while tracks are 1210 mm long, for the front track, and 1160 mm long for the rear track. These layout decisions were made by the team to obtain a small car, in order to reduce the total mass of the vehicle. In fact, the total weight of the car is around 200 kg, although it is an electric car and has at least 50 kg of batteries on board. Pneumatics rim were established by the team too, they are Hoosier 18.00 x 7.5-13. The frame is a monocoque, with main hoop, front hoop

and back hoop made of steel and connected to the frame as FSA rules impose. Connection between frame and suspensions are already designed and had to be used so, because of the monocoque frame. There are packaging restrictions too: the front suspensions must allow integration of two electrical motors, brakes; the rear part of the frame must fit battery's containment units. The car has aerodynamics appendixes, so the suspensions design must heed the additional vertical loads due to aerodynamic, in particular the suspension behavior should be satisfying as a whole $\pm$ 20 mm excursion. This is because the springs have to be preloaded to contrast the vertical loads in a way that the suspension travel should be zero for average velocity, but should not be zero when standing and when proceeding at very low speed.

2.2 Reference system

After a general introduction, an important topic for the vehicle design, the reference system, will be introduced.

The origin of GreenTeam reference system is set to the ground level in the middle of the the line connecting the two front tire path, with the *"z"* axis upwards, the "x" axis pointing to the rear part of the car and the *"y"* axis directed to have a normal right-handed Cartesian reference system. This way, regardless of the origin position, "x" and *"y"* axis have the same direction of the normal axis used in vehicle dynamics [10] , but with different verses. The software developed by the Eteam Squadra Corse, which I optimized too, has the normal vehicle axis: "x" axis directed from the rear axle to the front axle the *"z"* axis upwards and the *"y"* axis resulting as before. I used, like Eteam does, two reference systems with same orientation as explained above; the one located in the middle of the rear axle at the same level of the wheel centers, the other one with the origin in the barycenter of the car as usual.

The first system is used for geometrical modelling, the other is used to display common dynamical results like, *roll angle*, *pitch angle, yaw speed* and others.

First of all a visual display of the three reference systems, in figure 2.1

Below in the first member of 2.1 are the coordinates in the Eteam reference system in the second member the Green team one's and a translation vector: where "l" is the car's wheelbase equal to 1530 mm and "h_{wc}" is the unload wheel center height equal to 228.6 mm.

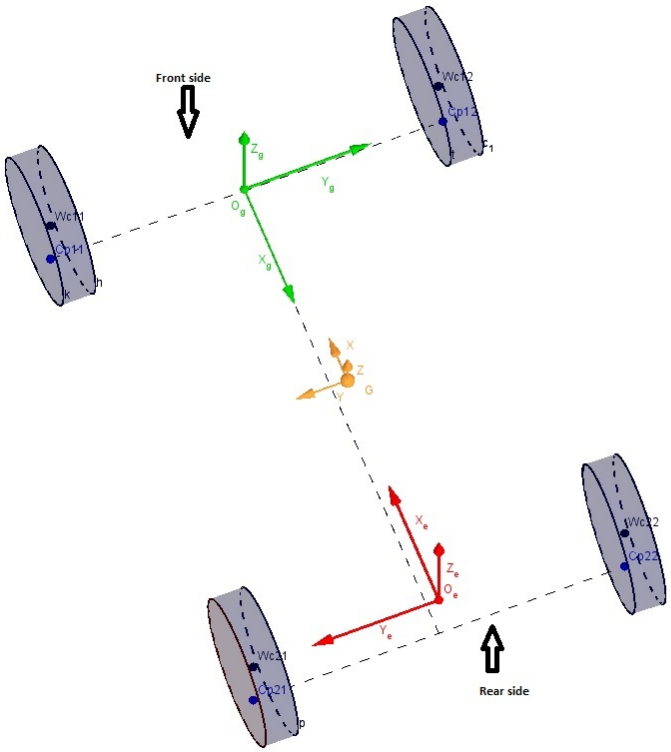

Figure 2.1: Reference systems: in green, the GreenTeam reference system, in red the Eteam one's and in orange the standard reference system situated in the barycenter.

$$\begin{pmatrix} X \\ Y \\ Z \end{pmatrix} = \begin{pmatrix} -\overline{X} \\ -\overline{Y} \\ \overline{Z} \end{pmatrix} + \begin{pmatrix} l \\ 0 \\ -h_{wc} \end{pmatrix} \tag{2.1}$$

It is easy to invert this equation to obtain the coordinate of GreenTeam system in the Eteam system. There are wheel's reference systems too, defined as in [12] , those have correct direction if used for left wheels. Right wheel's reference system is symmetrically oriented to the left system.

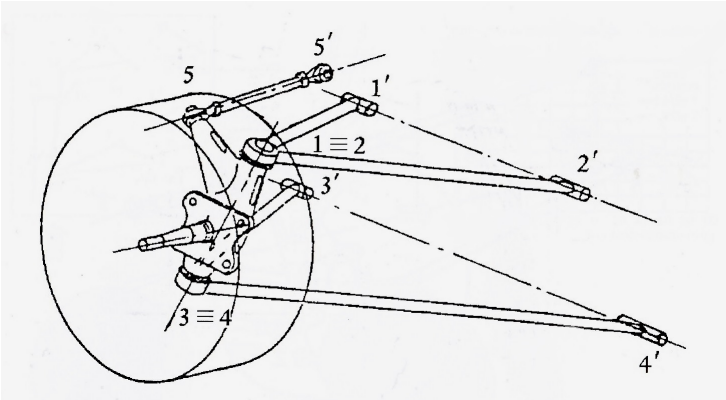

Figure 2.2: SLA rear suspensions example.

2.3 Suspensions architecture: Four-bar linkage

SLA suspension stands for Short-Long Arm suspensions is a generic name for a family of suspensions that have upper and lover control arm with the upper control arm shorter then the lower this arms can be A-arm also called fishbone arm.

These suspensions in a car's rear view are equivalent to a four-bar mechanism, that is used to study the kinematic.

The double A-arm and toe link is the most common suspensions type use in Formula Student, it is one of the most complicated suspensions systems but it has also a great range of design and if well conceived very high kinematic performances.

An example of a SLA suspension for the rear axle is illustrate in figure 2.2, as shown we have the two A-arm, the upper (points: 1',1,2') ,the lower (points: 3',3,4') and the toe link (points:5',5). The points 1 and 2 define the steering axle, in to the upright wheel around. The constrains are chosen to allow only one degree of freedom that is called suspension motion, usually is a combination of camber motion and steering motion, more will be explained later.

The constrains showed in the picture are two plane rotational joints and a spherical joint for each A-arm, this is a hyperstatic solution used more in standard cars for structural reason, usually in race cars like in FSAE cars the two rotational joints are replaced with two rod-ends (spherical joints) like the toe link ones.

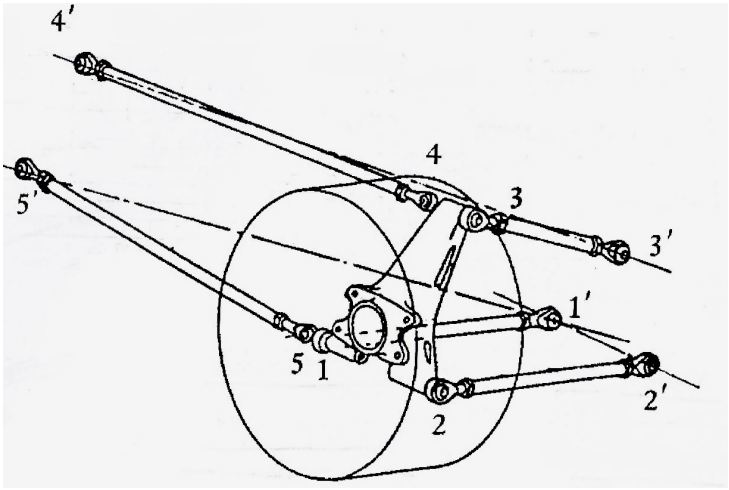

Figure 2.3: Multi-link rear suspension example.

All this introduce another type of suspensions: the multi-link suspensions, that can not be defined by four-bar suspension, because its motion is not a plane motion.

Multi-link is the name generically used when the upright is constrained to the frame with five links as shown in figure 2.3, but this definition is correct only when the straight lines, defined by every link, takes two by two, do not intersect themselves.

This is the most complex suspension design and is used only when extreme performances and set up possibility are required, due to the higher costs, designing and economic costs.

When the suspension is made by five links but they do intersect themselves as shown in figure 2.4 we still have a four-bar suspension, but we have more design possibility.

Making the triangles virtual, we can set the steering straight line position outside the physical range of an A-arm, that is important when we have fixed track and we have to deal with space problems do for example to brakes insertion, but we still want a particular steer straight line geometry. In some cases a hybrid solution could be the best solution.

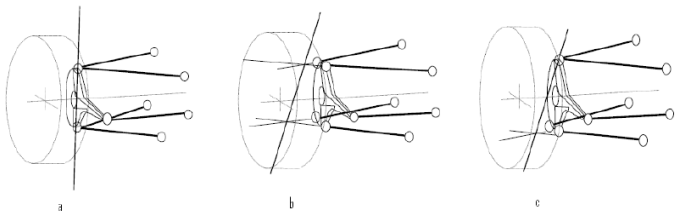

Figure 2.4: a) Normal SLA suspension b) Virtual triangles suspension c) Hybrid solution

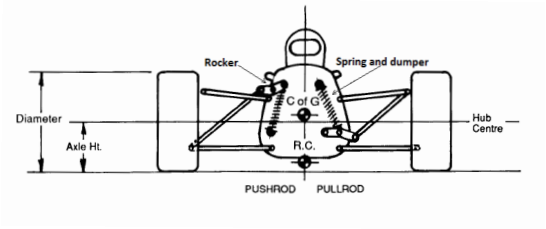

Figure 2.5: Pushrod architecture (left side) and pullrod architecture (right side)

2.4 Suspension architecture: Pushrod and Pullrod

In figure 2.5 are shown the two architecture concerning vertical motion control. Furthermore of the two A-arm and the tie rod there is the pushrod or pullrod mechanism which controls the vertical motion of the suspensions defining with springs and dumpers how much the suspension is allowed to bump how will be the motion kind in terms of oscillation (natural frequency and dumping factor).

The two architectures are quite the same, the difference is how the link between the rocker and the upright is stressed. In pushrod is compressed while the car move upwards, in pullrod in the same case is tractioned.

If springs are placed over the uprights and perfectly vertical each bump displacement will result in a equal spring displacement, this solution is not common anyway the ratio between uprights displacement and spring displacement is called *spring ratio,* also called *rocker's ratio.*

The rocker pushrod or pullrod system involve the possibility to set up spring ratios as wanted and allow to change the ratio during displacement, more will be discuss later when this system will be designed.

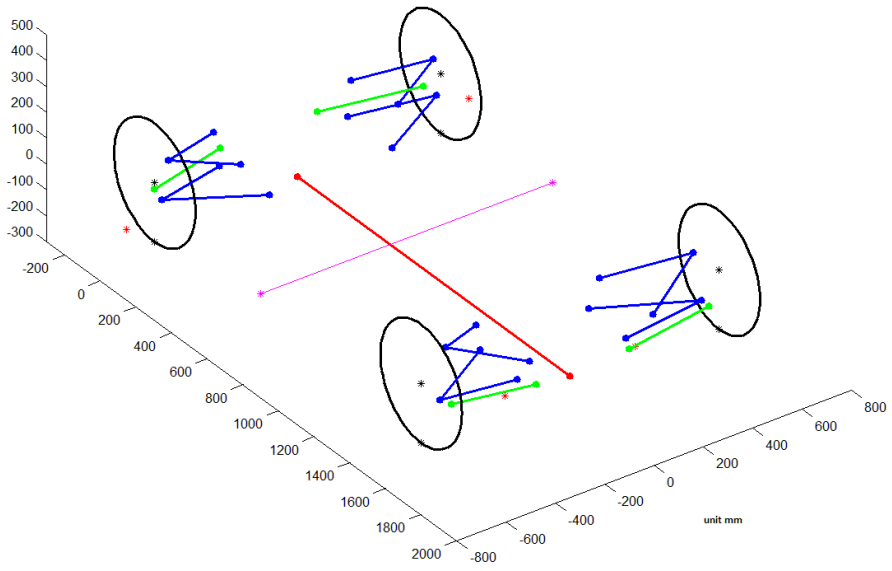

Figure 2.6: Geometrical view of the suspension system.

2.5 Suspension layout

The suspension layout of the car is in picture 2.6, this is the typical solution used in the Formula Student race cars, the suspension design is two double fishbone with rocker pushrod actuated and roll-bars with different set-up.

Chapter 3

Kinematic design

3.1 Instant center definition

Instant center, hereafter simply called IC is so defined: the word instant means at that particular linkage configuration and center refers to a projected imaginary point that is effectively the pivot point of the linkage in that instant. ICs come from the study of kinematics in two dimensions.

For all independent suspensions there are two instant centers, the front IC and the side IC. The side view IC controls force and motion factors predominately related to fore and aft accelerations, while the front view IC controls controls force and motion factors due to lateral accelerations.

As shown in 3.1in three dimension connecting the two ICs define the instant axle, this line can be thought as the instant axis of motion of the knuckle relative to the body.

3.2 Front view's instant centers: Roll center height, camber change rate and scrub

The front view IC location controls the roll center height, the camber change rate and tire lateral scrub. The roll center eight (in figure 3.2) is found by projecting a line from the center of the tire-ground contact patch trough the front view instant center. The roll center establishes the force coupling between the unsprung and sprung masses. the higher the roll center the smaller the rolling moment about the roll center (that as to be resisted to the springs), but

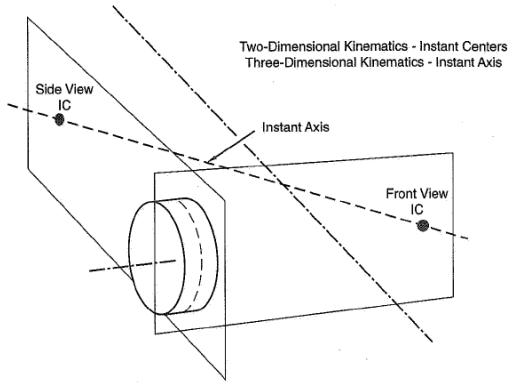

Figure 3.1: Instant centers of motion and instant axis.

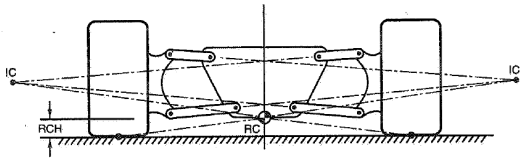

Figure 3.2: Roll-center and front view IC locations.

with higher roll centers the lateral force acting at the roll center is higher off the ground. The product of the lateral force and the distance to the ground is called *non-rolling overturning moment*, while the other is *rolling overturning moment*. Those two effects contribute in different way to the vertical load transfer of the tires belonging to the same axle. The better condition would be not to have load transfer, but it is impossible, so the roll center height is a trade off.

In our particular design, the roll-center heights should be as low as possible because the rolling moment contributes to the load transfer is bigger then the other. Also all this compatibly with the amount of space needed to the suspension components. Lower height for the front axle then to the rear axle is needed: less vertical change in the steering wheels is recommended to have an under-steering vehicle. Furthermore, it is very important that the roll center positions change little during suspension motion or at least that the relative position of front axle and rear axle rolling center height is the same when performing turns.

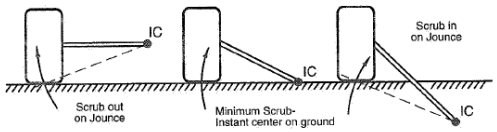

Figure 3.3: Scrub with reference to IC heights.

The ICs in front view define also the camber change rate, as function of the "*fvsa*" length, front view swing arm, ($f\bar{v}sa$). If the control arms of a suspensions are replaced with a single link that ran from the knuckle to the instant center the camber change rate ($\frac{d\gamma}{dz}$) per millimeter of ride travel degrees/mm is so defined:

$$(\frac{d\gamma}{dz}) = Tan^{-1}(\frac{1}{f\bar{v}sa}) \tag{3.1}$$

Camber change is less important then vertical load transfer but it has to be considered and restrained in a defined range.

Another front-view variable is *tire scrub*, this is a lateral motion relative to the ground resulting from the vertical motion of the wheel. Scrubs occurs ever and is minimum when the instant center is on ground, the amount is function of the absolute and relative lengths of controls arms and the ICs position relative to the ground.

In rough road the wheel path is not a straight line if there is scrub, significant amounts of scrub introduce lateral velocity to tires changing the slip angles, this will result in laterally car disturbs, and as to be avoided.

3.3 Side view's instant centers: "Anti features, wheel path and Caster change rate"

The side view swing arm controls motion and forces in the fore and aft direction. The IC position defines important parameters known as: *anti-dive*, *anti-lift*, *anti-squat* and *wheel path*.

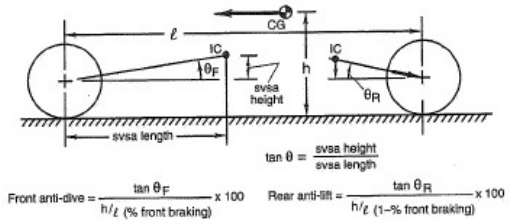

Figure 3.4: Front anti-dive and Rear anti-lift definition.

Those features describe the vertical force coupling between the sprung and unsprung masses, is important to remember that "*anti's*" do not change the steady state load transfer between front and rear wheel during accelerations.

However the anti features change the amount of load going trough the springs and the pitch attitude of a car.

The anti does amount is shortly defined in pictures 3.4.

Some general information:

- anti-dive geometry in front suspension reduces the bump deflection under forward braking;
- anti-lift only occurs, in front suspension if they the front wheels are driving wheels, and it reduces the suspension droop deflection under forward acceleration;
- anti-lift in rear suspension reduces the droop travel in forward braking;
- anti-squat in rear suspension reduces the bump travel on forward acceleration, if the wheels are driving wheels.

Another element controlled by the side view's geometry is the wheel path: the wheel centers relative to the sprung mass is controlled by the position of the instant center.

- If the IC is rearward and above the wheel center height or forward and below, the wheel will move forward as it rises.
- If the IC is behind and below or ahead and above, relative to the wheel center, the wheel will move rearward as it rises.

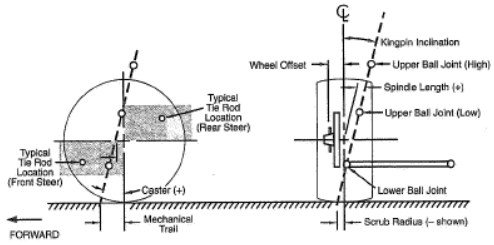

Figure 3.5: Steering axis main angles and sizes

The amount of curvature that the wheel center path has as the wheel rises or falls is only function of the swing arm length.

The last of this side view is the *Caster change rate*: just like camber in the front view, is only function of the side view swing arm, sally there is little reason to have caster change with suspension travel; the changing of Caster is generally accepted as a function of some others parameters. One result is that the bump-steer curve is more difficult to make linear, when there is much caster change during the suspension travel.

3.4 Front Suspensions design

3.4.1 General Issues

The most important thing is to remember that the position of the upper and the lower ball joints define the steering axis, the one around which spins the wheel. This axis is not generically vertical to the ground, so we have a *mechanical trail* an a *scrub radius*, these features are shown in figure 3.5.

The first task in designing a front suspension is to set up the packaging parameters that are fixed, then comes the wheel's package, tire's, brake's and bearing's, package. The tracks have to be established, if there are no rules limitations, then they have to be as wide as practical. In Formula Students competitions is established that: "*T2.4 Vehicle Track The smaller track of the vehicle (front or rear) must be no less than 75% of the larger track*"(from Formula Student's rulebook 2012-2013). Tire size and rim diameter and width have to settled, anyway the decision is taken from a not so wide list of Hoosier tires, designed for Formula Students competitions.

The wheel offset is worked out in parallel with fitting the brake caliper. Once

the caliper is located, is located also the brake rotor. With the rotor location comes the absolute farthest outboard location for the lower ball joint. For the bearings design the positions that minimize the force on them has to be selected.

The lower ball joint has been set, the height of the lower ball joint comes next, in this competition the are no more limitation about the wash rack clearance: "T6.2 Ground Clearance Ground clearance must be sufficient to prevent any portion of the car, other than the tires, from touching the ground during track events. Intentional or excessive ground contact of any portion of the car other than the tires will forfeit a run or an entire dynamic event."

So is also important to consider the deflected tire ground clearance.

The decision about the kingpin angle is the next in order to be discussed; the *scrub radius*, *spindle length*, and *Kingpin* angle are connected, so a compromise is needed. Usually in front-wheel drive car the spindle length must be minimized and the scrub radius should be negative, besides in rear-wheel-drive cars the lower ball joint as to be pushed out as far as possible and run a fairly low Kingpin angle, less then 8°, and accept the resulting scrub radius.

Kingpin angle effects on the car's lifting during steering, the more the kingpin the more the lift will result.

The camber of the wheels when steered is function of the kingpin and of the caster angle, we are not going to explain the details, but the reason that a low Kingpin angle is desirable is that kingpin angle reduce the negative camber gain, due to the caster, on the outside wheel.

For what concerns the rank location, is necessary to remember that: any difference in the lateral displacement of the ball joints in relation to the tie rod outer pivot will cause a steer angle. To assure stability is better *toe-out deflection* due to the lateral force instead of *toe-in deflection*.

3.4.2 Front View Geometry

The front view swing arm instant center is determinate by the desired roll center height and roll camber, the figure 3.6 shows how set up, in a simple way the relative center of motion between the frame and the wheels. To avoid bump steering, that is undesirable (try to imagine the car steering, due to the wheel meeting a depression in the ground) the straight line defined to the tie

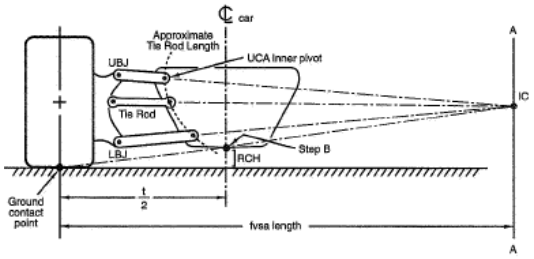

Figure 3.6: Tie rod set-up to minimize kinematic steering.

rod has to pass by the IC, and has to remain in a small range from the IC during the suspensions motion.

Packaging requirements will define the length of the lower control arm, but it should be as long as possible. The ratio between the upper and the lower control arms defines the shape of the camber curve: same length means that the camber-bump curve will be a straight line; if the upper is longer then the lower, the curve will be convex with its curvature toward positive camber; if the upper is shorter then the lower then the curve will be concave toward negative camber.

The goal is a curve which has negative camber in bump with less camber change in droop.

3.4.3 Side View Geometry

In this view the ICs position have to be designed as a result of calculating the desired anti-features. Often the ICs position is a compromise between antithetical needs, such as for example: in front-wheel drive, anti-lift and a receding wheel in bump are not compatible.

The side view geometry defines how the forces are distribute among the links of the suspension, for example: the more is the distance between the steering axis to the pivot of the tie rod, the less will be the force passing through this link.

3.5 Rear suspensions design

The same suspension type can be used easily as a rear suspension, the toe link is fixed to the frame, usually if a front suspension were to be used as rear

suspension the left front components should be installed as the right rear corner and the right front as rear left.

All this because the geometry toe considerations for front suspension are opposite for rear suspension to have roll under-steer. Anyway we are not going to modify front suspension to fit as rear, we are going to design it at all.

Sometimes the toe link could be attached to a control arm, this a way to save weight, but it can only be used when the toe link outer pivot is very close to the same eight as the ball joint. In our design we are not going to use this solution.

3.6 Steering system

The last part of this Chapter is about the steering system geometry and Ackerman geometry: referring to the picture 3.5.

As told before the steering axis has some main angle characteristics and also some lengths resulting from those angle, I am now describing the effects of those angle on the steering system behavior.

3.6.1 Kingpin

- With a positive *spindle length* , as shown in the picture, the car will raise when the wheels are steered, the more the *Kingpin* inclination the more the car will be raised, for a given *Kingpin* inclination a longer *spindle length* increase the lift during steering.
- At low speed the arsing of the front end aid the steering centering, while at high speed any trail will probably overcome this effect.
- *Kingpin* inclination affects the steer-camber characteristic, if the *Kingpin* is positive (toward the car at the upper end) the wheel will assume positive camber for both right or left steering. The amount of camber-steer is little, but in same cases could be important.
- When the wheel rolls over an uneven ground, the rolling radius is constantly changing, this also means wheel speed is changing therefore longitudinal forces are rising, the reaction of those forces will introduce kickback into the steering trough the spindle length. With a short *spindle length* or at lest zero, those forces will be less or even zero.

- A negative *scrub radius* as show in the previous picture introduce, during braking or driving, steer torque proportional to the *scrub radius*. If the forces are different (right wheel-left wheel), then there will be a steering torque felt by the driver, the only way to impose this torque to zero is to have zero scrub radius.

3.6.2 Caster angle and trail

- More trail entail higher steering forces.
- *Caster angle*, like *Kingpin* inclination entail the wheel to rise and fall with steer. Unlike kingpin the effect is not symmetric from side to side: the effect of left steer, with equal positive caster on left and right wheels, is to roll the car to the right causing a diagonal weight transfer. The stiffer the springs the higher will be the load transfer. If the caster is opposite (same value but one positive the other negative) then the car will only rise and fall, there will be no load transfer.
- *Caster angle* effects steer-camber but, the effects are different. With positive caster angle the outside wheel will camber in a negative direction, while the other wheel will camber in positive direction.
- The *pneumatic trail* that adds or removes to the mechanical trail, is nonlinear with the lateral force, and this effects steering torque and driver fell. The pneumatic trail reaches zero when the tire reaches the limit, and will result in lowering the self-centering torque. This could be a signal of the driver that the limit is near.

3.6.3 Ackermann Steering Geometry

The following pictures (figure 3.7 a and b) explain the problem due to the track sizes on the slip angles of the outboard and inboard tyre.

There are two major cases, low lateral acceleration curves, it's common to use *Ackerman steer*, in the way the wheels will have the same turn center. Furthermore on low speed curves the radius is small and similar to the track, so the wheels will have a significant different radius the inside front wheel must steer more than the outer wheel to have the same steering center.

At high lateral acceleration the tires will now work at significant slip angles, and the load on the inside wheel is much less then the other.

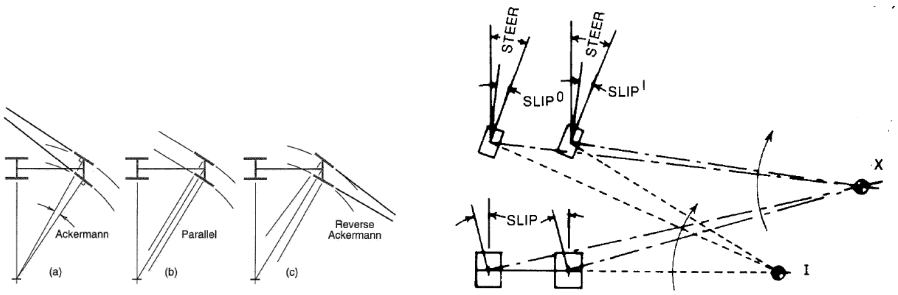

Figure 3.7: Ackerman steering, and effects to slip angles.

Those entail that the inside wheel should have a less slip angle to reach is lateral force peak, this means *reverse Akermann* or at least parallel steering. *Reverse Ackerman* is kind extreme solution because the car has to be moved or pushed at low speed. However during various years of texts the team decided to use implement at least 50% or reverse Ackermann due to the improvements they have got.

Chapter 4

Proposed solution

4.1 Kinematic solutions comparing

This Chapter discusses the selected solution, and compares the results with GreenTeam solution.

4.1.1 Basic Kinematics characteristics

Here are shown the kinematic basic characteristics (chart 4.1) , like *roll center heights*, *pitch-center height* and others. I am going to compare my solution with the one used by the GreenTeam in the race season 2012/2013.

The most important consideration to be made here is the difference between the two pitch-center heights. With the first solution the pitch-center is so low that during pitch the longitudinal position of the pitch-center changes drastically: this is not acceptable for the drivers and not only for him. If the longitudinal position changes, every vertical force changes its mechanical moment around the pitch-center, resulting in a difficult to predict dynamic. It is also important

Solutions	GreenTeam	present
Front roll center heights [mm]	42.8	39.0
Rear roll center heights [mm]	43.2	41.0
pitch-center height [mm]	15.3	110
pitch-center longitudinal position [mm]	492.2	612.3

Table 4.1: Kinematic characteristics, heights are measured from the ground level, and longitudinal position are in Eteam reference system: see Paragraph 1.1 .

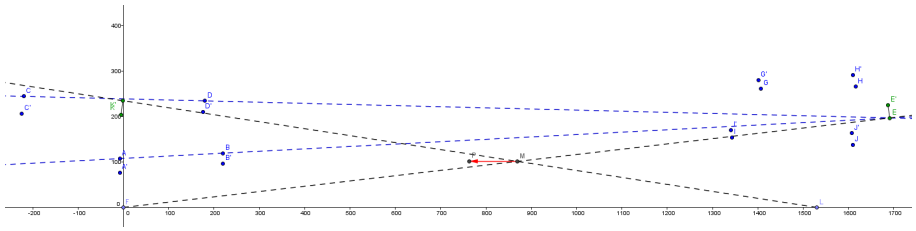

Figure 4.1: Pitch effects on longitudinal IC position, due to $+2°$ of pitch. In blue suspension's points, blue with " ' " are new point position, in violet wheel path's centers, point M and point P are IC position, first and after pitch respective, while points in green "E" are front suspension IC and "K" rear suspension IC.

to consider that the pitch-center has to be located approximately where the driver is, in a way that the body will not be shaken from the pitch movement.

The wheel base of this car is 1530 mm long, the driver head is approximately 600 mm far from the rear axle, so I tried to put the pitch-center in this position, as shown later: see 4.1.5, the position is changing .

Points position is defined with the Eteam reference system, see Chapter 1.

In picture 4.1, we have present suspension configuration points in blue, point in green are front "E" and rear "K" IC (see Chapter 3 to know how they are obtained); point "M" is the pitch-center and point "P" is the new location due to two degrees pitch. In red the displacement, it is small, around 100 mm, and almost horizontal. The other picture 4.2 shows GreenTeam configuration. We can see the pitch-center is not in the middle of the car for project configuration and it changes widely.

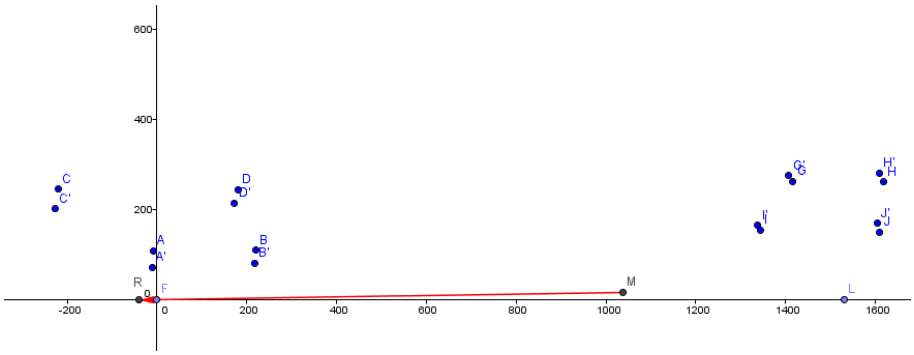

Figure 4.2: Pitch effects on longitudinal IC position, due to +2° of pitch. In blue suspension's points, blue with " ' " are new point position, in violet wheel path's centers, point M and point R are IC position, first and after pitch respective, front and rear suspension IC are not displayed, they are 10 meters (10000 mm) away from the car.

More about longitudinal IC is in Paragraph 4.1.4 and 4.1.6 .

Roll centers are changed too, but less, what I change is their relative position, from 0.5 mm, to 2 mm. The reason will be explained in Paragraph 4.1.4 and it has been discussed already in Chapter 3.

4.1.2 Toe angle and camber angle due to suspensions excursion

The pictures 4.3 and 4.4 show the two solutions: GreenTeam and present. Between the two curves the most important is the toe vs bump curve, positive bump means that if the wheel is not moving the frame is going down due to vehicle dynamic. The *kinematic steering* is wheels' steering movement coupled with wheel vertical motion. More precisely, suspension motion is always a mixture of vertical motion and steering motion. Kinematic steering is not desirable, and if not restrained in a small range, it is not acceptable. Anyway if well designed, it could push the car to performance limits. Let discuss shortly benefits and disadvantage of kinematic steering. First of all kinematic steering angle peak size can be designed, but it is always function of suspension travel therefore of vertical load on the present wheel, also function of the lateral acceleration and load transfer between the two axles. Kinematic steering, if well designed can nullify slip angle difference between inner and outer wheel or

it can adjust toe angle to satisfy wanted slip angles for both inner and outer wheels. All this can work in junction with Akermann or reverse Akermann steering for the front wheels.

Disadvantage are simple and really restrictive: try to imagine a wheel meeting a obstacle or a hole in the ground, the wheel will have a constrained vertical motion and it will assume a steering angle. This is absolutely undesirable if happens on the front wheel, because the driver has to correct the trajectory as it is undesirable for rear wheels too, because it entails greater driver correction. Great care must be taken of spring pre-loads (due to aerodynamic vertical loads), this means that a wheel could work with distance to statical configuration of 20 mm or more thus implying a steered wheel while the car is going straight. This can be corrected by static toe, but too many variables have to be controlled, risking an abnormal behavior if not very well studied and simulated.

For this last reason I decided to have the least possible kinematic steering, considering the possibility of and actuated steering system for the rear wheels in Chapter 6, that have same benefits and no disadvantage.

The solution used by the GreenTeam (figure 4.3) provides a range of circa ± 0.17 degrees. That is not far from zero, but is the curve's trend that is not correct. For the front axle we have negative toe when the car is higher then the project configuration (null vertical motion) and it reaches almost null value when the frame is moving down due to lateral forces. Usually a little negative toe angle is necessary at each velocity to have better performances, in particular for front suspension a -0.25 degrees toe angle grants best lateral acceleration performing constant speed low increasing steering angle, see Paragraph 4.2 . This means a toe angle of -0.4 degrees, when the car is moving at 50 or less km/h, which is too much in terms of pneumatics wear and for the resulting longitudinal forces when going straight. For this reason I reduced both the range (figure 4.4), front range to $-(0.02 \div 0.05)$ degrees, almost a null value, but less when the car is under lateral load and more when is going very slow. This way, using a -0.25 deg static toe, we always have a range of $-(0.27 \div 0.30)$ degrees.

Rear axle curve are usually symmetrical to front ones, in terms of curvature I prefer to have smaller excursion, from 0.08 degrees to 0.07 degrees, and relative change from -20 mm toe, to + 20 mm toe, instead of 0.17 degrees. With an optimized static toe of -0.1 degrees we have for the GreenTeam a range of $+0.07$ to-0.08 degrees while I have $-(0.03 \div 0.1)$ degrees, with less pneumatic wear

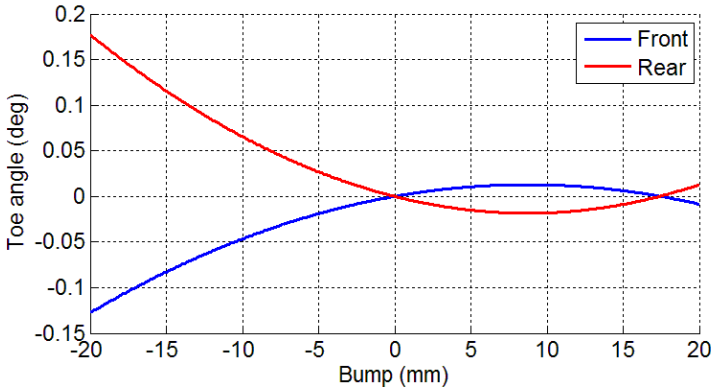

(a)

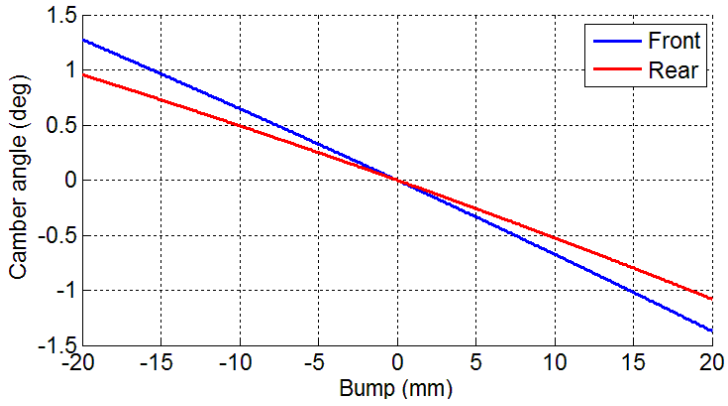

(b)

Figure 4.3: Toe angles (a) and camber angles (b) vs suspension excursion, GreenTeam solution.

and less kinematic steering.

Note that, optimized static toes, are almost the same for both the cars, Adams model confirms this, because they have to limit the slip angle difference from right and left wheels during a curve to have more lateral forces.

Camber curves are next in order. Here because of car size restrains, inboard and outboard, little can be done, I tried to reduce camber excursion for rear wheels, from circa $+1, -1.2$ degrees, to $+0.8, -1$ degrees, while front suspension camber changes, between the two solutions are not relevant.

I reduced camber excursion for rear wheels, because this axle is more preloaded then the front one, in a way to reduce static camber.

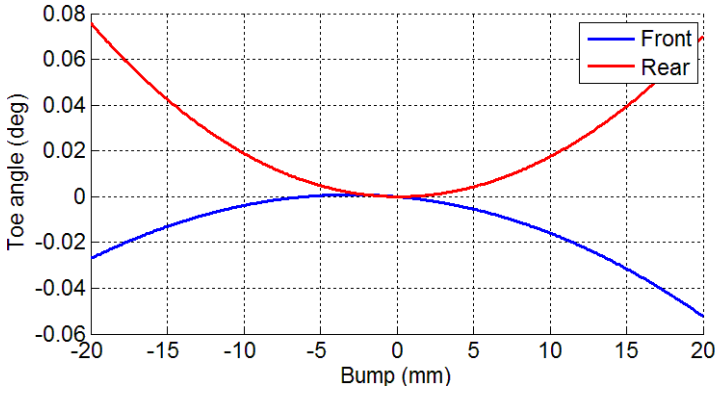

(a)

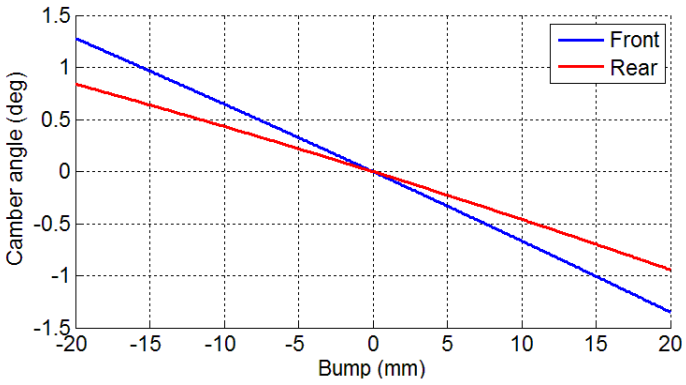

(b)

Figure 4.4: Toe angles (a) and camber angles (b) vs suspension excursion, present solution.

It is possible to see (figure 4.5) that front camber could reach positive value, anyway front suspension travel is limited to ±13 mm, while rear one can reach ±17 mm, so for common use, not particular cases, like accidents, camber curves for both the axles is always under zero level. It is necessary to say that a more negative static camber for front wheels results in a toe less camber for negative bumps, Adams optimizations suggests this value.

Before continuing I want explain the method used to get the results. The figure 4.6 shown the main points of the left front suspension in a "*z-y*" plain. I explain the front one, the other one is alike. The "*Z2*" point is the center point of the tire contact track, "*Z1*" and "*E2*" are the pivots of respectively the lower and the higher suspension triangles. "*Up-limit*" and "*low-limit*" points are the far

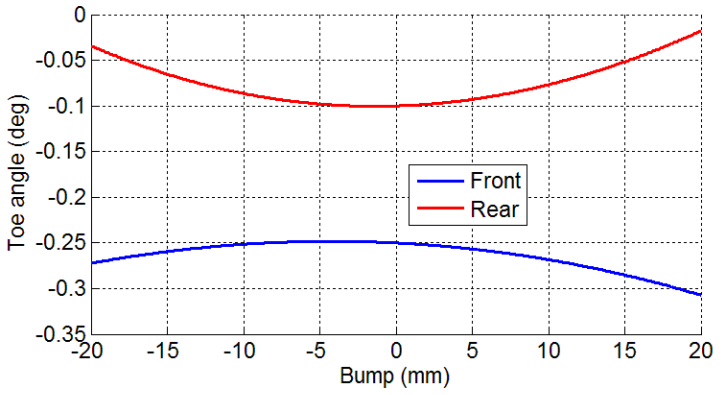

(a)

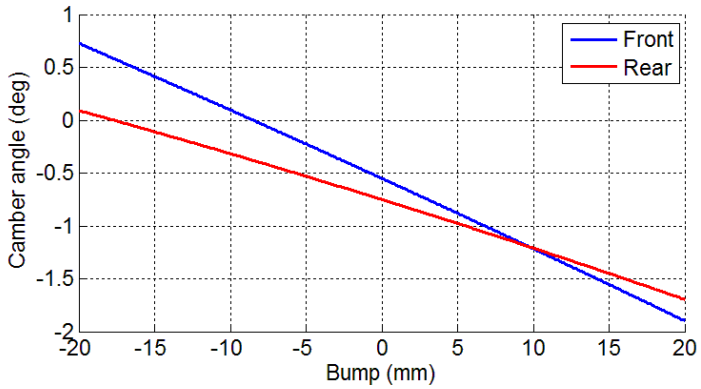

(b)

Figure 4.5: Toe angles (a) and camber angles (b) vs suspension excursion, present solution, with optimized static toes angles and static camber angles.

upper and lower position of the IC: normally triangles in this view are two over planning lines, if the inboard points have the same "z" position and "y" position. That can not be, it is necessary to have proper lateral IC position too, see Paragraph 4.1.1, so in this view IC is not a point but a line. More precisely is the line obtained from the intersection of the planes defined from the two triangles. For this reason I chose the points "$F4$" and "$P4$" defined by the bisector of the angles defined from the two triangles links. The four inboard points are chosen to have desired "$F4$" and "$P4$" point, so the average IC will as well as the desired roll center height. Note that in this first step solution, the four inboard points have the same "y", later in order to have the

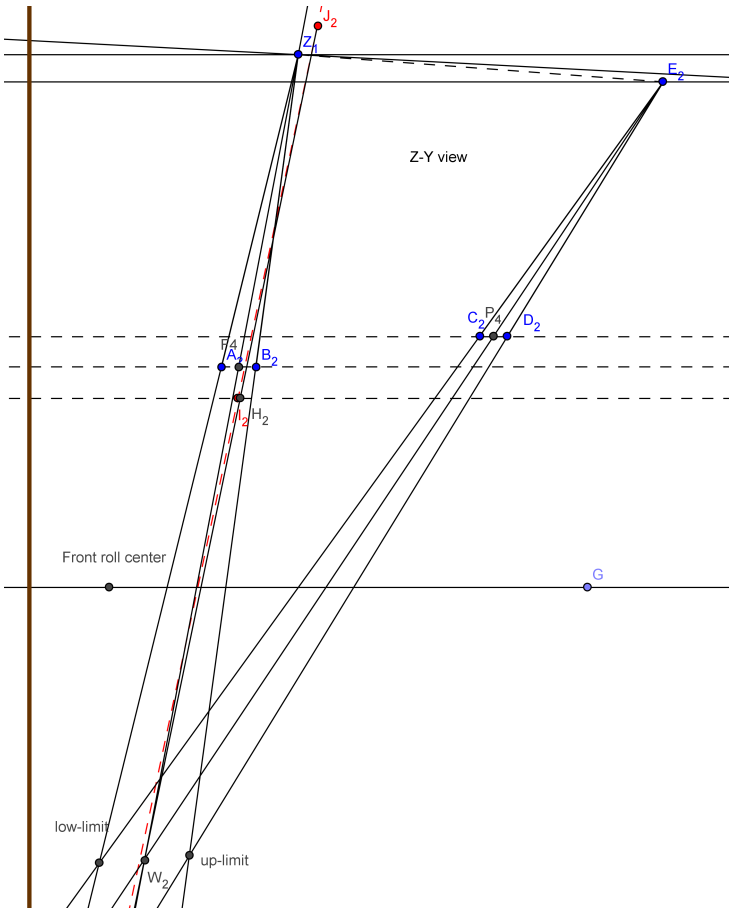

Figure 4.6: Geometrical method used to chose inboard toe arm point to have proper toe vs bump curve. G is the barycenter, and the brown line is the ground. Read below for the other points definition.

desired toe-bump curve these points will have to have a different "*y*".

Next step is to create a line from the out boarder toe arm point "*J2*" to "*W2*", this line defines the position of "*H2*", first approximation of the inboard toe arm position. The two extreme points represent the most outer position for the center of motion. Now we can get coordinates the of this point, ("*y*" position already defined by layout restrains) and using Matlab ® the position of the points "*A2*", "*B2*","*C2*", "*D2*" and the "*H2*" point we have the toe vs bump curves. Usually this first step solution gives already a good toe-bump curve, but to have appropriate longitudinal IC positions and to give the curve the wanted shape the inboard the four inboard arm points must be tuned as well as the "*H2*" point. After some simulation the wanted toe-bump shape is obtained and the final inboard point is "*I2*" is obtained, shown in red. It is good to notice that this point is really close to "*H2*" point that was the first approximation point .

4.1.3 Caster, Kingpin, Caster trail and Scrub-radius

Caster and Kingpin influence front wheel's vertical movement during steering. Anyway, it is more important to deal with Caster trail and scrub-radius consequences on steering stability and harmonize these results with wheel vertical movement. All this implies average Kingpin of 8 degrees, for both rear and front axes with a max excursion of± 1.5 degrees and an average Caster of $+3$ for the front suspension, and -3 for the rear one, with a excursion of $\pm$1degree.

Scrub-radius and *spiddle length* assume a very important task for steering stability, the trend I obtain has the aim to have more constant as possible wheel centered Scrub and spiddle, the other curves change according according with the problem explained below.

Before continuing it is necessary to show the effects of scrub-radius and spiddle length.

In picture 4.7 point "*up-joint*" and "*low-joint*" are the outboard joints in a "*z-x*" view with a reference system introduced in Chapter 1, they define steering axis, the same points are shown in a "*y-z*" view in the left picture. Considering a composite load, red is acceleration and blue is curve load we have a overturning moment around the steering axis. Normally braking or accelerating while the car is going forward do not represent a problem, because these forces on the toe links are the same so there is no overturning moment. It changes during a

curve, like shown under lateral forces have a ∼68 mm arm, while longitudinal forces have a ∼+53 mm arm (*scrub radius*).

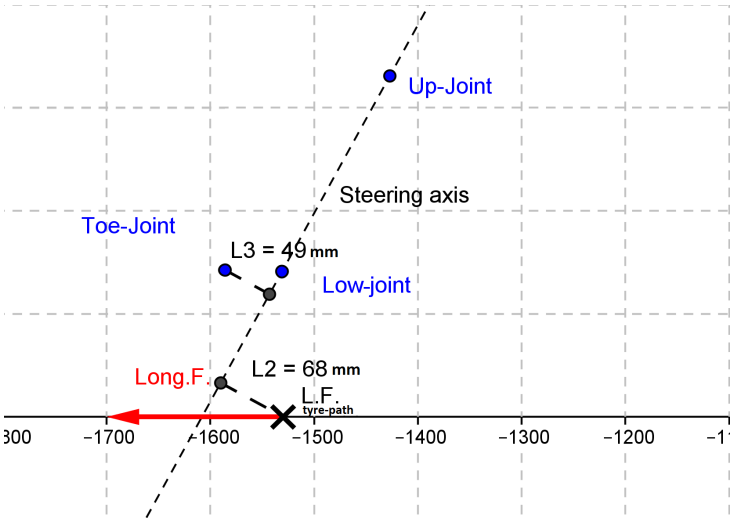

(a)

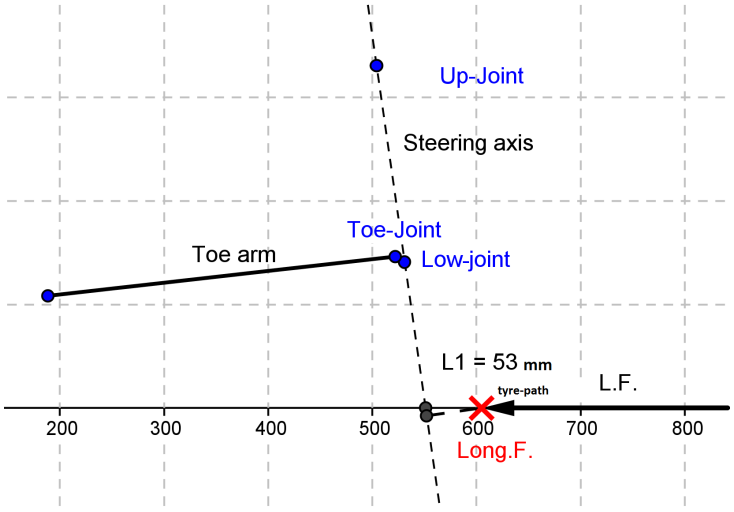

(b)

Figure 4.7: picture (b): "y-z" view of the main suspension points and forces: up and low joints are out boarder positions of A-arm, defining steering axis, toe-joint is the outboard position of the toe arm, Long forces in red, and Lateral forces in black (L.F.).Picture (b) shows same points and forces in a "x-z" view.

Lateral forces due to the position of the rank-pignon system are stabilizing

forces for this configuration as well as accelerating forces, braking could not happen.

Braking and turning can be divided in two cases: brake forces are almost the same and equal to the lower between the two, (no wheel blocking) or one wheel is blocked (inboard wheel) giving lower forces and another one is giving greater force. In this last situation we could have a mechanical moment that closes the curve, with consequences easy predictable. However lateral and longitudinal forces on the outboard wheel are almost the same, as well as on the inboard wheel is almost null (for a limit brake). Now considering that: while pneumatic trail plus mechanical trail has a range from $\sim 68 \div 100$ mm and the scrub radius is ~ 51mm then with this configuration we always have aligning moment on the driver's steering wheel.

4.1.4 Roll centers and pitch-centers heights variation vs suspension motion, Roll center height vs roll motion

In figure 4.8 the trend of roll center heights and pitch-center height and longitudinal position.

The first picture show how the roll center heights change during vertical motion of each axle. Roll center heights is one of the factor that determinate vertical load transfer on the wheels while the car is performing a curve, and these heights are one of the parameters that determinate the under-steering over-steering behavior of the car. Lower heights means less load transfer therefore better performances of that axle, like higher peak value and greater axle stiffens. Like suggested in literature, front roll center height should be should be lower then the other, this can grant on equal terms that the load transfer on the front axis, the steered one are less then the other. With reference on the following formula 5.8. We can see that vertical load transfer is divided in two terms, the one that can be directly modified changing spring set-up between the two axles, another one that is connected to the lateral load and to the roll center height. I designed the system in a way that the first term is always smaller for the front axis and the other one can be adjusted to have the desired vehicle behavior.

It is recommended in literature that the relative heights, between the two roll centers remains almost the same, or at least that the two lines do not intercept each other, this inverts the benefits granted by the roll center height in terms of load transfer.

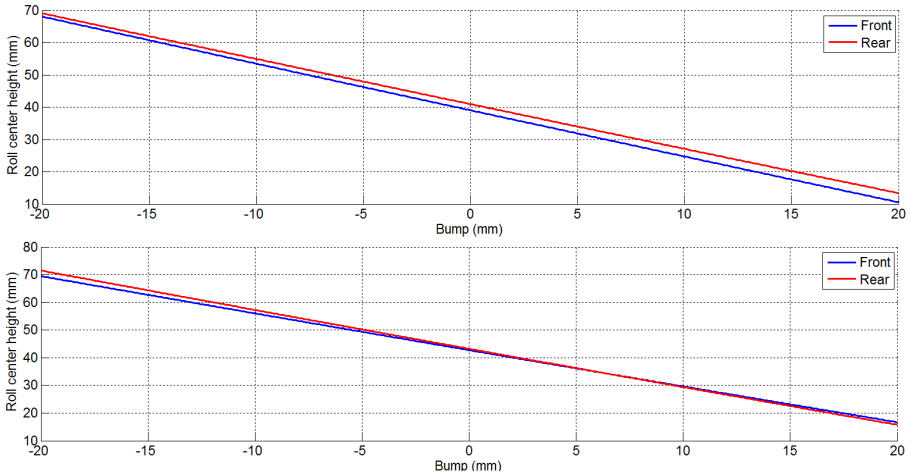

Figure 4.8: Roll center heights vs suspension excursion (bump), of present solution (above), GreenTeam solution (under).

We can see in the picture that if the suspension travel is equal for the front axle and for the rear one there's no line crossing, this is the first step, but this has to be true for all the dynamic condition. It is important here to remember that each suspension is preloaded to react vertical load, it is necessary to take some information from the Paragraph 4.2. We have to check if in the worst condition of relative bump of the two axles front roll center is always lower then the other.

Taking information of suspension travel from Adams ,performing a max lateral capacity at 120 km/h, we have:

1. Front suspension: average travel: 13.5 mm, max. value 14.7 mm, min. value 12.3 mm, corresponding to roll center heights→average 19.8 mm, min. 18 mm, max 21.5 mm.

2. Rear suspension: average travel: 15.1 mm, max. value 15.4 mm, min. value 14.8 mm, corresponding to roll center heights→average 20.1 mm, min. 19.7, max. 20.5 mm.

My purposes are satisfied, front roll center is always under rear roll center.

The picture 4.9 shows the pitch-center height and longitudinal position during vertical travel of both the axles, equals to vertical translation for the car, the main difference between present solution and the other one is that the vertical

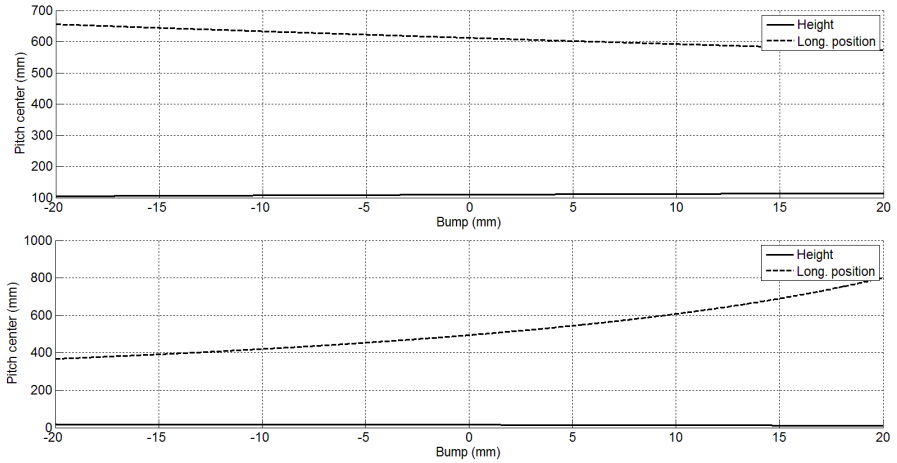

Figure 4.9: pitch-center heights and longitudinal position (above present solution, under GreenTeam solution) , with reference to Eteam reference system defined in Chapter 1.

position is grater and it is almost constant while the longitudinal position is set up in a way that for average velocity corresponding to -5,-10 mm of bump (car higher than project configuration), the pitch-center longitudinal position is in the middle of the car where the driver is, and the amount of change in longitudinal position is restrained in a range of 650 to 570 mm, while the other has 400 mm excursion and is not situated in the middle of the car.

The other picture (figure 4.10) shows GreenTeam E5-car solution, we can see the great variation during bump of the both height and longitudinal position resulting in a no so pleasant behavior for the driver and for the car dynamic too.

This last picture shows roll center heights during roll motion, it is possible to see that for a particular value of roll in the right picture front wheel center is higher then rear one's with consequences explained before. This roll value with default roll-bar can not be reached, but with lower roll stiffens could be reached, so I operate to prevent this phenomena.

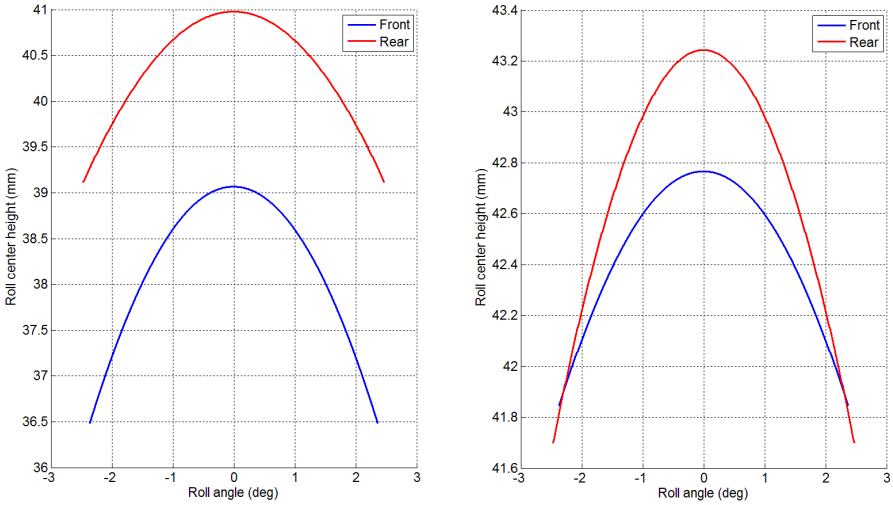

Figure 4.10: Roll center height trend due to roll motion. Present solution (left), GreenTeam solution, right.

4.1.5 Pitch-center height and longitudinal position vs pitch angle

As discussed in Paragraph 4.1, here (picture 4.11) differences between present solution and GreenTeam one are shown.

It is evident that, a so low pitch-center height comports during bump, see 4.1.4, and during pitch a great displacement of the pitch-center position. (figures 4.9 (b)).

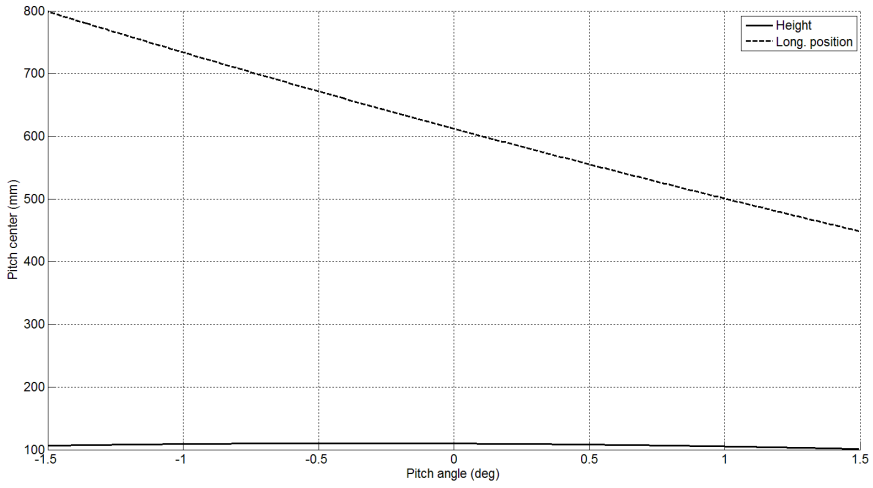

(a)

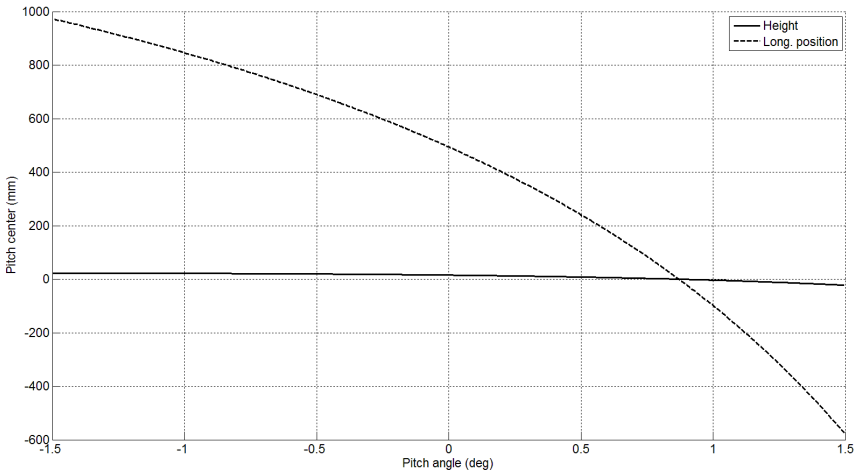

(b)

Figure 4.11: pitch-center height and longitudinal position vs pitch motion, present solution (a) GreenTeam solution (b).

Present solution grants a max. displacement of 350 mm, while GreenTeam has 1050 mm displacement of the pitch-center, relative speaking to the car wheel base we have:

22% for present solution, and 69% for GreenTeam solution, that is much low.

Explaining pictures 4.1 and 4.2, are not so accurate like this last picture, but

they show well the real trend.

4.1.6 Steering system set up: Ackerman

The picture (figure 4.12) shows the "x-y" view of the car, and the geometrical construction, to set-up Ackerman steering geometry, for references for how to construct it see [12].

In particular the design process starts with almost the entire geometry already designed, only the x-y coordinates of the outboard toe link arm have to be decided. The black line passing trow "Z4" is the line that define 100% Akermann steering geometry, starting with this geometry and proceeding with lines passing throw the circle the Ackerman changes in a range of circa 150% to 50%, the pink line represents final solution, with a Ackerman of -50%. This value is value that comports better performances after several Adams tests, and track tests.

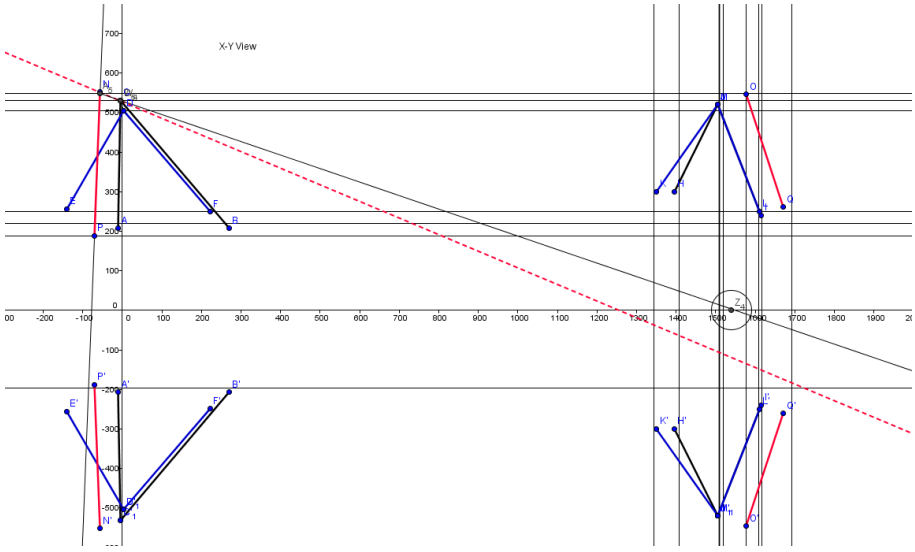

Figure 4.12: Ackerman-steering geometry construction.

Other consideration are:

- Toe-in deflection due to lateral load: arms are really stiff but lateral forces are not limited to little values, so it is important to set up rack pinion

system, like I did to have toe-in deflection due to these loads, because it influence steer stability, decreasing steering angle with their deformation.

- Steering ratio has to be in accord with available rack pinion systems and it should bigger for little steering wheels angle in a way that the steering angle on the wheel has more sensibility, important for high speed turns, and it has to decrease with steering angle for low speed curves where it is important to have greater variation of wheel steering angle with a smaller steering wheel angle.

- Dealing with anti-Akermann it is important that the difference between the wheel steering angle is smaller or at least null, parallel steering, for little steering angles: when the car make a large radius curves the difference between the two slip angles is smaller. Then it assumes trend as shown in picture 4.13.

A development for the future is to evaluate with more precision the difference between inboard and outboard slip angles, and set up Ackerman according to this.

In figure 4.13 Ackerman response as function of steering wheel angle (a) , and wheel's steering angle (b).

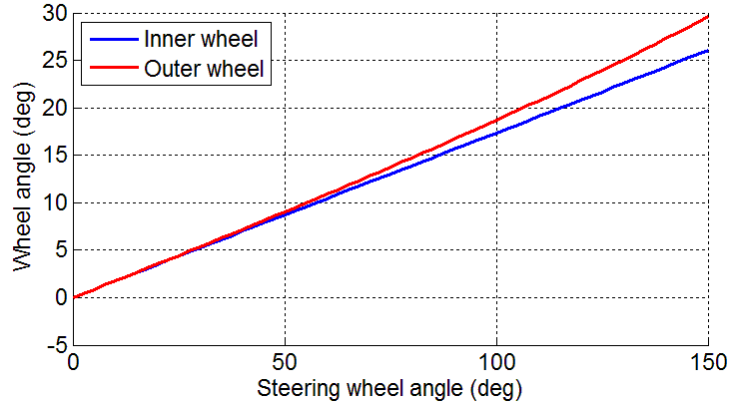

(a)

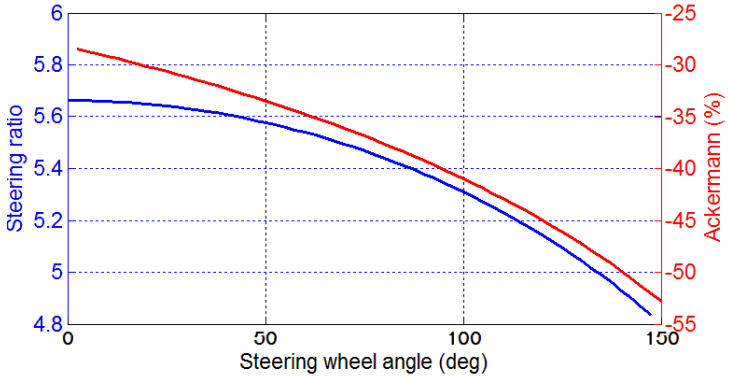

(b)

Figure 4.13: Wheels steering angle vs steering wheel angle(a). Ackermann respons vs steering wheel angle, steering ratio vs steering angle (b).

4.1.7 Anti-features

There is no much at this point of the design, anti-features are connected to pitch-center position and trend and with roll center position and trend, anyway I want here to discuss braking repartition, thus discussing connected anti-features.

Braking repartition should be set-up, like the ratio between vertical loads available on each axles, considering available wheel ground friction (wet and dry) ,

Anti-feature	present solution	GreenTeam solution
Anti-dive	54.8%	5.8%
Anti-lift	25.5%	3.6%
Anti-squat	7.5%	0.3%

Table 4.2: Anti-features evaluation.

load transfer due to longitudinal acceleration, and aerodynamics load , omitting calculation we have a range on the ratio between front and rear vertical loads of:

1. wet low speed-wet high speed: $0.65 \div 0.655$ (front/rear);
2. dry low speed-dry high speed:$0.765 \div 0.76$ (front/rear)

Now the bigger ratio has to be chose, in a way front wheels are the first to lose block: with this ratio we have the following anti-features with reference to figure 3.4.

As shown in chart 4.2, the values change from present solution and green team one's, these are the better solution according to other design factors like pitch-center and others.

4.1.8 Layout constraint

The main constraint to layout are the two front engines connected to the wheels and the rear propulsive system made up by two engine and two driveshaft show in picture.

It is necessary for the front engines to guarantee enough space between the two triangles and the toe arm to insert engines, while for the rear system suspension inboard point must allow enough space, in particular enough lateral space, other layout constrains are brake discs and battery compartment.

4.2 Dynamics Tests

4.2.1 Model

The model is a multibody model of the whole car: each part has the real inertia characteristics acquired from CAD. The model has 13 degrees of freedom but

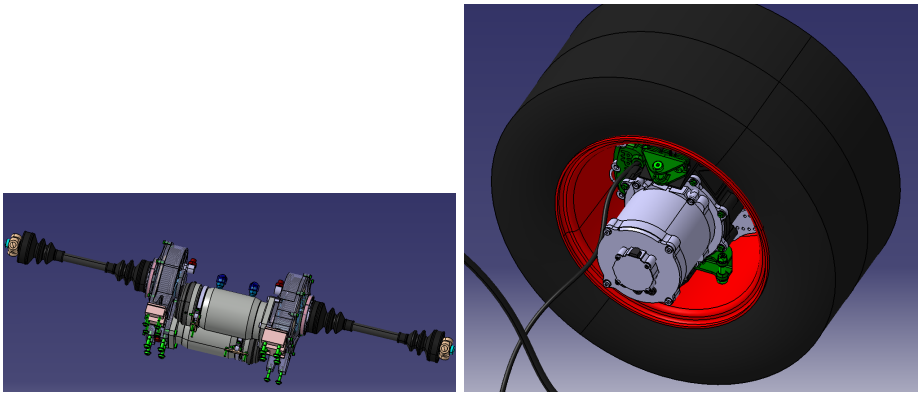

(a) (b)

Figure 4.14: Layout constrains: rear engines (a), front engines (b).

9 of those are important. Each suspension has 1 degree of freedom, the suspensions motion, that is a combined motion: vertical travel and toe variation. The other five degree of freedom are: forward velocity (traction is imposed to obtain a proper velocity), lateral velocity, roll, pitch, yaw.

For reference of multibody analysis see [17, 16]. Generally speaking Adams can solve dynamics equation for multibody systems for large displacement, something that is almost impossible to do easily with a paper and a calculator.

Another important part of the model are tires, there is no tire model for the particular type of tire used but there are tires models for two tires close to this one.

What I did, is to modify the physical parameters of those two tires available model, the one with the correct outer diameter the other with the correct width, in a way that the model I used should replicate the behavior of the real tires used.

In picture 4.15 is the entire model and further more (picture 4.16) a single wheel linkage with the used constraints. Each link used is not a deformable body so parts verification (stress and strain) takes place in the Chapter 7. Spring, dumpers and linkage geometry is set up respectively in Chapter 5 and in the first part of this Chapter.

The frame characteristics are allocated to the red sphere, barycenter position, front upright in green includes engine's inertia. Aerodynamics forces are evalu-

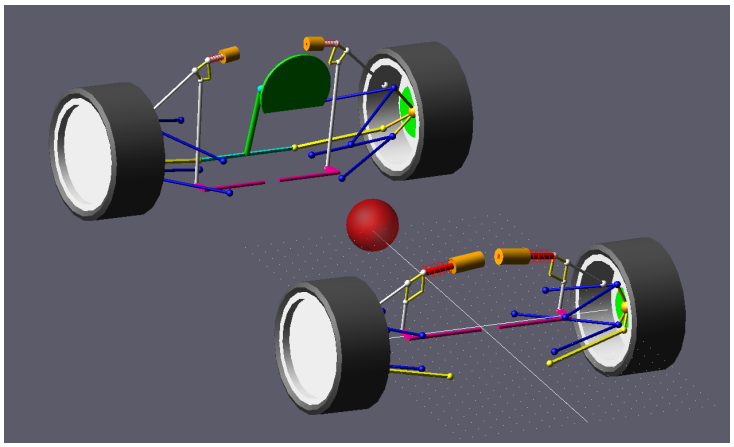

Figure 4.15: Multibody model of the car with Adams View.

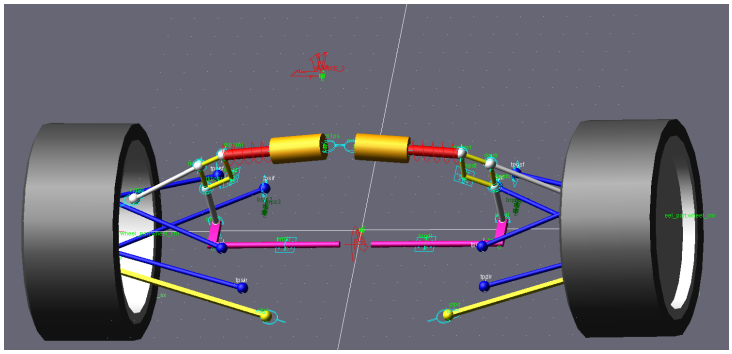

Figure 4.16: Rear axle suspension and joints view.

ated using experimental data and these forces are respectively (front-rear) 540 N and 695 N, while the total drag is 450 N.

More then joints it is possible to see the aerodynamic force in red, and the roll-bar mechanism. The entire stiffness of the roll-bar mechanism is allocated to a torsion spring, while bar-arms are infinitely stiff. Torsion spring value is obtained in Chapter 5, as well as springs and dumpers value, with Adams an optimization was made to reach greater lateral acceleration.

It is important to observe that each triangle has not three spherical joints but a revolute joint inboard and a spherical joint to connect with the uprights.

Proceeding with the Grouber count for a single suspension in both cases (considering 3 spherical joints each triangle or a revolute joint plus a spherical) we

obtain for the both cases:

Element type				Total
Bodies	2 triangle	1 toe link	1 upright	6 bodies
Constraints	4 spherical joint	2 spherical joint	2 spherical	
Grouber count	(12-12=0)	(6-6=0)	(6-6=0)	24-24=0

Table 4.3: Joints set up first case.

The first Grouber count (difference between DOF and joints grade) says that the suspension has no degree of freedom, this is not true, the single suspension has 2 DOF, the suspension motion and the revolution around the toe link. This is because this configuration of joints is hyperstatic, the two inboard spherical joints of each triangle are redundant constraints, if we decompose the constrains equation along the line connection the two inboard points and along a line perpendicular to this we have redundant constraints. In the real solution manufactured, the two spherical joints work like a revolute joint with the revolute axis along the line connecting the two inboard points of each triangle.

Element type				Total
Bodies	2 triangle	1 toe link	1 upright	6 bodies
Constraints	2 revolute joint	2 spherical joint	2 spherical	
Grouber count	(12-10=2)	(6-6=0)	(6-6=0)	24-22=2

Table 4.4: Joints set up second case.

1. The joints assignment is arbitrary, in a way that is only important the total sum of the single wheel suspension system.The partial Grouber count is between bracket, because it has not a proper physical meaning. The upright is not over-constrained and the toe link has no 3 DOF, this is simply the solution considering each body separate to the other.

We can see the total DOF in this case is two, an those two DOF are the two real-ones, because there are no redundant constraints equations.

4.2.2 Tests

Now that the model is clarified test are next in order. The car is just set up to work at a maximum speed of 120 km/h and a constant speed increasing steer angle from zero to a great value. roll-bars are default value, see Chapter 5.2 .

It is important to check that the suspension travel is inside the design range, there are no parts of the car touching the ground, camber values are negative or at least zero (for right wheels), and there's no abnormal behavior.

To make this some iterative tests are made to chose proper pre-load on the front and rear axles, starting with car standing, so only with pre-loads necessary to contrasts the weight force. When pre-loads, to have no suspension excursion are known, the next step is to find proper pre-loads compatible with vertical loads and max suspension excursion. When these value are known and the car is working properly, more test can be made.

Six optimization tests are made to increase lateral acceleration, starting with roll-bar stiffness, (front and rear) then, two are for front and rear static toes and last two are for static cambers.

Using geometry obtained from the kinematic design I designed rocker-pushrod geometry, spring ratios and roll-bar ratio, according with Chapter 5. (figure 4.17).

Springs dumpers and roll-bars are discussed in Chapter 5, but generically speaking they are connected to car's response frequency and wheels vertical loads variation as function of vertical load application frequency.

The most important task for the rocker-pushrod kinematic is to harmonize vertical suspension motion with available springs deformations and to grant enough spring pre-load to contrast vertical loads. It is not easy to make agreement with with all the parameters and it entails several simulations.

I chose a spring ratio (ratio between wheel center vertical motion and spring deformation, as known as rocker's ratio too) as constant as possible, to have a fixed parameter, that is not the only solution but it is easier to predict and easily simulated by mathematical models, spring ratios vs vertical displacement are in picture 4.17.

Now it is necessary to chose the four wheels engine's torque to have a desired forward velocity, negotiate maximum torque with the real torque available to each wheels. I can not make any trust of those values, because engine data are only in part available, so I must do some approximations.

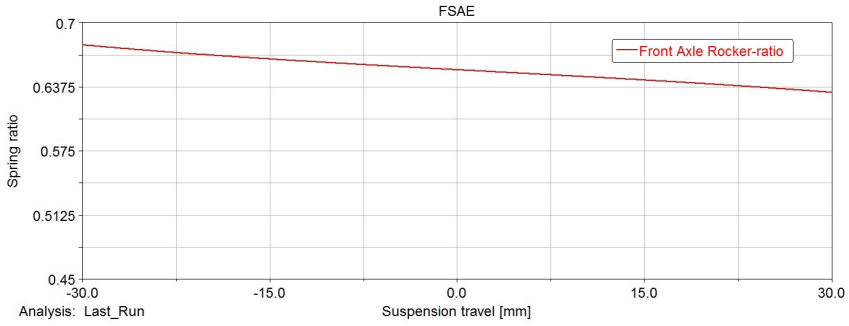

(a)

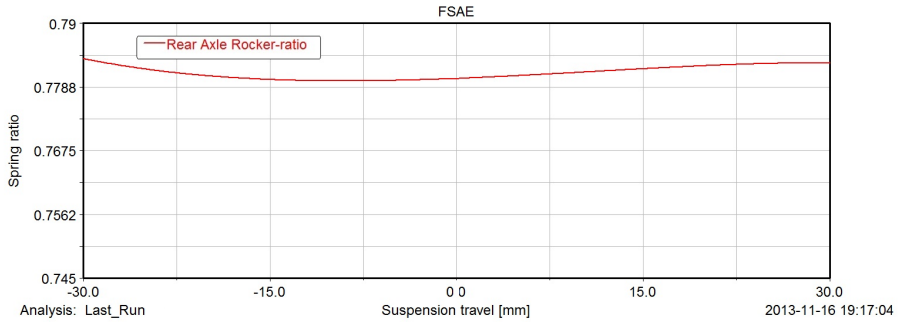

(b)

Figure 4.17: Rocker ratios vs suspension travel, front (a), rear (b).

I would like to remember that the exact amount of torque is only needed to evaluate acceleration performances, not an aim of this thesis, because during constant speed slowly increasing steering angle and steer step, torque thus longitudinal slip should be almost null.

It is known that the rear engines can reach 27 kW of power and can reach 50 Nm of torque while the front engines are 15 kW each and can reach 25 Nm. Gear ratios are respectively 6.5 for rear wheels and 7.4 for front wheels, with this value a torque controller is designed to have wanted forward velocity.

Caring on with tasks I performed the same task(constant speed slowly increasing steer angle) but at two different speeds 80 km/h and 50 km/h, and I checked car behavior. I also did optimization as before, usually obtaining different values, anyway for a real set-up it is necessary to know how the circuit is: how many 50, 80 and 120 km/h curves there are, then make a compromise between owned parameters.

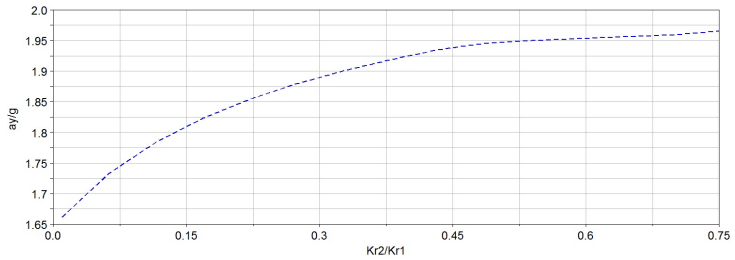

Figure 4.18: Design optimization for lateral acceleration hanging rollbars ratio, using a default front roll-bar of 20 Nm/degree.

Last simulations are I operate a "steer step" at 120, 90, 50 Km/h and I checked behavior as before

Test at 120 km/h

Now the car model is ready I made some design simulations. Starting with null static camber, static toes and with roll-bars design in Chapter 5, I obtained simulating best static toes, camber angles and roll-bars value to optimize the peak of lateral acceleration. Below an example of optimization, then most common results.

The picture 4.18 shows, the peak value of lateral acceleration expressed in g (9.81 m/s^2), fixing the front roll-bar to a $2 \cdot 10^4 Nmm/deg$ value, I changed rear roll-bar and I get improvements in peak value of lateral acceleration. It is here important to consider that beyond a certain value of the ratio K_{r2}/K_{r1} the car change is attitude see Chapter 5. I chose a 0.6 value for this ratio, that is a good compromise considering further tests too.

Something like this was made to find better static toe, front and rear, camber static front and rear, anyway benefits are limited so they will not be displayed.

Now that the car is completely optimized I first evaluate tasks discussed before, below most important features:

Picture 4.19, shows wheel-center travel relative to project configuration evaluating constant speed slowly increasing steer angle simulation, it is possible to see that when the car is stationary, (no forward speed), there is a negative displacement for both front and rear suspension, this means that the springs are preloaded, and without aerodynamics load the frame is above project configuration. Anyway the maximum excursion is under 20 mm for rear suspension and 7-8 mm for front one. While the vehicle is accelerating the frame is going

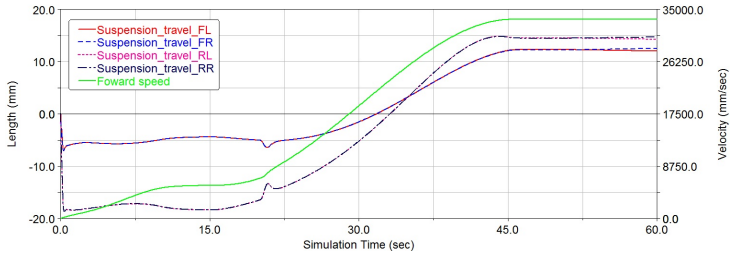

Figure 4.19: Suspension travel and velocity in the first part of the constant speed slowly increasing steer angle simulation. Task started at the 50th second.

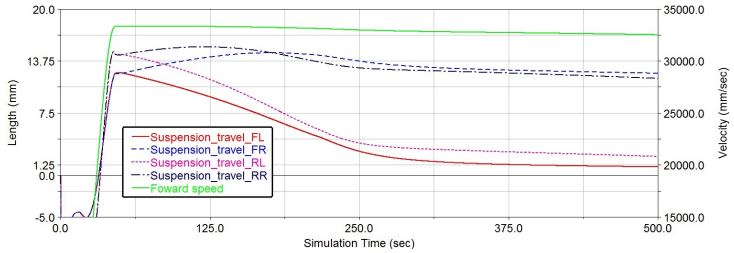

Figure 4.20: Suspension travel and velocity in the second part of the constant speed slowly increasing steer angle simulation.

down for both longitudinal load distribution and vertical loads, so suspension travel is increasing reaching for a particular velocity, function of both vertical loads and forward acceleration the project configuration. These particular values are not so important, what is important is that in a range of ± 10 mm from project configuration, corresponding to a range of velocity, for the rear suspension, of $31 \div 94\, km/h$, we have very good toe-bump curves, see figure 4.5, so the car for the most of the velocity has something really close to project parameters. For the front suspension we have a range of velocity even better.

In the last part of the previous graph velocity reach max value of 120 km/h, picture 4.20 shows suspension travel trend in the end of the task.

After the short time at constant speed, the car starts turning, it is possible to see how suspension travel between same axle's wheels assume a offset, the car is rolling that's the reason. What is important that suspension travel is inside design range $\pm$ 20 and that is. Can be seen, that velocity decrease, this is because of torque control function does not work perfectly, anyway speed difference is less then 2.5 %.

Now camber response in figure 4.21.

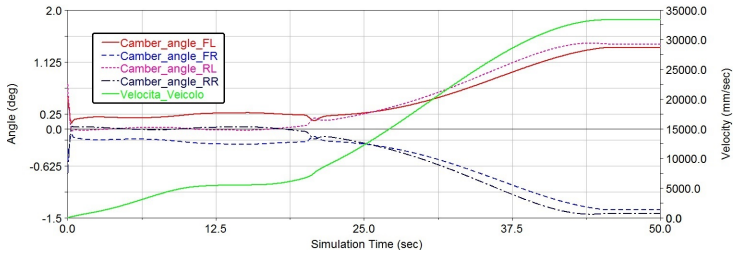

Figure 4.21: Camber angles and velocity in the first part of the constant speed slowly increasing steer angle. Task started at the 50th second.

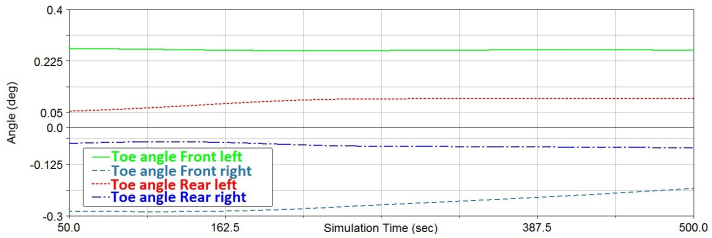

Figure 4.22: Toe angles, front one values are without steering angles contribute.

This picture is similar to previous one but it is about camber, it is here possible to see that for a simulation time included from 12.5 and 16 seconds, speed is constant (20 km/h) so no longitudinal load transfer, camber configuration is for all the four wheels negative (left wheels) or at lest null. (right wheels has symmetrical reference system, so positive camber correspond to negative for left wheels, see [12]).

It is now important to observe that for any other simulation time, velocity and steering wheel angle, wheels are always in a negative condition. It can be observed that for constant velocity camber angles of right side and left side are perfectly symmetrical, how should be.

In figure 4.22 there are toe angles during the test, it is possible to see how toe angles remain in the prescribed range as wanted and kinematic steering is limited to a little amount.

To complete the lateral acceleration during a steer step at 120 km/h and a steering wheel speed of 300 deg/s.

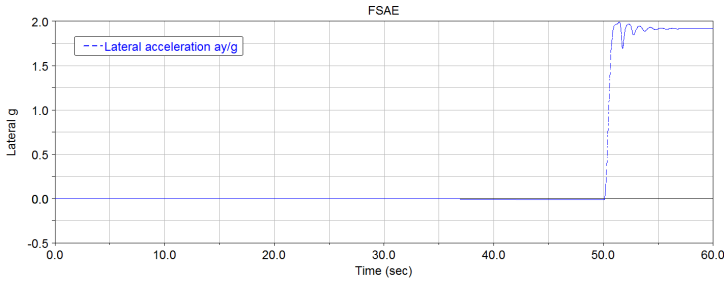

Figure 4.23

Test at 80 km/h

In picture 4.24 the same optimization test made to choose best K_{r2}/K_{r1} ratio between roll-bars, like before it is important to consider vehicle attitude too in terms of K_γ(understeer), see Chapter 5.4. .

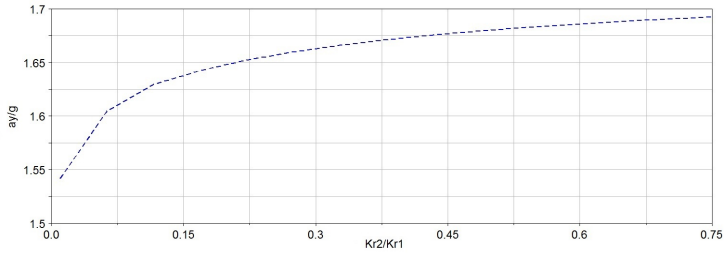

Figure 4.24: Design optimization for lateral acceleration hanging rollbars ratio, using a default front roll-bar of 20 Nm/degree.

Test at 50 km/h

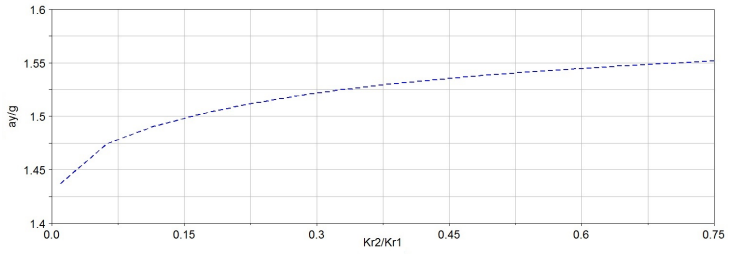

Figure 4.25: Design optimization for lateral acceleration hanging rollbars ratio, using a default front roll-bar of 20 Nm/degree.

The last picture, (picture 4.25) is the same optimization made before, it is possible to see how aerodynamics forces play an important role in vehicle maximum lateral acceleration. In this case at 50 km/h it is possible to reach "only" 1.55 g, that is still so much.

4.3 Other considerations

For future development a four-steering wheels model can be created modifying this model, in a way that benefits discussed in Chapter 6 can be compared with this model.

For the present concern this work is not a purpose of this thesis, because values of rear steer are not enough to proceed with this simulations, anyway I strongly recommend before a real introduction of this system to make more tests with Adams.

Chapter 5

Shock absorber setup

In literature are available many of methods to design spring and dumpers, most of them are based on comfort specifications. Olley's criteria impose a restrict range for the natural frequencies of the car's system, but these are useless in a race car, where performances only matter.

However some basic considerations should be made anyway: Olley suggests that frequencies should be in a range of $1 \div 1.5$ Hz. That is not only a matter of comfort but it is connected with static deformations in accord with the following formulae:

$$f = \frac{1}{2\pi}\sqrt{\frac{k}{m}} \tag{5.1}$$

and $\Delta z = \frac{m \cdot g}{k}$ resulting in:

$$f = \frac{1}{2\pi}\sqrt{\frac{g}{\Delta z}} \tag{5.2}$$

For frequencies from 1 and 1.5 Hz we have: $\Delta z = 248 \div 110$ mm.

For race cars to reduce those deformations we need greater frequencies. Other literature references for race cars suggest a range of $2 \div 2.9$ Hz ($\Delta z = 62 \div 30$) mm. and total roll stiffens $K_{\phi(g)}$of 1.2 degrees/g.

5.1 Springs setup

Initially is important to take care of springs available, is useless to design springs value that are not available. For Formula Student competition we have a particular range of stiffness required, something between mountain-bike and

light weight motorbike, fortunately Öhlins specialized in springs and dumpers make some high quality component for Formula student competitions.

Springs available are basically five: 26.2 N/mm, 30.6 N/mm, 35 N/mm, 39.4 N/mm, 43.4 N/mm, while pneumatic vertical stiffness is: p=169 N/mm.

Spring ratios are compromise between available excursion and equivalent stiffness of an axle, for this concern I create a simple model of the car, two degree of freedom, bump and pitch (like in [10]).

Remembering that:

$K_{wc} = K_m s_r^2$;

where $K_{wc}$is the equivalent wheel center stiffness, $K_m$is the spring stiffness, and $s_r$is the spring's ratio or rocker's ratio, furthermore: each axle has two springs and two pneumatic, so the axle equivalent vertical stiffness is:

$$K_e = 2\frac{K_{wc}p}{K_{wc}+p}; \tag{5.3}$$

Now I make this first step approximation:

$f = \frac{\omega}{2\pi} = \frac{1}{2\pi}\sqrt{(\frac{k_{e1}+k_{e2}}{m_s})}$;

I tried several springs and spring's ratios, according to Adams for spring preloads too, in a way to have a frequency of circa 2.2 Hz. Then I solved the two degree of freedom model, with proportional dumping and I obtained with $s_{r1} = 0.68$, $s_{r2} = 0.75$, $K_{m1} = K_{m2} = 26.2\ N/mm$:

bumping frequency f_b=2.23 Hz and f_p=2.94 Hz.

Using for both the axles the 35 N/mm springs we have:

f_b=2.55 Hz and f_p=3.36 Hz , acceptable if we consider that the driver should not be suggested to pitch motion, because is body is near the center of motion. Anyway, three different springs can be used for both the front and rear axle, with nine possible combinations, enough for tuning.

Dumping coefficients are obtained using proportional dumping. Results values are: $c1 = 1.76Ns/m$; $c2 = 1.74Ns/m$; while dumping coefficients are:

with dumping factor: $\zeta_1 = 0.67$ front, $\zeta_2 = 0.5$ rear.

Something more complex is needed to optimize bumping coefficient and to set up roll-bars, in other words is necessary to introduce roll and load transfer due to roll. For this purpose it's necessary to introduce pneumatic behavior vs vertical load, connected to $K_\gamma$understeer coefficient. In picture 5.1 an example

of the pneumatic force vs slip angle (from real used pneumatic data) as function of camber angle.

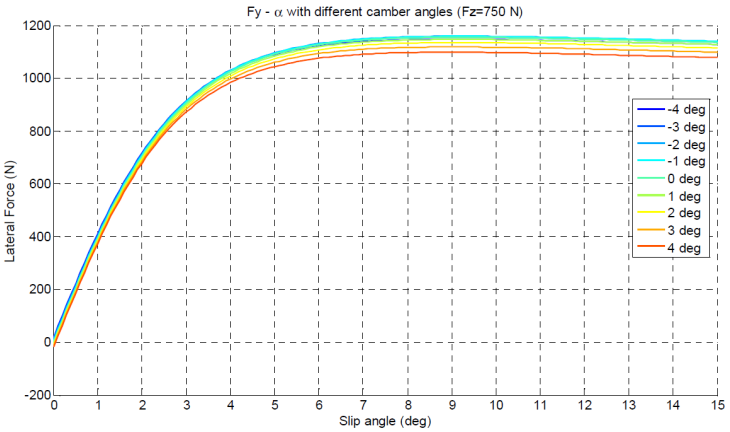

Figure 5.1: Lateral force vs slip angles for different camber angles for a vertical load of 750 N.

In picture 5.2 the influences of vertical load on lateral forces for the same slip angles.

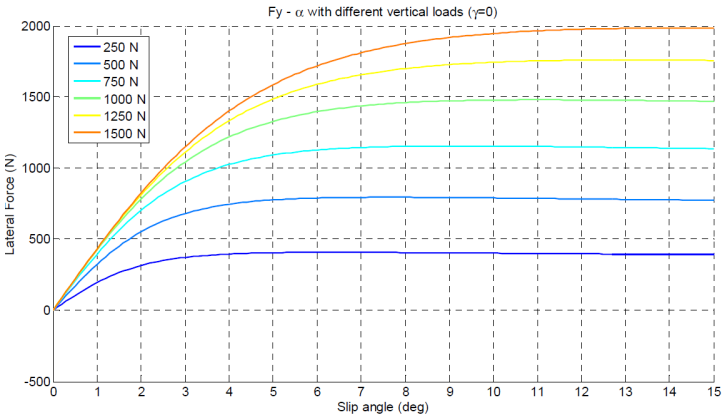

Figure 5.2: Lateral force vs slip angle changing vertical load.

The picture 5.3 shows instead longitudinal forces as function of vertical load and slip angle.

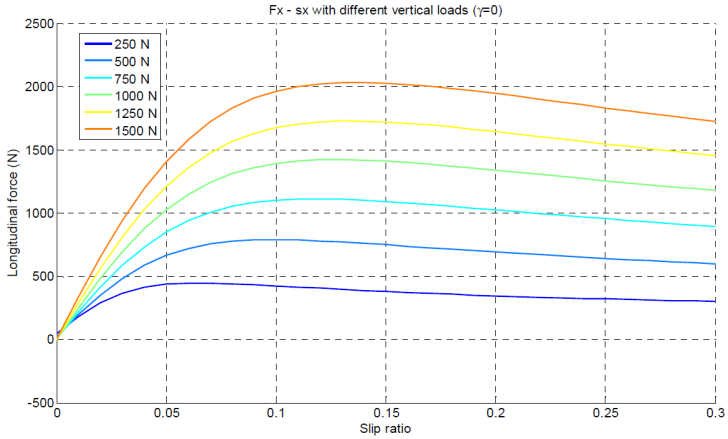

Figure 5.3: Longitudinal forces as function of slip ratio and vertical load.

Slip angles and practical slip ratio ($S_x$an S_y)are defined in [10], or [12].

Load transfer and axle characteristic

If pneumatic characteristic are known, axle stiffness C_i can be evaluated as function of lateral forces and lateral load transfer.

Below load transfer equations directly connected to the C_i, the more the load transfer the less is the resulting C_i, this causes the not linear behavior of the pneumatics. See [14].

$$\Delta F_{z1} = \frac{1}{t_1}[d_1 F_{y1} + \frac{K_{\phi 1}}{K_\phi}(h-d)(F_{y1}+F_{y2})]; \tag{5.4}$$

$$\Delta F_{z2} = \frac{1}{t_2}[d_2 F_{y2} + \frac{K_{\phi 2}}{K_\phi}(h-d)(F_{y1}+F_{y2})]; \tag{5.5}$$

where d_i are roll center heights, (1=front, 2=rear) and d is the roll axis height calculated at the same *"x"* of the barycenter.

In the expression 5.6, $K_{\phi i}$ are the total equivalent roll stiffness of each axle, and $K_\phi$is the total roll stiffness.

Each axle roll stiffness is so defined:

$$K_{\phi i} = K_{\phi i-S} + K_{\phi i-P} + K_{\phi i-B} \tag{5.6}$$

and the total stiffness is:

$$K_\phi = K_{\phi 1} + K_{\phi 2} \tag{5.7}$$

Where $K_{\phi i-S} = \frac{K_{wc_i} t_i^2}{2}$, $K_{\phi i-P} = \frac{2ps_{ri}^2 t_i^2}{2}$ and $K_{\phi i-Bi}$is the roll-bar stiffness (see Paragraph 5.2).

When all these parameter are defined, are therefore known the axle characteristic F_{yi}as function of both the slip angles.

Now the understeer coefficient can be defined and evaluated:

$$K_\gamma = \frac{m}{l}\frac{C_2 a_2 - C_1 a_1}{C_1 C_2} \tag{5.8}$$

Given that pneumatic behavior is not linear at all, another optimization model was used, this model optimize, dumping coefficients for front and rear wheel's as well as roll-bar stiffness granting a desired K_γ, a total roll stiffness and a bump frequency as wanted. It is important to consider that the car as vertical loads due to aerodynamic, so the two most far cases are evaluated, null velocity

Figure 5.4: Öhlins shock absorber designed for Formula Student competitions.

and 120 km/h velocity, requiring a 0.2 degree/g of K_γ and bump frequency of 2.2 Hz. with the following results.

$K_{m1} = 24.5\ N/mm$;

$K_{m2} = 24.3\ N/mm$;

This more precise model gives as output stiffness smaller then the previous one, however the frequency variation is function of:

$\Delta f = \frac{\Delta\omega}{2\pi} = \frac{1}{2\pi}\sqrt{\frac{\Delta k_{e1}+\Delta k_{e2}}{m_s}} = \sqrt{\frac{(2\cdot\frac{\Delta K_{wc1}\cdot p}{\Delta K_{wc1}+p}+2\cdot\frac{\Delta K_{wc2}\cdot p}{\Delta K_{wc2}+p})}{m_s}} = \sqrt{\frac{(2\cdot\frac{\Delta K_{m1}\cdot s_{r1}^2\cdot p}{\Delta K_{m1}\cdot s_{r1}^2+p}+2\cdot\frac{\Delta K_{m2}\cdot s_{r2}^2\cdot p}{\Delta K_{m2}\cdot s_{r2}^2+p})}{m_s}} \cong 0.12$ Hz;

if we use 26.2 N/mm springs we have an average bump frequency of 2.32 Hz according with simpler model.

In Chapter 4 wheel center displacements were into design range, it is necessary to control available range for shock absorber.

The max wheel center displacement is ever ±17 mm while the lower rocker ratio is 0.68 so the max spring displacement is ±25 mm and max shock absorber displacement is ±28.5 mm. This means a maximum exploitation of 88%, in case of overload, buffers are available in the shock absorbers, so the last few mm of displacement have a very high stiffness.

5.2 Roll-bars setup

To have a wanted 1.2 deg/g total roll stiffness is necessary to design roll-bars with the following values suggested from the optimization model.

Front roll-bar: 12000 Nmm/deg

Rear roll-bar: 9000 Nmm/deg

This value has to be configured to allow roll-bars set-up in a range of these suggested values.

For this matter a model has been created to easily choose roll-bar diameter, material and roll-bars arms with adjustable holes.

I have three roll-bars configurations, in the first we have roll-bars pipe and arms made by steel, then aluminum roll-bar pipe and steel arms then both aluminum.

Material proprieties and geometry are these listed below:

Roll-bars:

1. The rigid bar is made by steel and it is: $\phi_e = 20$ mm $\phi_i = 10$mm wide and it is 630 mm long.
2. The average bar is made by steel and it is: $\phi_e = 18$ mm $\phi_i = 14.5$ mm wide and it is 630 mm long.
3. The soft bar is made by aluminum and it is: $\phi_e = 24$ mm wide without hole and it is 630 mm long.

Roll-bars arms, have always the same geometry: two parallelepipeds 14 mm high, 4 mm deep and 100 mm long with holes. This is only a first step design, better geometry will be chosen according with this results. Anyway there are two series, one made by steel other one made by aluminum.

The total equivalent stiffness is evaluated calculating total strain for unit load, in picture 5.5 are the the three configuration, the first uses the first roll-bars of the list and steel roll-bars arms; the second uses the second roll-bars and the aluminum rollbars; the last uses the soft roll-bar and soft roll-bars arms. The middle stiffness configuration is enough for the most of the stiffness range needed, anyway other roll-bars can increase the stiffness range. Usually front roll-bars are set up with the medium configuration and rear with the soft, it changes only the roll-bar.

The total stiffness range with soft springs and soft roll-bars to hard-springs and roll-bars is: 9000$\div$ 31000 Nm/rad, with reference to 5.7 and 5.6

While with a degree/g measurement unit is: 3$\div$0.85, where in eq. 5.9 is the conversion equation:

$$K_{\phi(g)} = K_\phi m_s (h_g - d) g \tag{5.9}$$

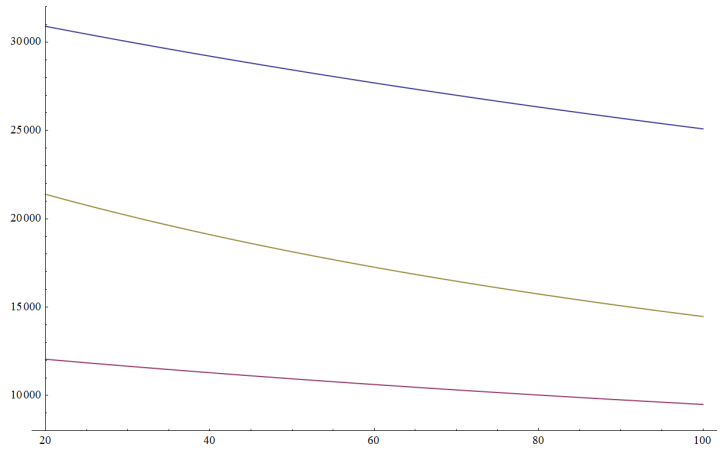

Figure 5.5: Rollbars stiffness, purple is soft configuration, yellow medium, blue stiff.

5.3 Dumpers setup

After a first step solution for dumper coefficients (Chapter 5.1) a more precise design has be done.

To choose a proper dumping coefficient it is necessary to know the force and wheel-center displacement overshoot.

These first pictures 5.6 show vertical force during braking and acceleration as function of dumping coefficient.

In this other pictures 5.7 are shown wheel center displacement overshoots for the front and rear axle caused by acceleration and braking as function of dumping coefficients.

The model evaluates two dumping values that harmonize dynamic force and wheel center displacement. The model suggest c1=1.74 Ns/m and 1.66 Ns/m corresponding to $\zeta_1 = 0.66$ and $\zeta_2 = 0.52$. These value are the best compromise between dynamic loads and wheel center displacements for the chosen tasks.

This value are available although dumpers have no-constant force vs speed response, see *Appendix B*.

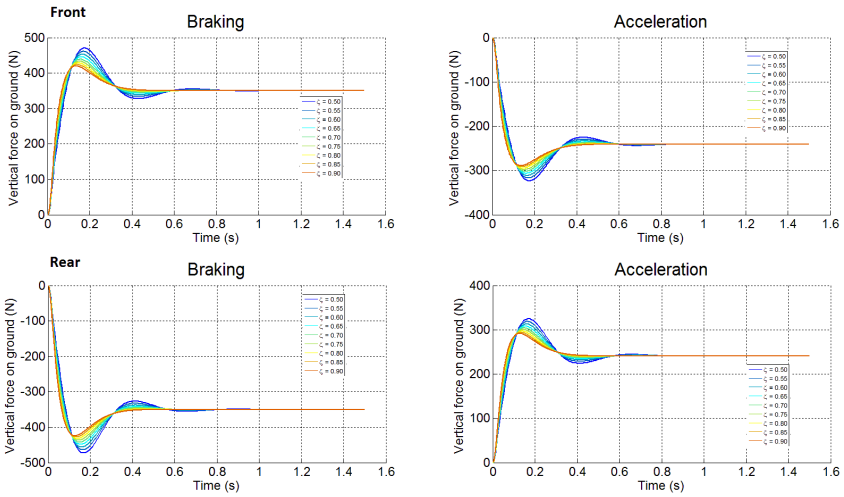

Figure 5.6: Vertical force due to braking and acceleration as function of dumping coefficient.

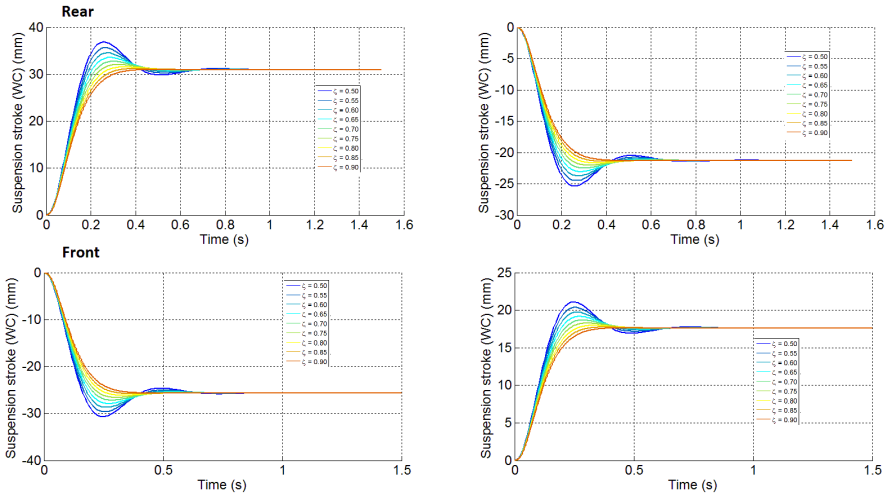

Figure 5.7: Suspension travel for acceleration (right) and braking (left) as function of dumping coefficient.

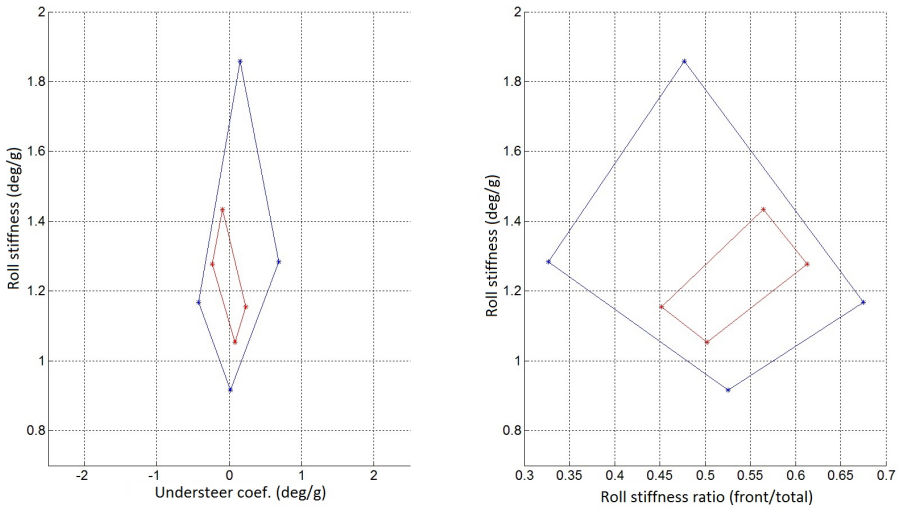

Figure 5.8: Understeering coefficient as function of roll stiffness (left), total roll stiffness as function of roll stiffness ratio (front/total) at a lateral acceleration of 1.6 g.In blue present solution in red GreenTeam one's.

5.4 Understeering oversteering: $\mathbf{K}_\gamma$

This last part shows resulting under-steer value as function of roll-bar set-up, when it is necessary a comparison between present solution and GreenTeam solution.

Starting with design values calculated to have 0.2 deg/g under-steer the program shows, changing in a range of $\pm 50\%$ these stiffness possible $K_{\phi(g)}$ and K_γ.

Blue curves in figure 5.8 are the present solution and red curves are from GreenTeam solution evaluated at a lateral acceleration of 1.6 g. Set-ups are wider with the same stiffness range, this means the car is more configurable and behavior range is wider than the GreenTeam solution.

These pictures 5.9 and 5.10 are respectively $K_{\phi(g)}$and consequent K_γ for 120 km/h, 1.95 g lateral acceleration and 50 km/h 1.5 g lateral acceleration. Set-up range influence on $K_\gamma$are limited, because it is at maximum lateral acceleration of the car, however it is possible to configure the car to have under-steer behavior at this lateral acceleration and to any other. In this way it is possible to have an understeering car in all the handling curve, or set roll-bars to have a wanted behavior.

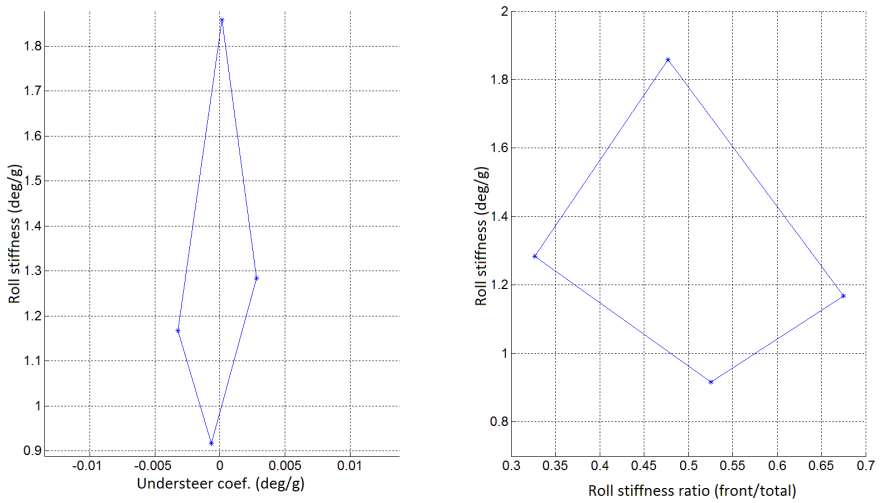

Figure 5.9: Understeering coefficient as function of roll stiffness (left), total roll stiffness as function of roll stiffness ratio (front/total) at a lateral acceleration of 1.95 g. In blue present solution.

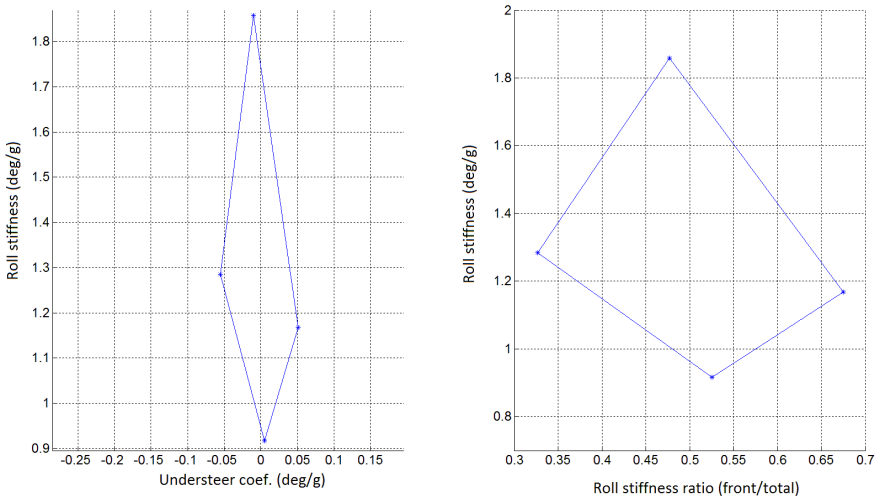

Figure 5.10: Understeering coefficient as function of roll stiffness (left), total roll stiffness as function of roll stiffness ratio (front/total) at a lateral acceleration of 1.5 g. In blue present solution.

Chapter 6

Four wheels steering approach

6.1 Model

This Chapter will present the model created and used to consider the introduction of a four wheels steering system in this type of race cars. The model is in *Appendix* A.

I will start describing the model part by part, then I will present the tests made, in conclusion of this Chapter I will show the results comparing the two and four wheel steering car.

6.1.1 Model explanation

The model is made with Mathematica ® and is composed of two main parts.

1. The first part is about the pneumatics curves plotting and characteristic.
2. The other part contains:

- the constitutive equations of the pneumatics obtained with the Pajecka *Magic Formula,* for reference see [14], the curve shape, the peek values and others are made to be similar to the tire data used in the Adams model.
- the congruences equations of the problem, like the car geometry: roll centers, tracks, wheelbases, center of mass eight, the definition of slip angles, wheels slip ratio. The model evaluate combined pneumatics load.(σ_x, σ_y)

- the dynamics equations of the car; the model has six degrees of freedom: yaw speed, lateral speed and the revolution speed of the four wheels, (not of the rims that is easily computable) as defined in the classic car reference system, with the origin placed under the barycenter at ground level, the forward speed as well as the steering angle are inputs. The model is a modified single track model, in a way that the wheels of the same axle have the same sleep angle as well as the steering angles, but the longitudinal sleep is different as well as the speed revolution of the inner and outer wheel while cornering. The model considers the vertical load variations due to a curve and can show the single wheel contribution on the lateral force or longitudinal force. For the previous reasons in addition to the three standards equations of motion there are three more equations: two for the two differentials (front axle and rear axle) and the last on for the central differential that distribute the traction between the two axles. The model consider aerodynamic too, but in approximate way: the drag is insert in the equations of motion and the vertical force contribution is considered modifying the shape of the axle characteristics.

What the models does not do:

- The model does not take in account the car pitching, therefore the vertical load transfer due to longitudinal accelerations.
- The toe angle variation due to the suspension motion, the camber angle the roll centers variation during suspension motions are not considered.

Those two main points are important for a complete dynamic analysis, but that is not the task of this model. In other words, what the model can not do is not important in a first approximation, and for further development can be implemented easily.

6.1.2 Model main parts

With reference to *Appendix A*, the first part called "*suspension*" is made by three cells and contains car's and suspension characteristic: tracks, wheelbase roll center heights and others, furthermore we aerodynamics load evaluation, then "*Magic Formula*" to model pneumatics and axle force response, in the last cell we have wheel's slip definition, lateral and longitudinal slip as well as combined slip and forces obtained from slips: longitudinal and lateral.

The second part called "*equations*" is made by four cells, first steering wheels angles as function of the time, then wheel slip angles definition, then the six equation to be solved, three Newton equation of motion, using ref. system shown in figure 2.1: forward acceleration, lateral acceleration, and yaw acceleration as function of forces and inertia, fourth and fifth are open differential equation for the front and rear axles, then last equation subdivide the traction from the front an rear axle as function of the present vertical load, it is something like the third differential in other types of cars, but this car is electric one, so the traction is electronically subdivided.

The third cell solve the system as function of the four ω_c(rim revolution speed, directly connect to longitudinal slips), lateral velocity and Yaw speed. The fourth cell take results from the solver.

Then we have the part called "*Traction force*" made by three main cells, the first cell redefine all the pneumatic forces using results obtained: this part is necessary if we want to make several simulation without the need to reset Mathematica's kernel, because if we substitute solution obtained with force definition used in the first part the model can not work again without a reset. The second cell plots some results, then the third cell makes last definition, like slip angles Ackerman angle, lateral acceleration, turning radius, yaw angle and distance traveled during a curve as function of the solutions.

Under we have the part called corrector, that is only one cell, this cell using actual solution and evaluate a function to obtain $\beta = 0$ as discussed in the first part of this Chapter. In conclusion we have last part made by one cell that evaluate last plot, in particular we have "axle exploitation".

Pneumatics

In pictures are shown pneumatics and axles lateral forces as function of theoretical slips σ_1 and σ_2 evaluated with the Magic formula. At a forward velocity of 50 km/h vertical forces are scarce. Last picture, (figure 6.1 (c)) shows axles response as function of both slip ratios.

6.1.3 Additional features

The model solve the equations of motions and in addition plot all the most important results, as it will be shown later.

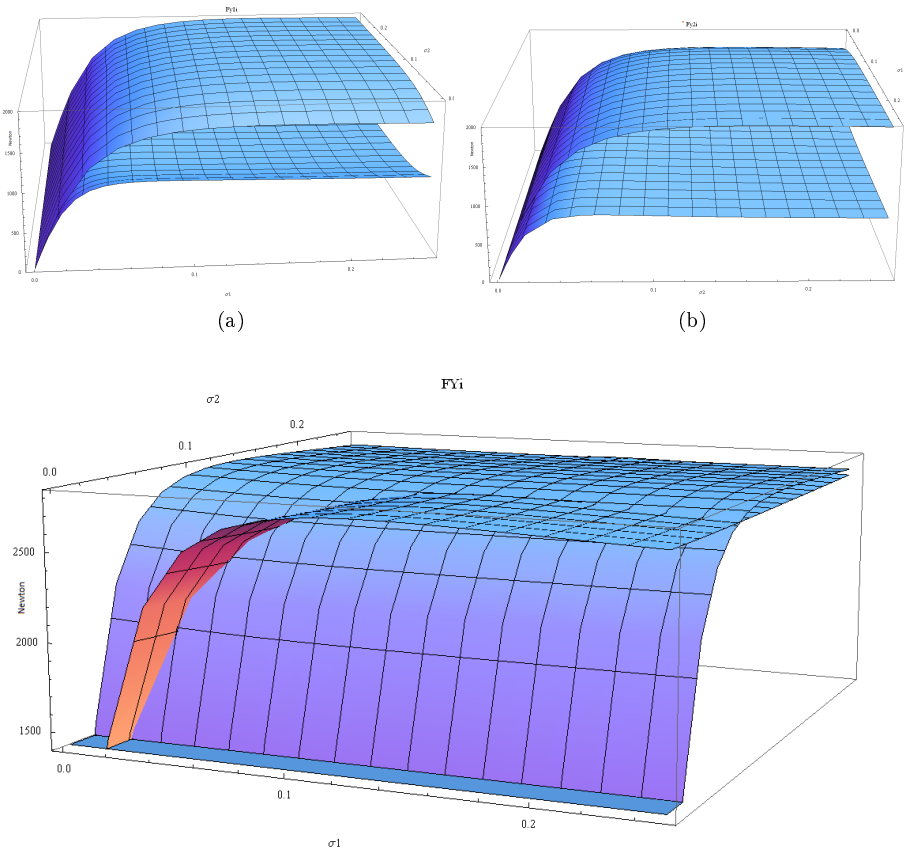

(a) (b)

(c)

Figure 6.1: Pneumatics lateral force as function of both the slip $\sigma_1 and\, \sigma_2$, front pneumatics (a), rear pneumatics (b), axles lateral forces (c).

For what concerns the four wheels steering system the task of the model is to evaluate a function that describe the evolution of the rear steering to obtain a desired vehicle slip angle. After several bibliography consultation and several reasoning in a first instance I suppose that a null vehicle slip angle, could improve the car performances. The task of this model is to verify those supposition, because this problem can not be solved without the support of a simulation model.

6.2 Tests

6.2.1 Test carried on

Tests attempted are step steer angle of three different velocity: 50km/h, 80km/h, 120km/h.

For these simulations important feature like later acceleration slip angle and others will be discussed and displayed. Then a four wheels steering system will be introduced, in a way that the car has the same velocity and it has the same steady state turning radius, then the same lateral acceleration. The other exception is, considering a real applications of this system, the electronic control unit of the rear steer can not instantly responds to a given steering wheel input, but it takes some time, in the vicinity of 0.1 seconds or more. The function depends to the forward velocity, the steering wheel velocity and angular displacement, if the the other car parameters are fixed, so a control unit to work fine should be a "look at table, memory based" control unit, because it has not enough time to solve simultaneously the equations of motion and to impose the correct rear wheels steering. This means that the memory has to be mapped by points and between those point there will be some sort of interpolations. For those two main reasons the "correction function" should be approximate and delayed.

6.2.2 Two-four steered wheels simulations

Below are the parameters used for three test for which I simulated step steering at three different velocity: $50km/h, 80km/h, 120km/h$. The amount of steer is different for each case, but the steer velocity is always in the range of $200 \div 400deg/s$ at the steering wheel, naturally less to the wheels.

Results steer step 50 km/h

This are the steer angles imposed to the wheels, and it is a function like:

$\delta_1[t] = A \cdot (1 - e^{-\frac{t}{\tau}})$ where A and τ are regulated to have wanted lateral acceleration and steer step velocity $\dot{\delta_1}[t]$ while $\delta_2$is an interpolation function calculated to have $\beta = 0$ as discussed before. In picture 6.2 steering angles as function of time for both, two wheels and four wheels car model.

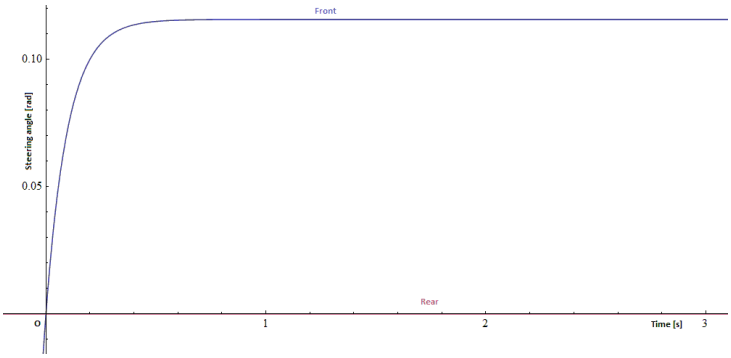

(a)

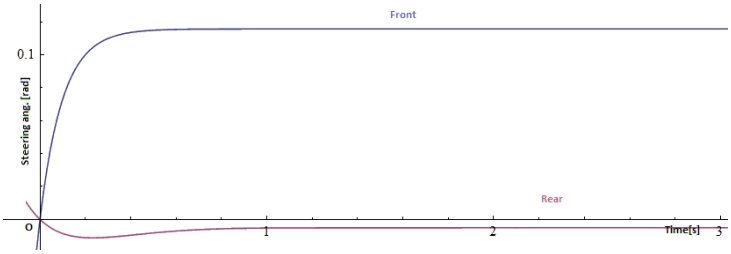

(b)

Figure 6.2: Wheel center steering angles: two wheel steered car (a), four wheel steered car (b), for the 50 km/h steer step simulation.

In picture 6.3 wheels slip angles for both the simulations, it is possible to see that for the four wheels steered car, slip peaks are higher.

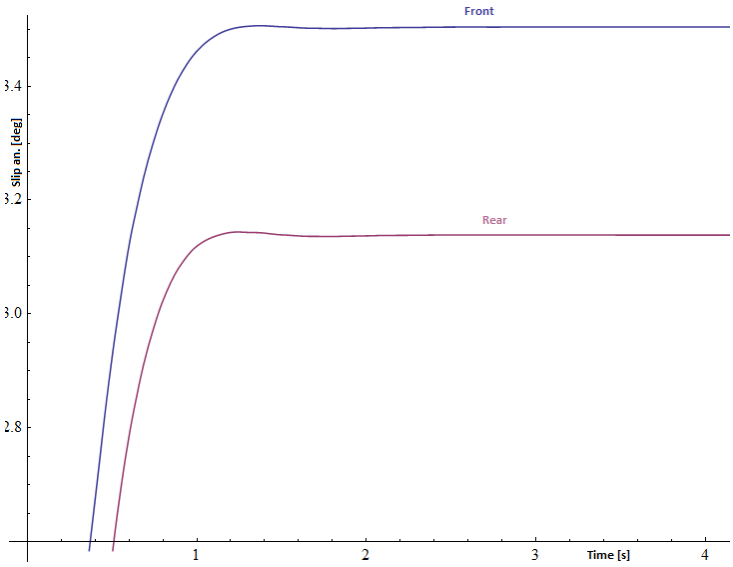

(a)

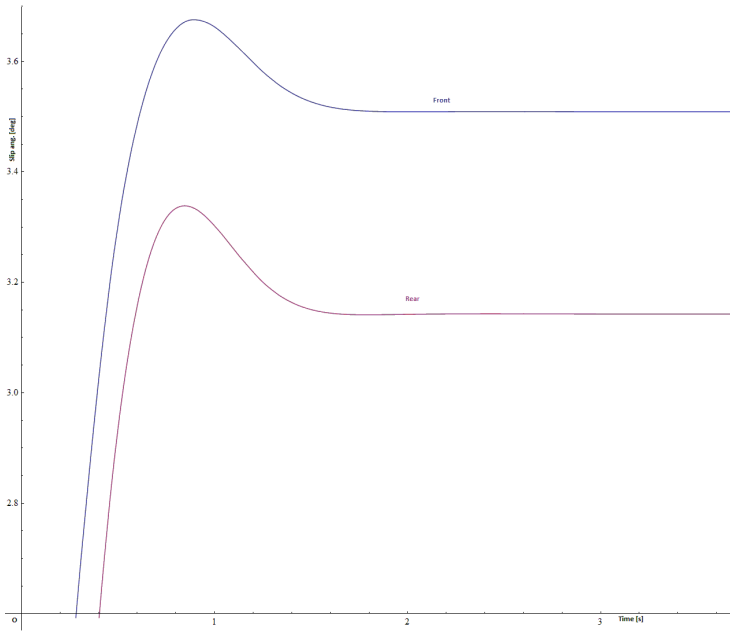

(b)

Figure 6.3: Slip angles for the two wheels steered car (a) and four wheels steered car (b), for the 50 km/h steer step simulation.

Pictures 6.4 shows vehicle slip angle for the two and the four wheels steered car model. As wanted figure (b) shows that the corrector works properly in a way that the slip angle is null.

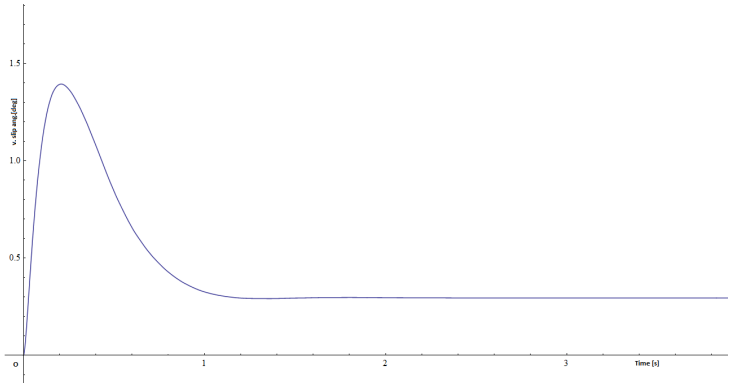

(a)

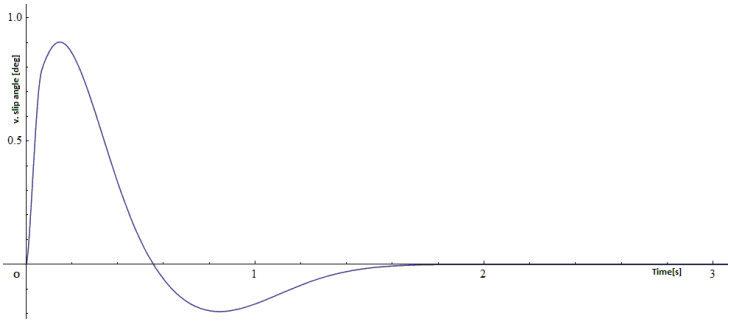

(b)

Figure 6.4: Vehicle slip angle, two wheels steered car (a), four wheels steered car (b), for the 50 km/h steer step simulation.

These pictures 6.5 prove that stady-state lateral acceleration is the same for the two model.

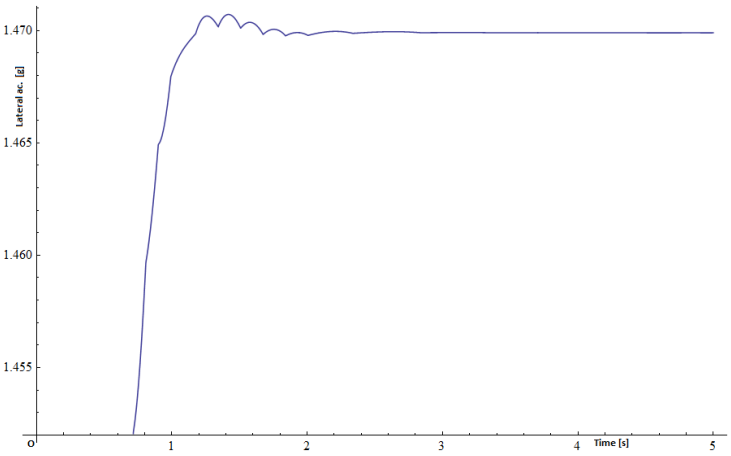

(a)

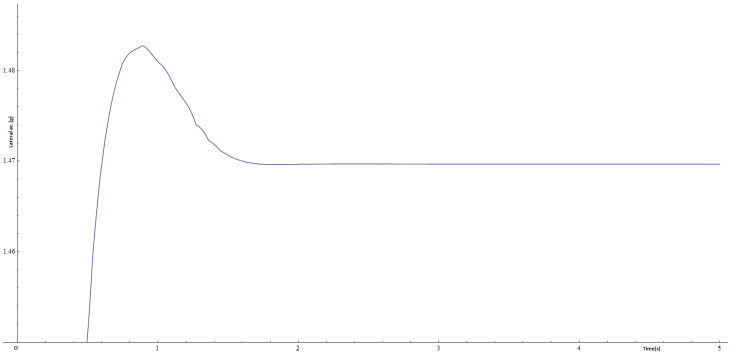

(b)

Figure 6.5: Lateral acceleration, two wheels steered car (a), four wheels steered car (b), for the 50 km/h steer step simulation.

Following pictures 6.6 (a) and (b) show yaw speed for both the vehicle, two wheels steered and four wheels steered. It is possible to see the different trend of the two curves, curves (b) has a greater peek in the not steady part of the simulation then reach same steady state value. This difference in the trend can grant benefits in vehicle yaw angle in a way that it can reach the same Yaw angle in less time.

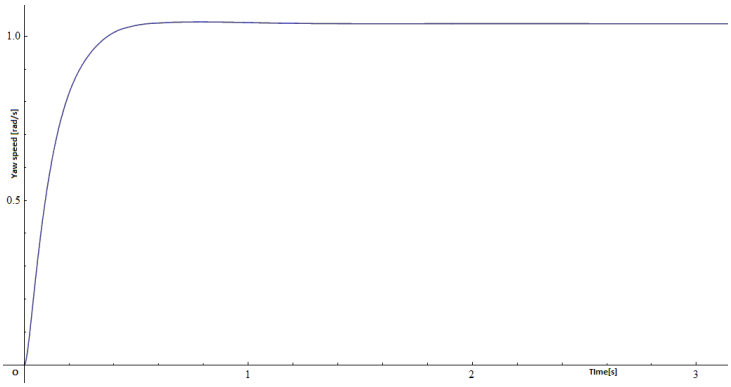

(a)

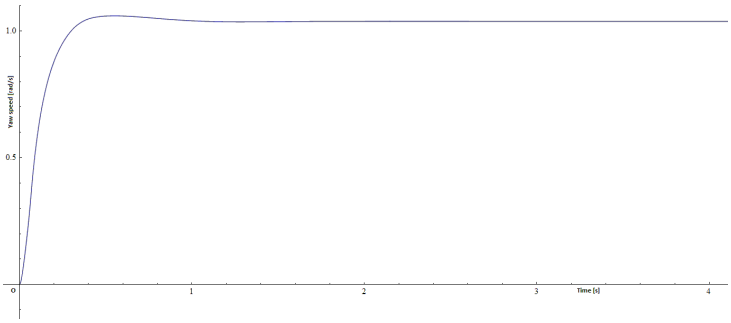

(b)

Figure 6.6: Yaw speed, two wheels steered car (a), four wheels steered car (b), for the 50 km/h steer step simulation.

Picture 6.7 (a) and (b) are the most important, they shows total axles exploitations for both the two vehicle, trends are different we have greater value for four wheels vehicle in the not-steady phase, then the difference between the two exploitation is less then the normal vehicle, to much less but the trend is to have the limit condition to maximum exploitation reached for both the axles.

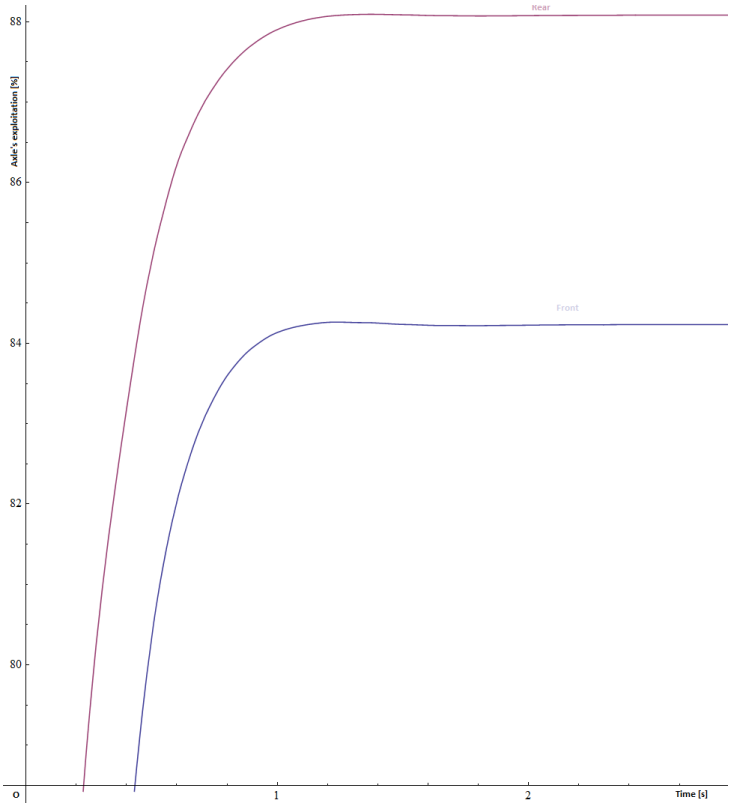

(a)

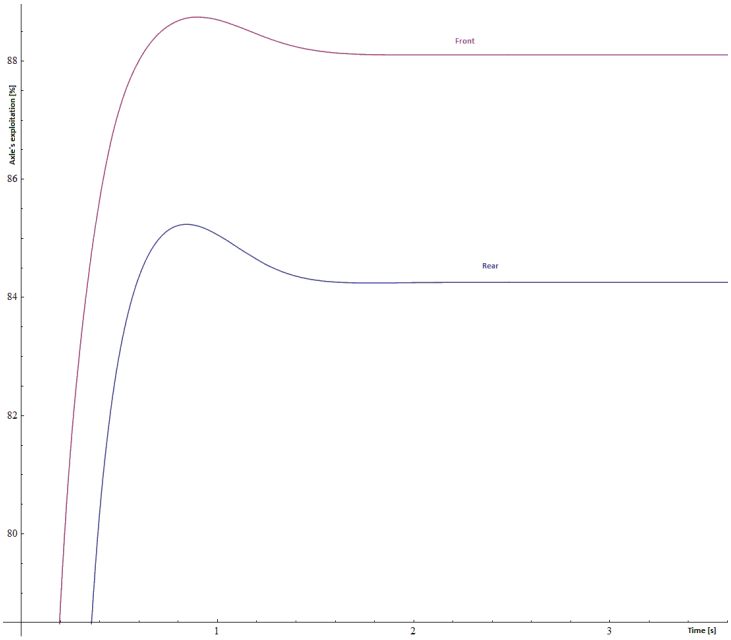

(b)

Figure 6.7: Axle's exploitation, two wheels steered car (a), four wheels steered car (b), for the 50 km/h steer step simulation.

Results steer step 80 km/h

These below are most important curve for 80 km/h steer step simulation, see 6.2.2 for reference. Picture 6.8 show how after a first phase of counter-phase steering (front wheels and rear wheels steered in different directions), we have a in-phase steering because velocity it is increased.

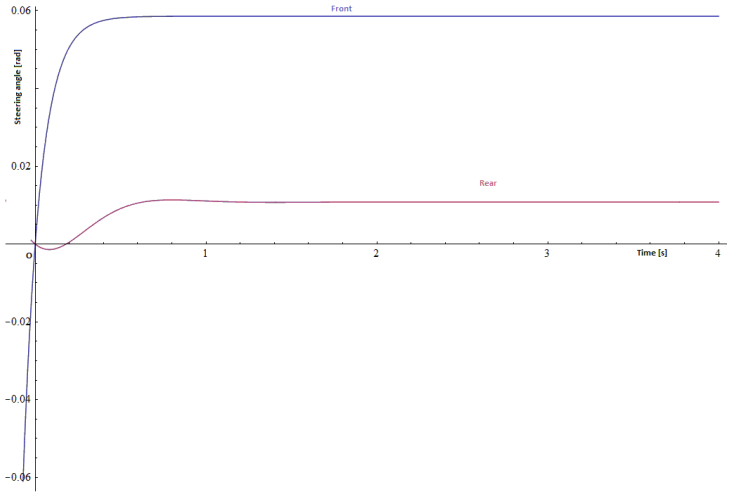

Figure 6.8: Wheel center steering angles: two wheel steered car (a), four wheel steered car (b), for the 80 km/h steer step simulation.

These pictures 6.9 (a) and (b) show vehicle slip response with and without four-wheels steering system. Slip angle for the four wheels steered car is tending to a very low value as wanted.

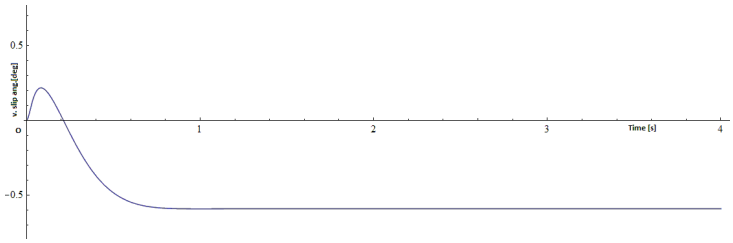

(a)

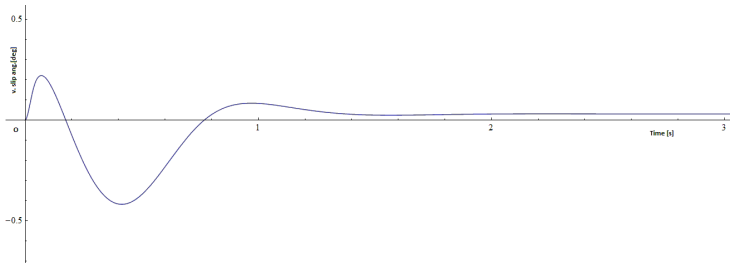

(b)

Figure 6.9: Vehicle slip angle, two wheels steered car (a), four wheels steered car (b), for the 80 km/h steer step simulation.

Results steer step 120 km/h

This last four are same curve as before but for 120 km/h steer step simulation, see 6.2.2 for reference. In this case solution is more oscillatory, because the car is reaching its maximum performances.

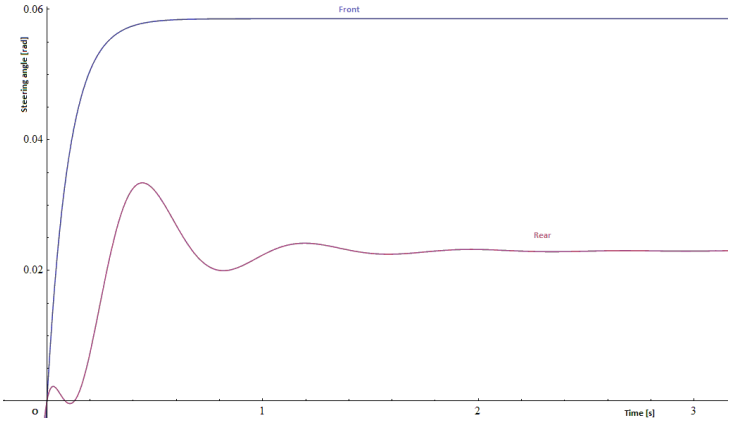

Figure 6.10: Wheel center steering angles: two wheel steered car (a), four wheel steered car (b), for the 120 km/h steer step simulation.

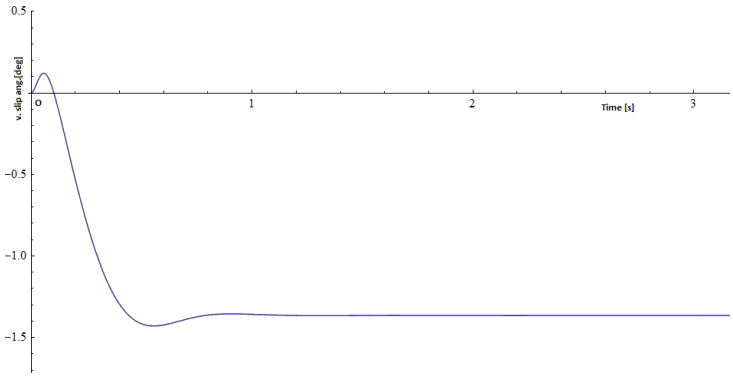

(a)

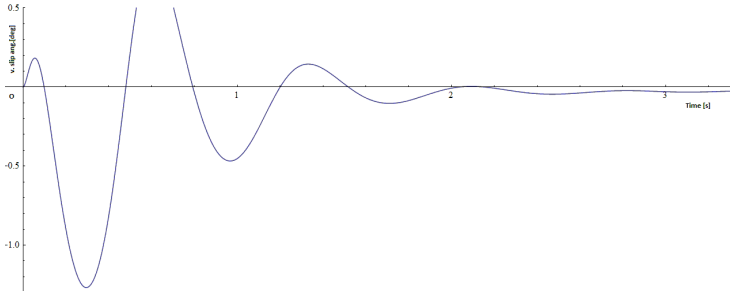

(b)

Figure 6.11: Vehicle slip angle, two wheels steered car (a), four wheels steered car (b), for the 120 km/h steer step simulation.

6.3 Result confrontation and lap time improvements

In this section I will compare results and benefits obtained so far, in terms of times improvements were the car running in the most common circuit of Formula Student's competition: Formula Student Germany circuit of the season 2011, obtained with a data logger during a real competition. The circuit changes each year but it is a good reference, because it does not change through and through every year.

Comparing results obtained at 50 km/h we can see that main improvements are in terms of distance travelled at same velocity and steady state turning radius, then we have higher lateral speed peak and yaw speed peak at last we have a better axle exploitation.

Similar results are obtained for different velocity with different improvements, greater at higher speed. Below a summary chart:

Forward velocity (km/h)	50	80	120
time for 45° (s)	0.89	1.39	1.61
time for 90° (s)	1.63	2.65	3.13
time for 120° (s)	2.15	3.49	4.20
time for 180° (s)	3.16	5.21	/
turn radius (m)	13.3	36	64.5
steady state a_y	1.47	1.4	1.75

Table 6.1: Time need for different turn angles at three different velocity and lateral acceleration. (two wheels steered car).

Forward velocity (km/h)	50	80	120
time for 45° (s)	0.86	1.34	1.59
time for 90° (s)	1.61	2.61	3.12
time for 120° (s)	2.12	3.46	4.14
time for 180° (s)	3.13	5.17	/
turn radius (m)	13.3	36	64.5
steady state a_y	1.47	1.4	1.75

Table 6.2: Time need for different turn angles at three different velocity and lateral acceleration. (four wheels steered car).

Forward velocity (km/h)	50	80	120
Δtime for 45° (s)	30	50	20
Δtime for 90° (s)	20	40	10
Δtime for 120° (s)	30	30	60
Δtime for 180° (s)	30	40	/
averageΔtime (ms)	27	40	30
steady state a_y	1.47	1.4	1.75

Table 6.3: Time benefits between two and four steered car, for different turn angles at three different velocity and lateral acceleration.

Benefits for each curve are small, nonetheless results are precise till the the third decimal number because of the numerical solver precision.

Considering that in a complete race circuit, like the one exposed before has sixteen or more curves, and the benefits is constant considering a single velocity: is gained in the not steady state phase we can do this first step valuation.

Dividing these curve with a distribution of *40%* with a max velocity of 50 km/h, *40%* in a range from 50 to 80 km/h, *20%* in a range from 80 120 km/h we have:

$16 \cdot 0.4 \cdot 27 + 16 \cdot 0.4 \cdot 40 + 16 \cdot 0.2 \cdot 30 = 525ms = 0.525s$

These results have to be viewed against an average lap time that runs at 55-60 seconds, therefore this system could increase performance of 1%. This result is considerable, but real tests must be done to prove these result.

Chapter 7

Mechanical design

7.1 Loads calculation

With reference to [12]a small Matlab ® program is been created to calculate loads in tires contact paths.

In chart 7.1 loads direction are computed with the Eteam reference system, see Chapter 1.1; vehicle weight 2010 N, driver 690 N.

All tasks are evaluated at a $120km/h$ speed velocity, so aerodynamic is in place. Evidently curve and combined tasks are evaluated at maximum performances as well as braking. Some tasks are omitted because not critical for load concern: for example brake for the rear axle as well as acceleration for the front ones.

Turns are always on the right, so left front and rear tire path loads will be displayed.

Now that loads are known each part will be design and mechanical verifications

Tasks and task number	Axle	X direction	Y direction	Z direction
1. Static load	Front	0	0	951
2. //	Rear	0	0	989
3. Brake	Front	-2491	0	1484
4. Acceleration	Rear	2292	0	1364
5. Curve	Front	0	-2106	1526
6. //	Rear	0	-2158	1564
7. Curve+acc.	Rear	1804	-1804	1692
8. Curve+brake	Front	-1848	-1848	1733

Table 7.1: Wheel-path loads, only important configurations.

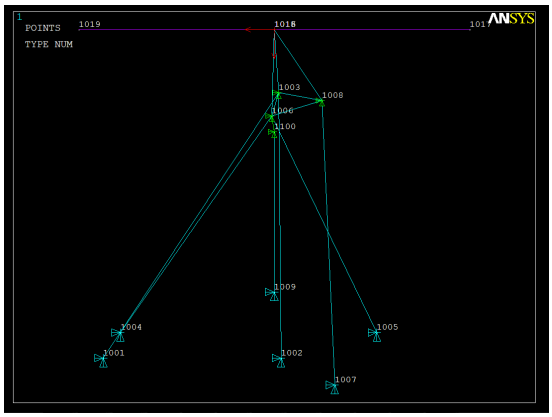

Figure 7.1: Ansys classic front suspension links geometry.

will be accomplished.

Structural verification consists in: maximum stress equal or less to material ultimate stress, fatigue and safety coefficient evaluation.

7.2 Beam parts

Now that loads in contact paths are known, carbon fiber links will be processed as beam parts, glued links between links and aluminum alloy inserts will be discuss in the next Paragraph.

Given that geometry and load configuration is in three dimension, no simplification possible, a Ansys ® classical model must be used.

Input of this model are load in load paths computed before, carbon fiber links will be sketch as beam parts, deformable, uprights and wheel will be considered as rigid (no deformation) parts, inserts are not considered in this preliminary part, they will be analyzed later.

Wheel center travel from static configuration it is acquired from the Adams model.

Below a graphical view of the model (figure 7.1)

The wheel is connected to the upright with no degree of freedom, the wheel center height changes, and the amount is taken from the Adams model for each

task, Chapter 4. Each triangle is made by two arms, they are connected to the up rights with a no displacement joint, situated where the joint really is, as well as to the ground that represent the car frame, (spherical joints). Push rod, and toe link are constrained with two no displacement joints, all links are beam element, so normal load, shear the two bending moment and twisting moment can be evaluated, however due to the joints configuration only normal load are significant.

Each of the eight cases listed before (chart 7.1) , will be evaluated. To understand results each part is called "element" followed by a number with reference to the legend below.

- Element 1: Lower triangle, rear link.
- Element 2:Lower triangle, front link.
- Element 3:Bottom triangle, rear link.
- Element 4:Bottom triangle, front link.
- Element 5:Toe link.
- Element 6: Pushrod link. (connection between upper triangle and rocker).

Now that elements are well defined each task will be simulated and loads will be summary with charts.

Beam loads: front axle static load, task one

With reference to chart 7.1, first task in place is number one, results are in local beam reference system with center in the outboard part of the element, "X" axis along link axis directed inboard, "Z" axis upward perpendicular to "X" axis and "Y" axis as result of right hand rules. :

Element	Nxi (N)	Tyi (N)	Tzi(N)
1	31	0.08	0
2	541	0.09	0
3	176	0.8	0
4	266	-0.9	0
5	-70	0	0
6	-1153	0	0
Max compressed element:6	-1153	0	0
Max tractioned element: 2	541	0.09	0

Table 7.2: Element loads under task one with reference to chart 7.1.

In red most stressed elements, before continuing with stress and safety factor calculation all the tasks have to be evaluated to consider only most critical parts.

Beam loads: rear axle static load, task two

From now only most stressed part will be displayed, for local beam reference system and loads see task one.

Element	Nxi(N)	Tyi(N)	Tzi(N)
Max compressed element: 6	-1671	-0.13	0
Max tractioned element: 4	1239	4.15	8.82

Table 7.3: Element loads under task two with reference to chart 7.1.

Beam loads: front axle braking, task three

Element results for task three, for local beam reference system and loads see task one.

Element	Nxi(N)	Tyi(N)	Tzi(N)
Max compressed element: 1	-7729	-1.35	-0.14
Max tractioned element: 2	4800	1.62	0.01

Table 7.4: Element loads under task two with reference to chart 7.1.

Beam loads: rear axle acceleration, task four

Element results for task four, for local beam reference system and loads see task one.

Element	Nxi(N)	Tyi(N)	Tzi(N)
Max compressed element: 1	-5896	-0.73	-0.07
Max tractioned element: 2	5731	0.7	0.03

Table 7.5: Element loads under task four with reference to chart 7.1.

Beam loads: front axle curve, task five

Element results for task five, for local beam reference system and loads see task one.

Element	Nxi(N)	Tyi(N)	Tzi(N)
Max compressed element: 2	-2993	-0.46	-0.01
Max tractioned element: 4	1326	0.42	0.01

Table 7.6: Element loads under task five with reference to chart 7.1.

Beam loads: rear axle curve, task six

Element results for task six, for local beam reference system and loads see task one.

Element	Nxi(N)	Tyi(N)	Tzi(N)
Max compressed element: 2	-2643	-0.11	-0.01
Max tractioned element: 4	2546	0.12	0.07

Table 7.7: Element loads under task six with reference to chart 7.1.

Beam loads: rear axle curve plus acceleration, task seven

Element results for task seven, for local beam reference system and loads see task one.

Element	Nxi(N)	Tyi(N)	Tzi(N)
Max compressed element: 3	-4815	-1	-0.1
Max tractioned element: 1	7116	1.14	0

Table 7.8: Element loads under task seven with reference to 7.1.

Beam loads: front axle curve plus braking, task eight

Element results for task eight, for local beam reference system and loads see task one.

Element	Nxi(N)	Tyi(N)	Tzi(N)
Max compressed element: 1	-5740	-1	-0.1
Max tractioned element: 3	2379	1.22	0.9

Table 7.9: Element loads under task eight with reference to 7.1.

7.2.1 Stress safety factor and buckling for beam parts

Suspension links are made by carbon fiber pipes, to the edges are glued Ergal inserts.

Below carbon fiber pipes characteristics:

$E_c = 100$ GPa, Young module;

$\sigma_{uc} = 1$ GPa, ultimate tensile strength;

$d = 16$ mm, outer pipe diameter;

$d_i = 11$mm, pipe's internal diameter;

$A_r = \frac{\pi}{4} \cdot (d^2 - d_i^2) = 106$ mm^2;

$I = \frac{\pi}{64} \cdot (d^4 - d_i^4) = 2498$ mm^4;

For more information about carbon fiber pipes see [4, 7, 9].

Now a little summary of symbols and formulae:

L_{ij} :axial load of the element "i", under task "j", see 7.1. .

$\sigma_{xx}max = \frac{L_{ij}max}{A_r}$: where "L$_{ij}max$ is maximal traction or compression load in module, and "xx" stays for axial load, I used "xx"instead "z" or "zz" to have congruence with previous formulae. So *"xx"* is the local normal direction as defined in Chapter 7.1 .

$P_i = \frac{\pi^2 \cdot E \cdot I}{l_i^2}$, where $P_i$is the critical eulerian loads for elastic instability of the element "i", "l_i" is the length of element "i" and "I" is the polar surface moment of the pipe along its axis.

For each element must be $P_i > L_{ij}$, for instability and of course only on compression loads, then will be evaluated:

$\eta_{inst} = \frac{P_i min}{L_{ij} min}$ while $\eta = \frac{\sigma_{xx} max}{\sigma_u}$ that are safety factor the one for instability the other regarding stress.

Normal verifications are made with an equivalent static configuration, that can be true if the car is under is static load, but during dynamics events the following formula can be used:

$F_d = F_s \cdot (1 + \sqrt{}(1 + \frac{2 \cdot h}{\delta_s})$ or equivalent:

$$F_d = F_s \cdot (1 + \sqrt{}(1 + \frac{v^2}{g \cdot \delta_s}) \tag{7.1}$$

where F_d is the dynamic equivalent load F_s is the static load, h is the height from where the mass $m = \frac{F_s}{g}$ is falling or equivalently, "v" is the velocity of the load application, $h = 0$ means null velocity but still not static it could be called "leaned load", with a Fd=$2Fs$.

Consulting Paragraph 7.2 to acquire critical load we obtain:

$L_{ij} max = L_{13} = 7728$ N, in module.

For instability concern, we have to compare all $P_i$with $L_{ij}$and select the most critical.7.1.

Here a chart with $P_i$for all the six elements, then maximal compression load for that element then η_{inst}. Elements position are explained in Paragraph 7.2 .

In red the most critical situation with a $\eta_{inst} = 2.3$ verified and with a not static load amplification of two, see eq

Element one is the most loaded for stress concern too in this case we have:

$\sigma_{xx} max = \frac{7728}{106} = 73$ MPa while $\eta = \frac{1000}{73} = 13.7$ verified, pipes are not critical, bonding are next in order.

7.3 Inserts bonding verification

In this section bonding between inserts and carbon fiber links will be verified, the most complicated triangle inserts will be verified later.

Element front axle	$P_i[N]$	$L_{ij}min$[N]	η_{inst}
1	$1.78{\cdot}10^4$	-7728	2.3
2	$2.53{\cdot}10^4$	-2293	11
3	$2.34{\cdot}10^4$	/	/
4	$2.83{\cdot}10^4$	-1700	16.6
5	$2.18{\cdot}10^4$	/	/
6	$4.6{\cdot}10^4$	-1706	27
Element rear axle	P_i[N]	$L_{ij}min$[N]	η_{inst}
1	$2.53{\cdot}10^4$	/	/
2	$1.95{\cdot}10^4$	-5896	3.3
3	$3.14{\cdot}10^4$	-4815	6.5
4	$4.41{\cdot}10^4$	/	/
5	$1.81{\cdot}10^4$	-38	476
6	$71.2{\cdot}10^4$	-2643	27

Table 7.10: Stability check for link pipe elements.

Carbon-fiber aluminum bonding

Dismissing details, available in see [4], for bonding matter is important:

1. Choose a geometry to reduce skinning forces (tangential stress).
2. Use the max available area to reduce middle stress value.

Bibliography suggests to prefer gloving to work with shear stress over traction. Another important matter is width and gloving length. Experience shows that increasing joint substrate width (in this case substrates are the material that are going to be glowed) increase linearly ultimate strength, but increasing length is not linearly connect to ultimate stress it is less then linearly and over a certain ration between length and width there is no more benefit in ultimate strength of the joint.

Thanks to the know-how acquired from Eteam and after biographical consulting I decided for a 30 mm joint length with a thickness of 2.5 mm substrate of carbon fiber and 2 mm for aluminum.

It is important to choose a roughness included between Ra=$1.5 \div 3$ μm, this is to guarantee correct surface wetting, and the use of a primer in place to remove impurity end to optimize surface wetting.

The bonding thickness is 0.5 mm, it is important to consider that over a certain thickness there are no more benefits in the joint quality.

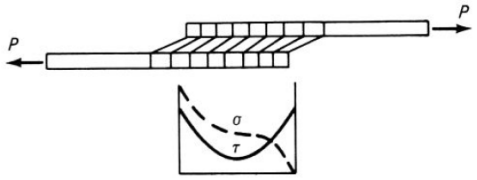

Figure 7.2: Volkersen, stress distribution.

Now I will summary two of the formulae used to compute shear stress in glowed joints.

Shear stress evaluation

The most simple evaluation of the shear stress is given by:

$$\bar{\tau} = \frac{P}{A} = \frac{P}{b \cdot L} \tag{7.2}$$

Where P is the shear load, A the area subjected to stress equal to length "L" multiplied "b" in this case the perimeter of a pipe.

This formula consider the both glowed material infinitely stiff, that is an approximation, more precise models are available, like Volkersen (1938).

$$\frac{\tau}{\bar{\tau}} = \frac{\omega}{2}\frac{Cosh(\omega\frac{x}{2})}{Sinh(\frac{\omega}{2})} + \frac{(t_1 - t_2)}{(t_1 + t_2)}\frac{\omega}{2}\frac{Sinh(\omega\frac{x}{2})}{Cosh(\frac{\omega}{2})} \tag{7.3}$$

this is the solution when same material are going to be glued.

Where $\omega^2 = \frac{G}{\eta}(\frac{t_1+t_2}{Et_1t_2})L^2$, G is shear module of the joint, $t_1$and t_2 are the two joint thickness, η is the resin thickness and L is the joint length.

In figure 7.2 a typical trend of Volkersen stress distribution:

Verifications are thus evaluated: first a $\bar{\tau}$ for the most critical glowed part will be calculate then, with the previous formula 7.3 the tangential peak stress can be calculated finally compared with available epoxy resin characteristic.

These two pictures show the two main part to be glued, the one is the insert used

For the first case, picture 7.3(a) we have, with reference to eq. 7.2:

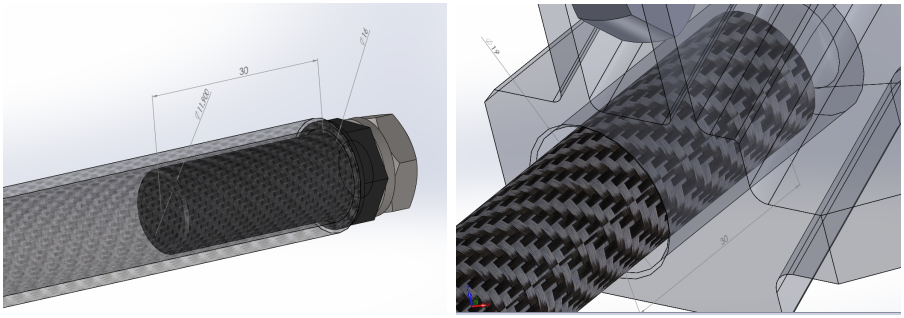

(a) (b)

Figure 7.3: Main parts joined with resins. (a) pipe carbon fiber link, b aluminum triangle insert.

$P = -7728$ N; $L = 30$ mm, and $b = \pi \cdot d = 50.25$mm;

$\bar{\tau}_{max} = 5.12$ MPa;

While $\frac{\tau_{max}}{\bar{\tau}_{max}}$ =2.16, then $\tau_{max} = 11.07$ MPa.

Before proceeding some data:

I chose Loctite R, Hysol R with a $\sigma_{ur} = 46$MPa, and a $\tau_{ur} = 23$MPa;

then we have a safety factor of $\eta = \frac{23}{11.07} = 2.07$, verified also with a intensification factor of 2 due to dynamics load or fatigue.

For what concerns triangle inserts (figure 7.3 (b)), we have at least a $t1 = 4mm$;

then $\frac{\tau_{max}}{\bar{\tau}_{max}} = 1.27$ MPa $\tau_{max} = 7.81$MPa then a $\eta = \frac{23}{7.81}$=2.95.

7.4 Three dimensional parts

In this Paragraph, parts too complicated to be correctly verified without a FEM analysis. In this case Ansys ® is used.

Inserts are made by Ergal alloy, Al 7075, with impressive mechanical specifications, as shown below:

$E_e = 77$ GPa, Young module;

$\sigma_u = 572$ GPa, ultimate stress;

7.4.1 Triangle inserts verification

Below Ansys Workbench ® verification for suspension triangle inserts, will be displayed only critical load configuration and as before, safety coefficient will

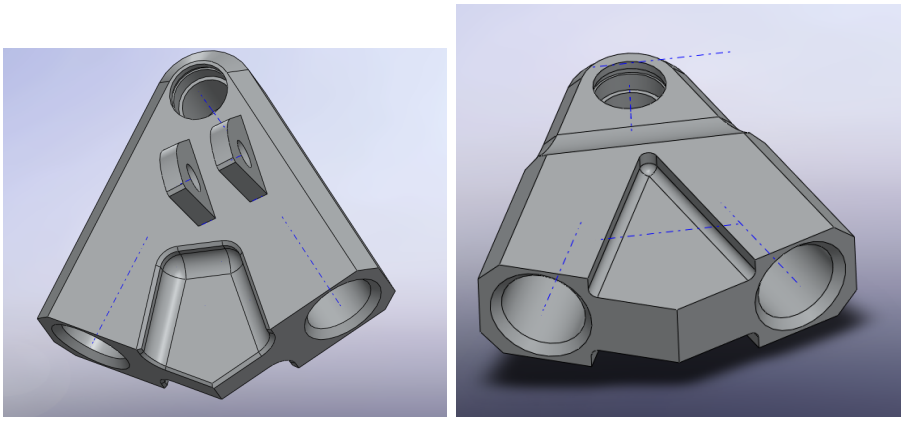

(a) (b)

Figure 7.4: Ergal triangle inserts: (a) front suspension, top insert; (b) rear suspension, lower insert.

be evaluated.

To have correct load application in the three-dimensional model are added some constrain geometry, for example a short part of the pipes is added and an approximation of the screwed connection. In this way it's possible to have easier load direction set up, and joint interface evaluation with only one simulation.

In picture 7.4 CAD view of two Ergal inserts.

I chose two joints: a no displacement joint situated in the uniball hole and a compression only support where the uniball insert will be in touch to contrast vertical load. The joint can allow little displacement and works like a spherical joint with a determinate rotation angle, in fact no displacement means that the outer uniball's ring will not rotate, but generally there can be a relative angle between planes containing wider ring sections.

As we can see the maximum Von Mises equivalent stress is σ_{max-e} =125 MPa, while the most of the body is under a tension of 50÷60 MPa. I preferred not to reduce inserts material because those parts have to be stiff to reduce total deformation and anyway the mass would not change so drastically (30÷40 grams), this means less then 200 grams in the whole car could be saved with less rigid inserts, I preferred not to.

For what concern shear stress it is possible to see in picture 7.6 (b), that all the pipe-insert connection zone is "green" so with a max shear stress of 9 MPa,

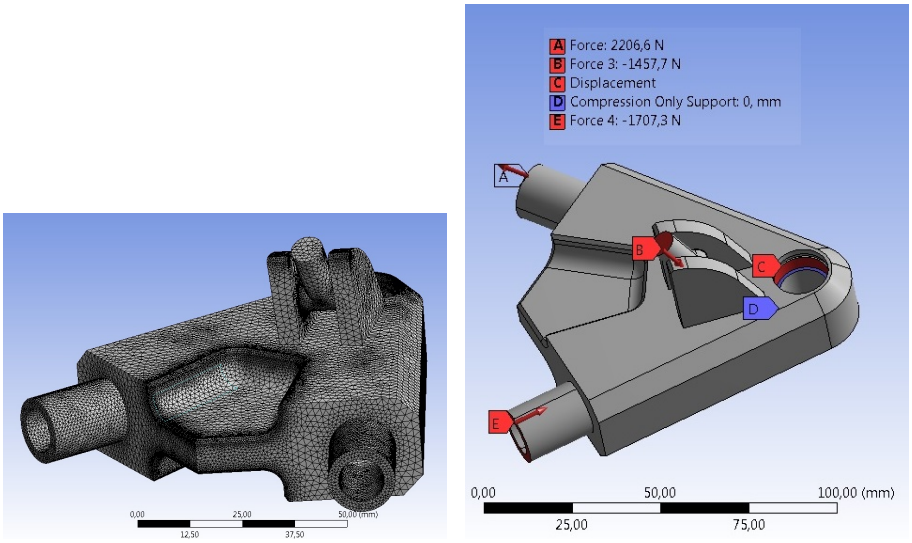

(a) (b)

Figure 7.5: Mesh (a) and load-constraint (b) configuration for insert (a) in picture 7.4.

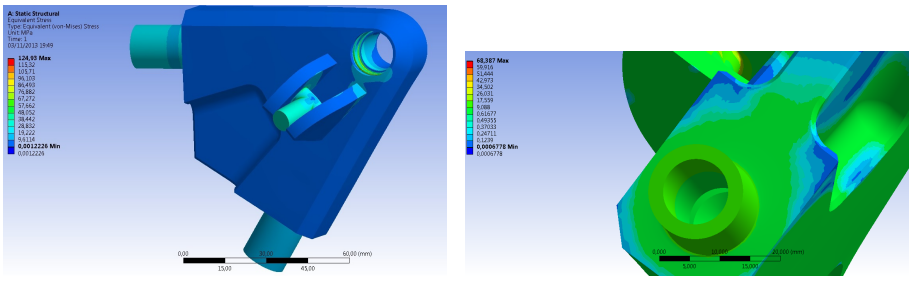

(a) (b)

Figure 7.6: Equivalent Von Mises stress (a) and max. shear stress (b), for insert (a) in picture 7.4.

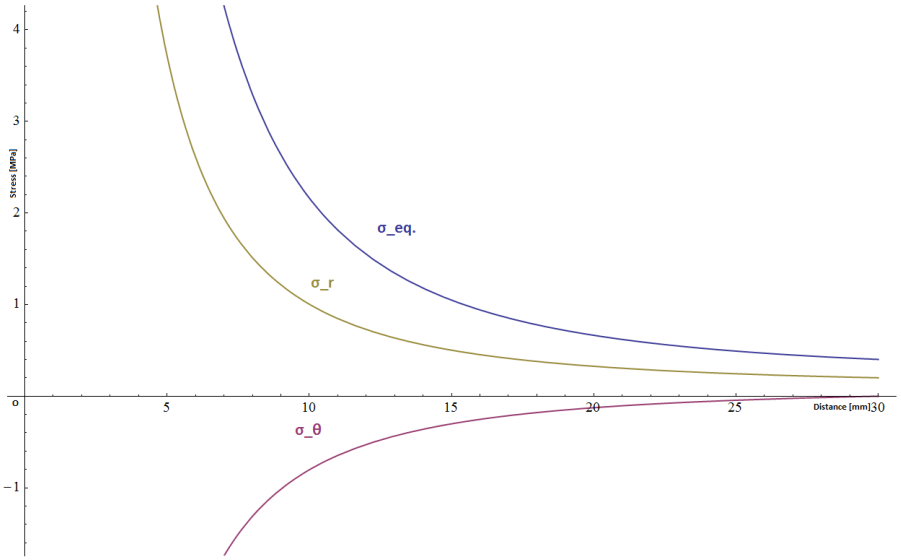

Figure 7.7: Stress due to forced conjunction of an uniball spherical joint and the Ergal insert.

value concordant with the one obtain in previous Paragraph.

Before evaluating safety check it is here necessary to introduce stress introduced from the uniball. The uniball, is under vertical load too, and it has to be slotted inside the supporting hole with a certain constrain, to grant with friction vertical load resistance. In addition a Seeger ring is inserted to prevent the uniball in emergencies situation to exit its position.

However this junction introduce stress in the material near to the hole so before continuing this stress has to be evaluated then a superimposition of effects is necessary to calculate real the stress.

Below a little theory summary:

$\sigma_r(r) = A - \frac{B}{r^2}$;

$\sigma_\theta(r) = A + \frac{B}{r^2}$;

With reference to figure 7.7, σ_r is the radial stress function of the radial distance "r", while "σ_θ" is the tangential stress function of the radial distance "r", "A" and "B" are constants function of the particular problem.

Assuming that $\sigma_r(d_{ext}) = 0$, no load applied, and $\sigma_r(d_{int}) = -p$, radial pressure due to forced inserts we have:

$\sigma_r(r) = \frac{p}{a^2-1}(1 - \frac{r_{ext}^2}{r^2})$;

$\sigma_\theta(r) = \frac{p}{a^2-1}(1 + \frac{r_{ext}^2}{r^2})$;

Where $a = d_{ext}/d_{int} = \frac{2 \cdot r_{ext}}{d_{int}}$;

equivalent Von Mises stress:

$\sigma_e(r) = \sqrt{(\sigma_r(r)^2 + 4 \cdot \sigma_\theta(r))}$;

The vertical load is granted by the friction of the two bodies:

$P_z = p \cdot A \cdot \mu$ where "S" is the interface area equal to 1230 mm^{2}and μ is the static friction coefficient between steel and aluminum equal to 0.61 and $P_z$is 1310 N we have:

$p = \frac{1530}{1230 \cdot 0.61} = 1.74$ MPa and $\sigma_e(d_{int}) = \sqrt{(\sigma(d_{int}/2)^2 + 4\sigma_\theta(d_{int}/2))} = 4.26$ MPa;

then total equivalent stress is 130 MPa so for this part we have: $\eta = \frac{\sigma_u}{\sigma_{max-e}} = \frac{572}{130} = 4.4$

Other inserts are less critical but it will displayed an example of lower insert. In figure 7.8 is the front lower insert, joint are the same of previous cases, see picture 7.5.

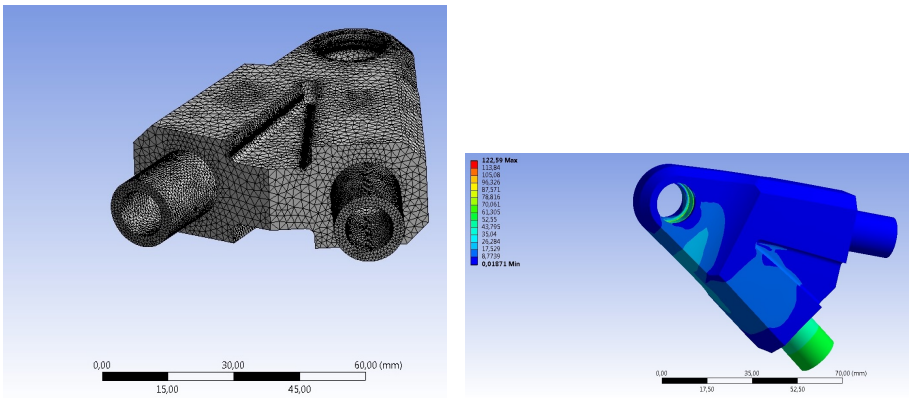

(a) (b)

Figure 7.8: Mesh (a) and equivalent Von Mises stress (b), for insert (b) in picture 7.4.

In this case we have almost the same maximal stress and using pre-load of the previous case is precautionary so safety factor is almost the same or little less.

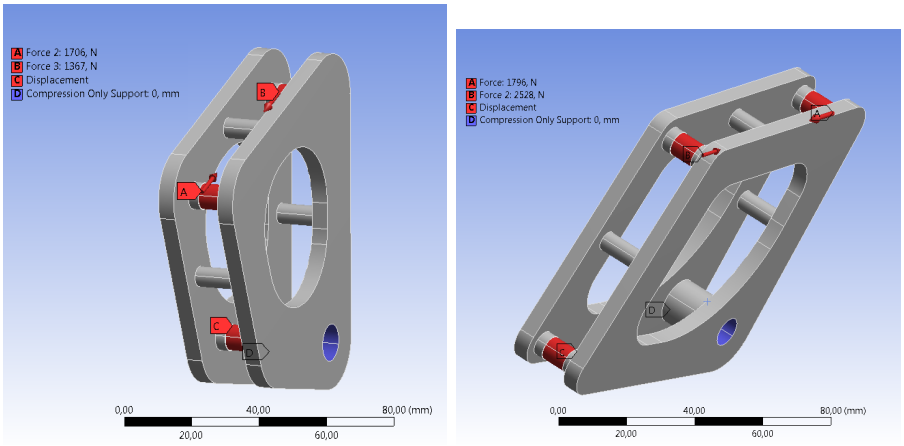

(a) (b)

Figure 7.9: Load and constraints for front axle rocker (a) and rear axle (b).

7.4.2 Rockers

Rocker loads are verified using greater loads available from springs and from push-roads, these loads are already known. Joints are rocker joint force and roll-bar arms force, both evaluated by Ansys. The two constrains are simulated by a compression only support for the rocker joint, in fact there is a bush to permit rotation and to avoid friction, while where the roll-bar arm is, I used a no displacement joint. (called displacement in picture 7.9, but is 0 mm displacement).

Loads are here summarized:

- Front: spring load is 1367 N, pushrod load 1706 N.
- Rear: spring load is 1796 N, pushrod load 2528 N.

In figure 7.10 equivalent stress for both front and rear rockers.

Ansys provide joints forces and equivalent Von Mises stress.

Maximum stress is in the two cases on bolts, and bolts are made by steel. For what concerns rockers maximal tension is 40 MPa for the front one and 70 MPa for the rear one, safety factors are $\eta_a = \frac{\sigma_u}{\sigma_{max-e}} = \frac{572}{40} = 14.3$ and $\eta_p = \frac{\sigma_u}{\sigma_{max-e}} = \frac{572}{70} = 8.2$. More then enough, more important in this case were deformations: I inserts some pins, to be welded to make rocker structure more stable.

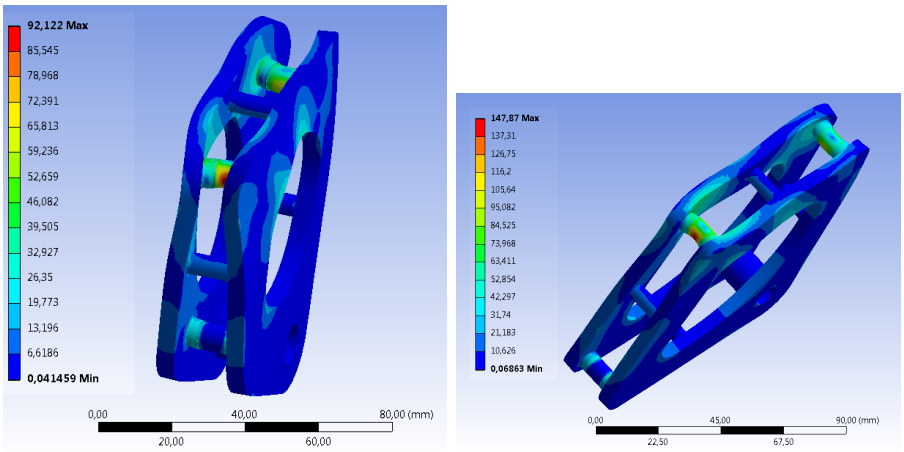

(a) (b)

Figure 7.10: Equivalent Von Mises stress for the front axle rocker (a) and rear axle rocker (b).

Ansys provides joint forces: rocker joints forces, in particular the rear have 710 N space resultant and 480 N space result the front one they will use to verify rocker supports see 7.4.4 .

7.4.3 roll-bar mechanism

Roll-bars mechanism is sketched in figure 7.11 (b) ,while the other figure (a) is the CAD. The worst load configuration is chosen, the most rigid one considering maximal wheel-centers excursions converted with bar-ratio (ratio between wheel-center displacement and most distant roll-bar hole displacement).

Roll-bars are designed in tree configuration, as explained before. Load configuration in the worst case is shown in picture 7.11 using design geometry in the connection between roll-bars pipes and arms there is a $\sigma_{zz} = 417$ MPa, this stress can grant with a steel ultimate stress: $\sigma_{u-s} = 740$ MPa a $\eta = \frac{740}{417} = 1.77$.

While the roll-bar pipe is subject to tangential stress of $\tau = 70$ MPa, while normal stress is $\sigma_{zz} = 139$ MPa therefore $\sigma_e = 197$ MPa, lesser than the other.

To better design the roll-bars, some Ansys simulation have been done to find a proper junction between roll-bars arms and roll-bar pipes.

The new maximal equivalent stress is: 352 MPa that correspond to: $\eta = \frac{740}{352} = 2.1$.

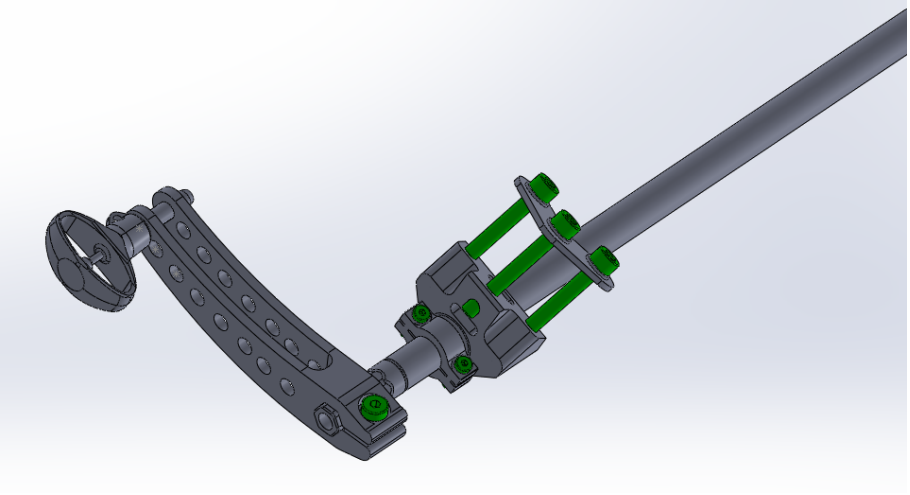

(a)

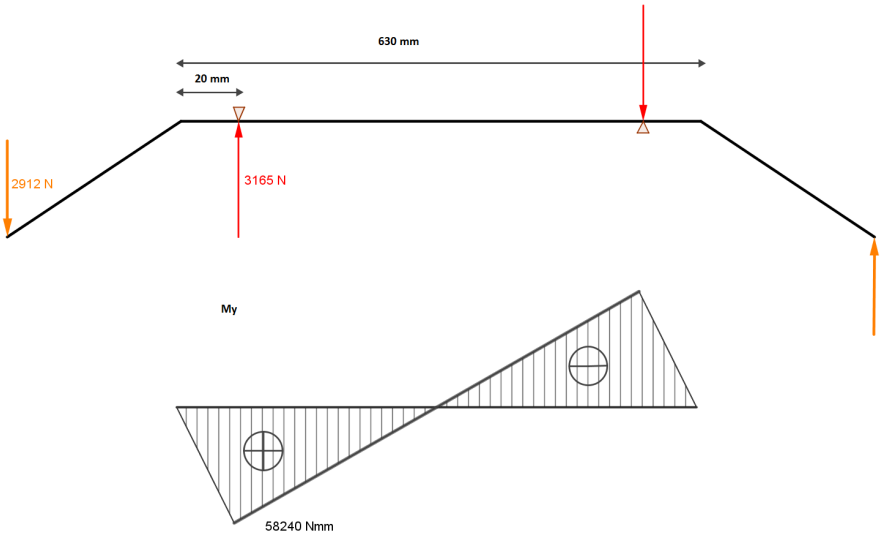

(b)

Figure 7.11: Roll-bar system CAD (a) and sketch (b).

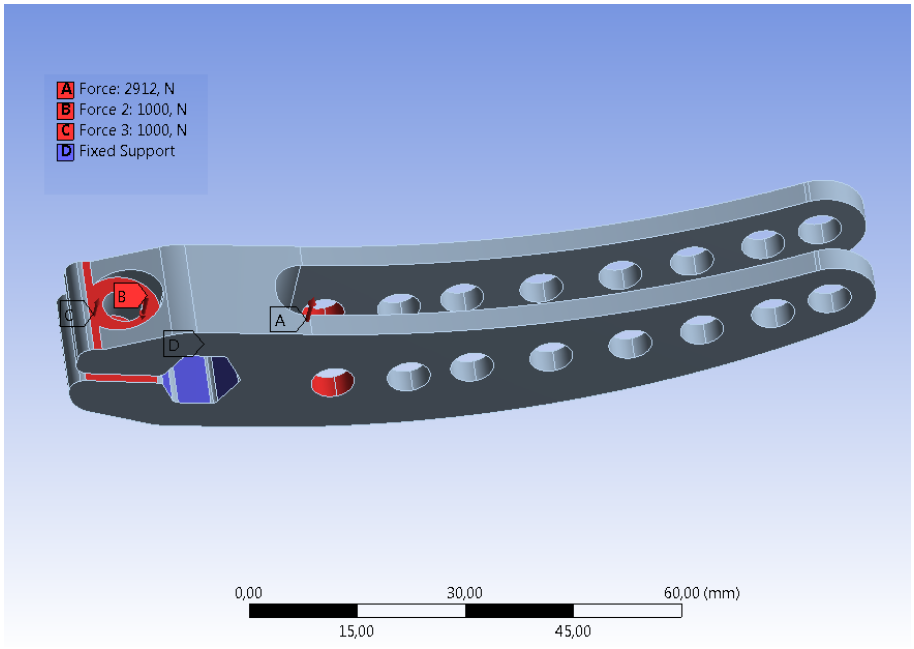

(a)

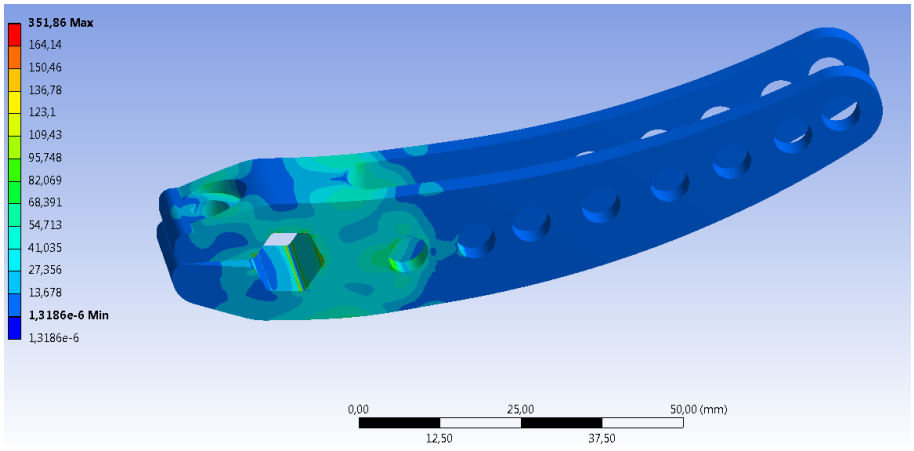

(b)

Figure 7.12: Roll-bar arms load and joint (a), equivalent Von Mises stress (b).

7.4.4 Frame supports and linking

In this Paragraph connection between main parts and the monocoque frame or between each other will be shortly checked.

There two main connection: arms connections and rockers connections, the other connection like rollbars to the frame and steering system to the frame are bush-pin type, so it is enough to confront average pressure with max pressure for that type of bushes.

Frame arms links

In picture 7.13 is the standard connection link between the frame and an arm.

The worst load condition is 7700 N. It is possible to see that maximal stress are considerable, for this reason it is advisable to use high-strenght screws. Very high-strenght screws can reach 1200 MPa of ultimate stress. Anyway at least 800 MPa ultimate stress screws must be used, and they must be replaced each race event.

Anyway other arms, thus links, are not under these loads: this is the worst case scenario.

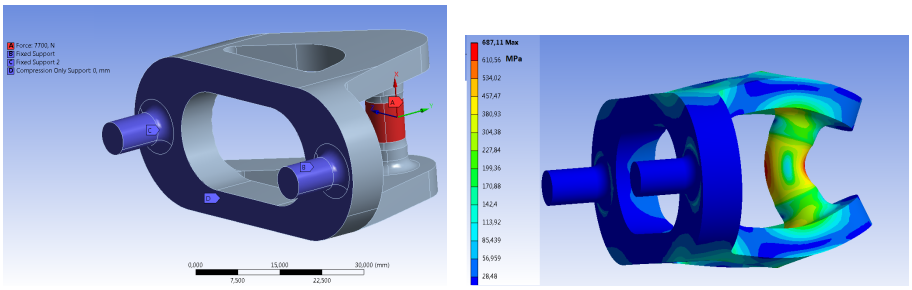

(a) (b)

Figure 7.13: Load and joints for standard frame support (a), equivalent stress (b).

Frame rockers links

Below in picture 7.14, maximal stress is 50 MPa, ultimate Ergal stress is 570 MPa, so there are no safety problems.

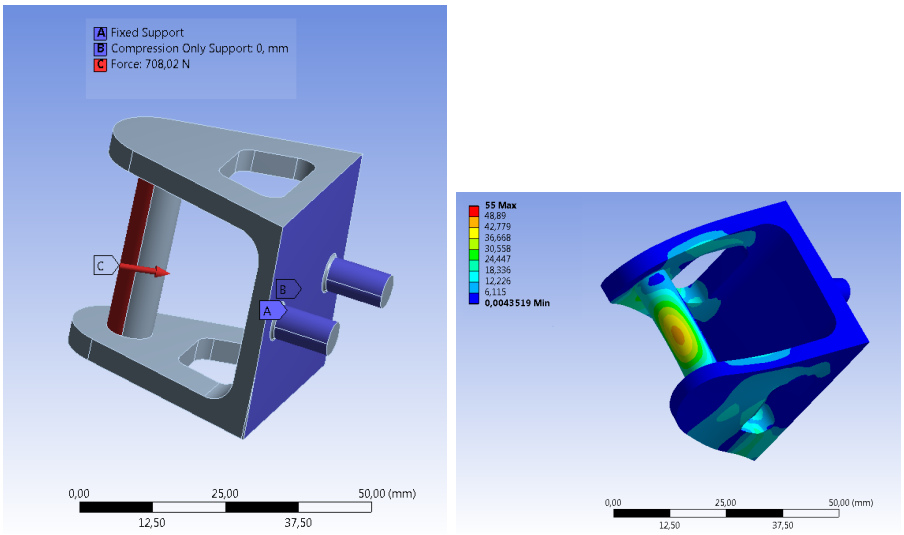

(a) (b)

Figure 7.14: Rocker support load and joints (a), equivalent Von Mises stress (b).

Rod-ends and uniballs

Rod-ends are connection between carbon fiber pipes and other components, technical specifications are in picture 7.15, while the greater load is 7700 N. Then $\eta = \frac{12.9}{7.7} = 1.67$.

Principal dimensions						Angle of tilt	Basic load static	Mass
d	d_2 max	B	G 6g	C_1 max	h		C_0	
mm						°	kN	kg
8	25	8	M 8	6,5	42	15	12,9	0,029

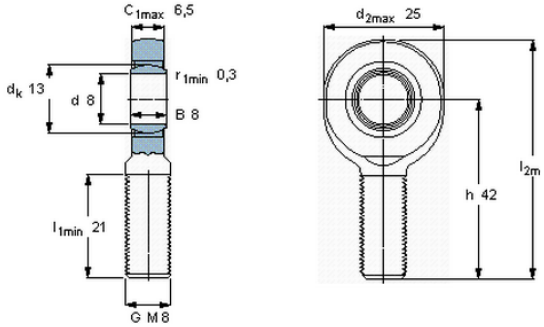

Figure 7.15: SKF rod-ends technical specifications.

Other connection between up-rights and Ergal triangle inserts are uniball, technical specifications are in picture 7.16 , while the greater load is 4100 N. Using dynamics max value for uniball (5.5 kN) is:

$\eta = \frac{5.5}{4.1} = 1.34$.

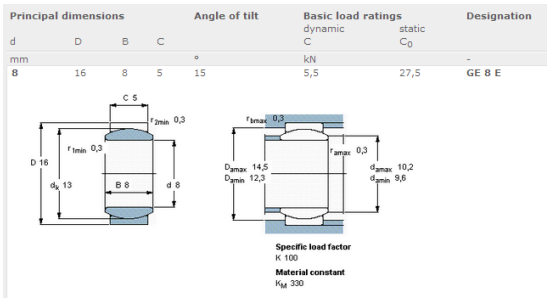

Figure 7.16: SKF uniball technical specifications.

Other connections

Each rocker-link has two pre-tensioned bushes with a bolt, the maximal radial load is evaluated in Chapter 7.4.2 and is 710 N, while dynamical load sustainable from this bushes is under C letter and it is 12 kN in figure 7.17), there are non safety problem. I suggest at least 10 Nm pre-load on the bolt that is a M10 to have proper bush functioning.

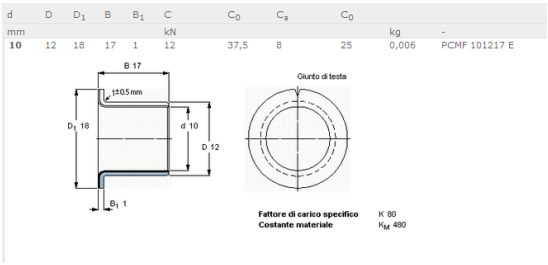

Figure 7.17: Rocker's bushes (SKF).

Other bushes are the one from the roll-bar mechanism, each is a 18 mm external diameter, 15 mm long with an available area of 3664 mm^2 but only half of this work when a load is applied, however the load coming from 7.4.3 is about 3200 N so we have an average pressure of 1.74 MPa without complication for the bush that can operate at 250 MPa pressure. See *Appendix C* for bushes technical data.

Other bushes have a small load, so there is no reason to check the pressure.

7.5 Parts already available: steering system

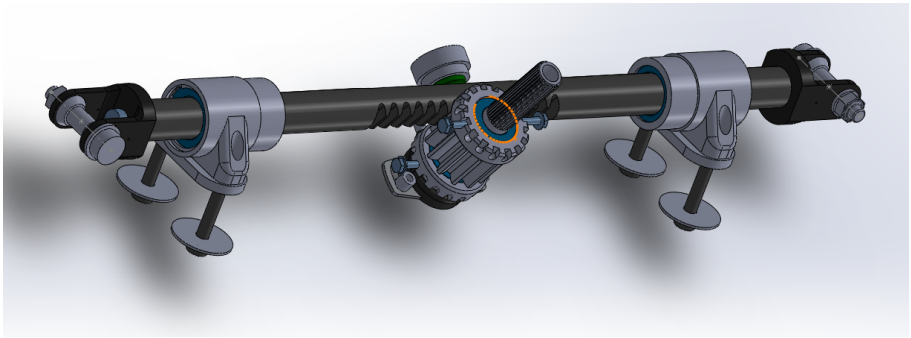

Figure 7.18: Rack pinion steering system with supports, and pre-load spring system in green.

The steering system is already available from the GreenTeam. For this reason the same rack pinion system will be used anyway main feature will be verify because of the new load configuration.

In figure 7.18 the the CAD layout, there are the rack pinion system a pre-load spring and two bushes to let the rank slide properly.

Next figure 7.19 shows load configuration in the worst case scenario, the steering load it is thought to be done with one hand only, in the middle of the picture the rack pinion system, below the steering column.

Maximal load for the rank is $\sigma_{zz} = 513$ MPa while the column have $\sigma_{zz} = 194$ MPa, $\tau = 108$ MPa so$\sigma_e = 290$ MPa, with safety factor of respectively:

$\eta = \frac{850}{360} = 2.36$;

$\eta = \frac{850}{290} = 2.93$;

These below are fatigue safety factor see Paragraph 7.6 .

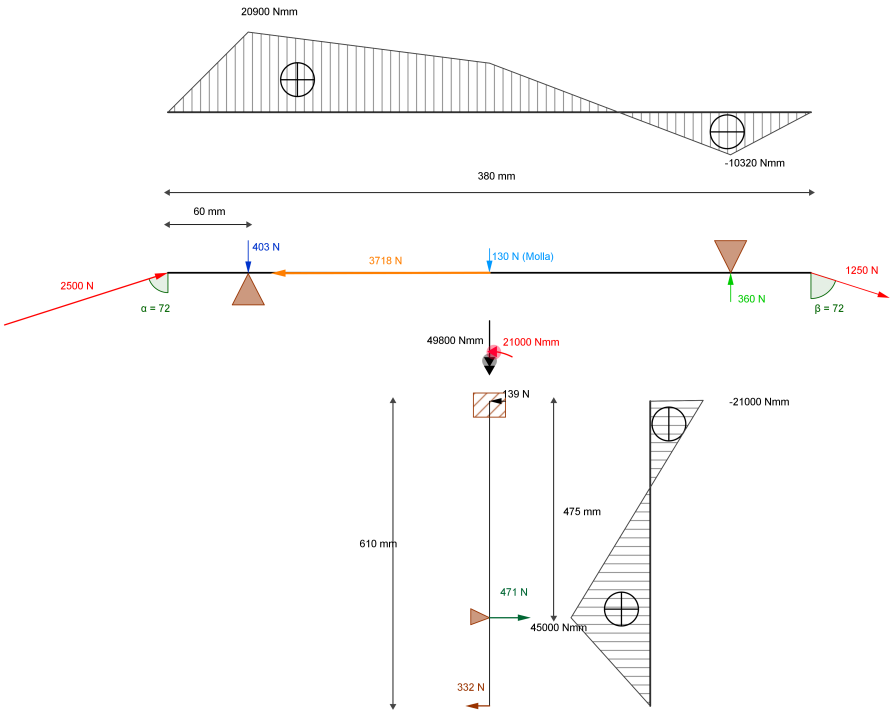

Figura 7.19: Steering system worst load configuration.

$\eta_f = \eta \cdot \frac{S_\infty}{\sigma_u} = 1.18;$

$\eta_f = \eta \cdot \frac{S_\infty}{\sigma_u} = 1.46;$

Now the gear verification: the gear is supported by two bushes like in figure 7.20.

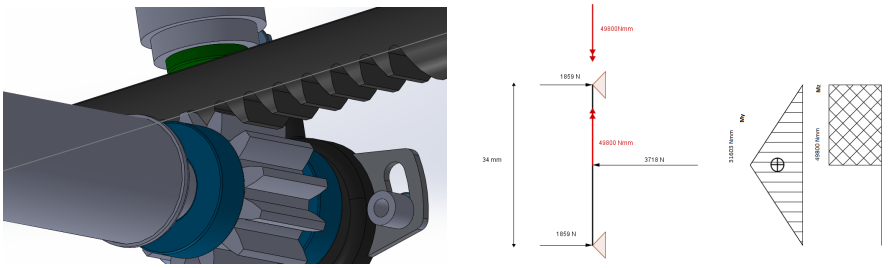

(a) (b)

Figure 7.20: Rank pignon bushes support details (a), load and constraint (b).

To check the gear I used this formula (eq. 7.4), from [11]:

$$\sigma = \frac{F_t}{bpy} \tag{7.4}$$

Where F_t =3178 N is the tangential force to be transmitted, "b" is the tooth width 19 mm, "p" is pitch of the gear ($\frac{\pi d}{Z}$), "d" is 20.8 mm, "Z" teeth number and it is 12 and "y" is the Leweis factor in this case: 0.25.

Then we have a $\sigma_{max} = 123$ MPa under at least 740 MPa of ultimate stress, so $\eta = 6$.

The shaft is splined to connect with the steering column, in our case we have:

$$T_{max} = 0.58\pi\frac{d^3}{8}\sigma_u = 2.9 \cdot 10^5 Nmm$$

where "d" is the shaft diameter 12 mm and σ_u is still the ultimate stress of the shaft, the torque is instead 49800 Nmm, so we have:

$\eta = 5.84$

To finish this part the normal verification for the small shaft between the two bushes and the bushes average pressure:

$\sigma_{zz} = 189$ MPa, $\tau = 145$ MPa so$\sigma_e = 348$ MPa, with a $\eta = 2.12$.

7.6 Fatigue

This last part takes in consideration effects of fatigue. It is important to remember that this type of cars will hardly travel more then 100 km overall in their lifetime, that corresponds to something like 10000 load cycles.

There is some know-how available to evaluate a load spectrum to have a more precise decrease factor for ultimate stress due to fatigue. However these calculation are complex and not reliable, I preferred precautionary fatigue factor from [11], the lower between bending, torsion and traction.

So with S_{10^3} I mean maximal stress for one thousand cycle, and it is:

$S_{10^3} = 0.72\sigma_u$, while S_∞ is the equivalent stress for unlimited fatigue life for more important parts, like rank pignon system.

This way, the lowest safety factor are $\eta_{fr} = \eta_r \cdot \frac{S_\infty}{\sigma_u} = 1.27$ for the roll-bars arm and $\eta_{fs} = \eta_s \cdot \frac{S_\infty}{\sigma_u} = 1.18$ for the rack pinion system and $\eta_{fsh} = \eta_{sh} \cdot \frac{S_\infty}{\sigma_u} = 1.06$ and $\eta_{ft} = \eta_t \frac{S_{10^3}}{\sigma_u} = 3.17$ for the triangle insert.

Chapter 8

Appendix

Appendix A: mathematical model

Below the mathematical model used to prove benefits of a four wheel steered car, see Chapter 6.

```
Dynamic
Suspensions
t1 = 1.210;"carreggiata anteriore";
t2 = 1.160;
l = 1.530;"passo";
x = 52;"rapporto molle ant/post";
σmax = 0.25;"Sigma massimo nei grafici";
xl = 0.516;"rapporto semipasso ant/l";
dr1 = 0.039;"alteza centro di rollio ant";
dr2 = 0.041;"altezzacentro di rollio post";
h = 0.255;"altezza baricentro";
mv = 205;"massa veicolo";
mp = 65;"massa pilota";
m = mp + mv;
u[t_] = 50/3.6; If[t < 2, 80/3.6, 80/3.6 − 1/2 ∗ 1 ∗ 2 ∗ 1.1 ∗ (20/3.6)^2/270 ∗ (t − 2)];


"km1=30.6*10^3
km2=26.6*10^3
s=160000;
ke1=km1*s/(s+km1)*t1;
ke2=km2*s/(s+km2)*t2;
kr1=
kr2=
k1=ke1+kr1;
k2=ke2+kr2;"
tinx = 0;
tmax = 5;

kφt = kφ1 + kφ2;
a1 = (l ∗ xl ∗ mv + 3.5/10 ∗ l ∗ mp)/(m)
a2 = l − a1
a1/l
t1
```

```
t2
t1/t2
dr = (a2 * dr1 + a1 * dr2)/l;"altezzacentro di rollio a baricentro";
kϕ1 = x;
kϕ2 = 100 − x;
c1 = c2 = 1.3;
e1 = e2 = 0.35;
d1 = d2 = 2000;
b1 = 40000/(c1 * d1);
b2 = 40000/(c2 * d2);

Areo
kappa = 0.6;
h1 = 0.175;
h2 = 0.700;
fz1 = 0.75 * kappa * u[t]^2;
fz2 = 1.1 * kappa * u[t]^2;
Z:=n1 + n2 − fz1 − fz2 == 0;
X:= − 0.7 * kappa * u[t]^2 + t == 0;
My:= − t * h + n2 * a2 − n1 * a1 + (0.3 * kappa * u[t]^2)*
(h − h1) − (0.4 * kappa * u[t]^2) * (h2 − h) + 1.160 * fz1 − 0.71 * fz2 == 0;

areo = Solve[{Z, X, My}, {n1, n2, t}]

n111 = n1/.areo[[1, 1]];
n112 = n2/.areo[[1, 2]];
T = t/.areo[[1, 3]];
 "km1=30.6*10^3
km2=26.6*10^3
s=160000;
ke1=km1*s/(s+km1)*t1;
ke2=km2*s/(s+km2)*t2;
kr1=
kr2=
k1=ke1+kr1;
k2=ke2+kr2;" "km1=30.6*10^3
km2=26.6*10^3
s=160000;
ke1=km1*s/(s+km1)*t1;
ke2=km2*s/(s+km2)*t2;
kr1=
kr2=
k1=ke1+kr1;
k2=ke2+kr2;"


Plot[u[t], {t, 0, tmax}]
y1[t_] = d1 * Sin[c1 * ArcTan[b1 * σ1[t] − e1 * (b1 * σ1[t] − ArcTan[b1 * σ1[t]])]];

y2[t_] = d2 * Sin[c2 * ArcTan[b2 * σ2[t] − e2 * (b2 * σ2[t] − ArcTan[b2 * σ2[t]])]];

y[t_] = y1[t] + y2[t];



y1f[t_] = d1 * Sin[c1 * ArcTan[b1 * σ1f[t] − e1 * (b1 * σ1f[t] − ArcTan[b1 * σ1f[t]])]];

y2f[t_] = d2 * Sin[c2 * ArcTan[b2 * σ2f[t] − e2 * (b2 * σ2f[t] − ArcTan[b2 * σ2f[t]])]];

yf[t_] = y1f[t] + y2f[t];
```

```
"magic formula";

N1[t_] = y1[t] * a1 - y2[t]a2;

N1f[t_] = y1f[t] * a1 - y2f[t]a2;
"N della dinamica come da guigginai";

Δfz1[t_] = 1/t1 * (dr1/l * (y[t] * a2 + N1[t]) + kϕ1/kϕt * (h - dr) * y[t]);

Δfz2[t_] = 1/t2 * (dr2/l * (y[t] * a1 - N1[t]) + kϕ2/kϕt * (h - dr) * y[t]);

Δfz1f[t_] = 1/t1 * (dr1/l * (yf[t] * a2 + N1f[t]) + kϕ1/kϕt * (h - dr) * yf[t]);

Δfz2f[t_] = 1/t2 * (dr2/l * (yf[t] * a1 - N1f[t]) + kϕ2/kϕt * (h - dr) * yf[t]);

Tyre

A11 = A12 = -0.05 * 1000^(-1);
A21 = A22 = 1;
A31 = A32 = 40000;
A41 = A42 = 2000;

Fz10 = (n111 + m * 9.81 * (a2/(l)))/2;
Fz20 = (n112 + m * 9.81 * (a1/(l)))/2;

Fz101 = (m * 9.81 * (a2/(l)))/2;
Fz201 = (m * 9.81 * (a1/(l)))/2;

"Fz10=(m*9.81*(a2/(l)))/2;
Fz20=(m*9.81*(a1/(l)))/2;"

Fz12[t_] = Fz10 + Δfz1[t];
Fz11[t_] = Fz10 - Δfz1[t];
Fz22[t_] = Fz20 + Δfz2[t];
Fz21[t_] = Fz20 - Δfz2[t];

Fz12f[t_] = Fz10 + Δfz1f[t];
Fz11f[t_] = Fz10 - Δfz1f[t];
Fz22f[t_] = Fz20 + Δfz2f[t];
Fz21f[t_] = Fz20 - Δfz2f[t];

D12[t_] = (A11 * Fz12[t] + A21) * Fz12[t];
```

```
D11[t_] = (A11 * Fz11[t] + A21) * Fz11[t];

D22[t_] = (A12 * Fz22[t] + A22) * Fz22[t];

D21[t_] = (A12 * Fz21[t] + A22) * Fz21[t];

D12f[t_] = (A11 * Fz12f[t] + A21) * Fz12f[t];

D11f[t_] = (A11 * Fz11f[t] + A21) * Fz11f[t];

D22f[t_] = (A12 * Fz22f[t] + A22) * Fz22f[t];

D21f[t_] = (A12 * Fz21f[t] + A22) * Fz21f[t];



B12[t_] = A31 * Sin[2 * ArcTan[Fz12[t]/A41]]/(c1 * D12[t]);

B11[t_] = A31 * Sin[2 * ArcTan[Fz11[t]/A41]]/(c1 * D11[t]);

B22[t_] = A32 * Sin[2 * ArcTan[Fz22[t]/A42]]/(c1 * D22[t]);

B21[t_] = A32 * Sin[2 * ArcTan[Fz21[t]/A42]]/(c1 * D21[t]);


B12f[t_] = A31 * Sin[2 * ArcTan[Fz12f[t]/A41]]/(c1 * D12f[t]);

B11f[t_] = A31 * Sin[2 * ArcTan[Fz11f[t]/A41]]/(c1 * D11f[t]);

B22f[t_] = A32 * Sin[2 * ArcTan[Fz22f[t]/A42]]/(c1 * D22f[t]);

B21f[t_] = A32 * Sin[2 * ArcTan[Fz21f[t]/A42]]/(c1 * D21f[t]);

gain = 1.52;

X1 = gain;
X2 = gain;
X3 = gain;
X4 = gain;


Fy12[t_] = X1 * D12[t] * Sin[c1 * ArcTan[B12[t] * σ12[t] - e1 * (B12[t] * σ12[t] - ArcTan[B12[t] * σ12[t]])]];

Fy11[t_] = X2 * D11[t] * Sin[c1 * ArcTan[B11[t] * σ11[t] - e1 * (B11[t] * σ11[t] - ArcTan[B11[t] * σ11[t]])]];

Fy22[t_] = X3 * D22[t] * Sin[c2 * ArcTan[B22[t] * σ22[t] - e2 * (B22[t] * σ22[t] - ArcTan[B22[t] * σ22[t]])]];

Fy21[t_] = X4 * D21[t] * Sin[c2 * ArcTan[B21[t] * σ21[t] - e2 * (B21[t] * σ21[t] - ArcTan[B21[t] * σ21[t]])]];


Fy12f[t_] = X1 * D12f[t] * Sin[c1 * ArcTan[B12f[t] * σ12f[t] - e1 * (B12f[t] * σ12f[t] - ArcTan[B12f[t] * σ12f[t]])]];

Fy11f[t_] = X2 * D11f[t] * Sin[c1 * ArcTan[B11f[t] * σ11f[t] - e1 * (B11f[t] * σ11f[t] - ArcTan[B11f[t] * σ11f[t]])]];

Fy22f[t_] = X3 * D22f[t] * Sin[c2 * ArcTan[B22f[t] * σ22f[t] - e2 * (B22f[t] * σ22f[t] - ArcTan[B22f[t] * σ22f[t]])]];

Fy21f[t_] = X4 * D21f[t] * Sin[c2 * ArcTan[B21f[t] * σ21f[t] - e2 * (B21f[t] * σ21f[t] - ArcTan[B21f[t] * σ21f[t]])]];
```

```
Y1[t_] = (Fy12[t] + Fy11[t]);
Y2[t_] = (Fy22[t] + Fy21[t]);

Y1f[t_] = (Fy12f[t] + Fy11f[t]);
Y2f[t_] = (Fy22f[t] + Fy21f[t]);


 "σ11[t_]=If[(σ11x[t]^2+σ11y[t]^2)>0,(σ11x[t]^2+σ11y[t]^2)^(0.5),1];
σ12[t_]=If[(σ12x[t]^2+σ12y[t]^2)>0,(σ12x[t]^2+σ12y[t]^2)^(0.5),1];
σ21[t_]=If[(σ21x[t]^2+σ21y[t]^2)>0,(σ21x[t]^2+σ21y[t]^2)^(0.5),1];
σ22[t_]=If[(σ22x[t]^2+σ22y[t]^2)>0,(σ22x[t]^2+σ22y[t]^2)^(0.5),1];


σ1[t_]=If[(σ1x[t]^2+σ1y[t]^2)>0,(σ1x[t]^2+σ1y[t]^2)^(0.5),1];
σ2[t_]=If[(σ2x[t]^2+σ2y[t]^2)>0,(σ2x[t]^2+σ2y[t]^2)^(0.5),1];";


"ω012[t_]=If[Abs[r[t]]>0,u[t]/0.228*(u[t]/r[t]+t1/2)/(u[t]/r[t]),u[t]/0.228];
ω011[t_]=If[Abs[r[t]]>0,u[t]/0.228*(u[t]/r[t]-t1/2)/(u[t]/r[t]),u[t]/0.228];
ω022[t_]=If[Abs[r[t]]>0,u[t]/0.228*(u[t]/r[t]+t2/2)/(u[t]/r[t]),u[t]/0.228];
ω021[t_]=If[Abs[r[t]]>0,u[t]/0.228*(u[t]/r[t]-t2/2)/(u[t]/r[t]),u[t]/0.228];";

ω012[t_] = u[t]/0.228 * (u[t]/r[t] + t1/2)/(u[t]/r[t]);
ω011[t_] = u[t]/0.228 * (u[t]/r[t] - t1/2)/(u[t]/r[t]);
ω022[t_] = u[t]/0.228 * (u[t]/r[t] + t2/2)/(u[t]/r[t]);
ω021[t_] = u[t]/0.228 * (u[t]/r[t] - t2/2)/(u[t]/r[t]);


σ11x[t_] = ω011[t]/ωc11[t] - 1;
σ21x[t_] = ω021[t]/ωc21[t] - 1;
σ12x[t_] = ω012[t]/ωc12[t] - 1;
σ22x[t_] = ω022[t]/ωc22[t] - 1;

σ11y[t_]:= - ω011[t]/ωc11[t] * Tan[α11[t]];
σ12y[t_]:= - ω012[t]/ωc12[t] * Tan[α11[t]];
σ21y[t_]:= - ω021[t]/ωc21[t] * Tan[α21[t]];
σ22y[t_]:= - ω022[t]/ωc22[t] * Tan[α21[t]];

σ1x[t_] = (σ11x[t] + σ12x[t])/2;
σ2x[t_] = (σ21x[t] + σ22x[t])/2;
σ1y[t_] = (σ11y[t] + σ12y[t])/2;
σ2y[t_] = (σ12y[t] + σ22y[t])/2;


σ11[t_] = (σ11x[t]^2 + σ11y[t]^2)^(0.5);
σ12[t_] = (σ12x[t]^2 + σ12y[t]^2)^(0.5);
σ21[t_] = (σ21x[t]^2 + σ21y[t]^2)^(0.5);
σ22[t_] = (σ22x[t]^2 + σ22y[t]^2)^(0.5);


σ1[t_] = (σ1x[t]^2 + σ1y[t]^2)^(0.5);
σ2[t_] = (σ2x[t]^2 + σ2y[t]^2)^(0.5);

fx1[t_] = -σ11x[t]/σ11[t] * Fy11[t] - σ12x[t]/σ12[t] * Fy12[t];
fx2[t_] = -σ21x[t]/σ21[t] * Fy21[t] - σ22x[t]/σ22[t] * Fy22[t];

fy1[t_] = -σ1y[t]/σ1[t] * Y1[t];
```

```
fy2[t_] = -σ2y[t]/σ2[t] * Y2[t];
 Equations

"δ1[t_]=If[t<5,0,0.001*(t-5)]";
i[t] = Interpolation[{{0, 0}, {5, 0}, {5.5, 0.1}, {6, 0.1}, {7, 0.1}, {7.5, 0}, {8, 0}}, InterpolationOrder → 3];
δ11[t_] = 0.015 * (1 - e^(-(t)/0.05)) - 0.005(t - 2.3);
δ1[t_] = 3 * (1 - e^(-(t)/0.1)) * (12.86 - 2) * 0.00355;
delay = 0.2;
power = 0.5;
δ21[t_] = 0.5 * (-0.01 * (1 - e^(-(t-delay)/0.05)) + 0.001 * (0.5 * t - delay - 0.9) + 0.02 * (1 - e^(-(t-0.5)/0.8)) - 0.517516581182798 * e^(-(t)/0.05))
"δ2[t_]=Corr;"
δ2[t_] = 0.485 * Corr; Delta2; If[t < 2.3, 0, 1 * corr[t]];
δ2[0.1]
δ2[0]
Plot[{δ1[t], δ2[t]}, {t, -2 * delay, tmax}]

J = 125;

α1[t_] = (δ1[t] - (v[t] + r[t] * a1)/u[t]);
α2[t_] = (δ2[t] - (v[t] - r[t] * a2)/u[t]);

α11[t_] = α1[t];
α21[t_] = α2[t];  eq1 = {u'[t] == (fx1[t] + fx2[t] - fy1[t] * δ1[t] - fy2[t] * δ2[t] - T + v[t] * r[t] * m)/m};
eq2 = {v'[t] == (fy1[t] + fy2[t] + fx1[t] * δ1[t] + fx2[t] * δ2[t] - u[t] * r[t] * m)/m};
eq3 = {r'[t] == (fy1[t] * a1 - fy2[t] * a2 + fx1[t] * a1 * δ1[t] - fx2[t] * a2 * δ2[t])/J};
eq4 = {(Fz12[t] + Fz11[t])/(Fz22[t] + Fz21[t]) == fx1[t]/fx2[t]};
eq5 = {-σ11x[t]/(σ11[t]) * Fy11[t] == -σ12x[t]/σ12[t] * Fy12[t]};
eq6 = {-σ21x[t]/(σ21[t]) * Fy21[t] == -σ22x[t]/σ22[t] * Fy22[t]}; "soluzioni del sistema";

t0 = 0;
solu1 = NDSolve[{eq1, eq2, eq3, eq4, eq5, eq6, v[t0] == 0, r[t0] == 10^ - 4, ωc11[t0] == u[0] * 1.0/0.228, ωc12[t0] == u[0] * 1.0/0.228,
ωc21[t0] == u[0] * 1.0/0.228, ωc22[t0] == u[0] * 1.0/0.228}, {v, r, ωc11, ωc12, ωc21, ωc22}, {t, 0, tmax}, PrecisionGoal → 2];

ωc11f = ωc11[t]/.solu1[[1, 3]];
vf = v[t]/.solu1[[1, 1]];
vf' = v'[t]/.solu1[[1, 1]];
rf = r[t]/.solu1[[1, 2]];
rf' = r'[t]/.solu1[[1, 2]];
ωc12f = ωc12[t]/.solu1[[1, 4]];
ωc21f = ωc21[t]/.solu1[[1, 5]];
ωc22f = ωc22[t]/.solu1[[1, 6]];


EmitSound[Play[Sin[100000t^2], {t, 0, 0.1}]]
 ForzaMotrice

α1f[t_] = (δ1[t] - (vf + rf * a1)/u[t]);
α2f[t_] = (δ2[t] - (vf - rf * a2)/u[t]);

ω011f[t_] = u[t]/0.228 * (u[t]/rf - t1/2)/(u[t]/rf);
ω012f[t_] = u[t]/0.228 * (u[t]/rf + t1/2)/(u[t]/rf);
ω021f[t_] = u[t]/0.228 * (u[t]/rf - t2/2)/(u[t]/rf);
ω022f[t_] = u[t]/0.228 * (u[t]/rf + t2/2)/(u[t]/rf);

σ11xf[t_] = ω011f[t]/ωc11f - 1;
σ21xf[t_] = ω021f[t]/ωc21f - 1;
σ12xf[t_] = ω012f[t]/ωc12f - 1;
σ22xf[t_] = ω022f[t]/ωc22f - 1;

σ11yf[t_] = -ω011f[t]/ωc11f * Tan[α1f[t]];
σ12yf[t_] = -ω012f[t]/ωc12f * Tan[α1f[t]];
σ21yf[t_] = -ω021f[t]/ωc21f * Tan[α2f[t]];
```

```
σ22yf[t_] = −ω022f[t]/ωc22f * Tan[α2f[t]];

σ1xf[t_] = (σ11xf[t] + σ12xf[t])/2;
σ2xf[t_] = (σ21xf[t] + σ22xf[t])/2;
σ1yf[t_] = (σ11yf[t] + σ12yf[t])/2;
σ2yf[t_] = (σ12yf[t] + σ22yf[t])/2;



σ11f[t_] = (σ11xf[t]^2 + σ11yf[t]^2)^(0.5);
σ12f[t_] = (σ12xf[t]^2 + σ12yf[t]^2)^(0.5);
σ21f[t_] = (σ21xf[t]^2 + σ21yf[t]^2)^(0.5);
σ22f[t_] = (σ22xf[t]^2 + σ22yf[t]^2)^(0.5);



σ1f[t_] = (σ1xf[t]^2 + σ1yf[t]^2)^(0.5);
σ2f[t_] = (σ2xf[t]^2 + σ2yf[t]^2)^(0.5);


fx1f[t_] = −σ11xf[t]/σ11f[t] * Fy11f[t] − σ12xf[t]/σ12f[t] * Fy12f[t];
fx2f[t_] = −σ21xf[t]/σ21f[t] * Fy21f[t] − σ22xf[t]/σ22f[t] * Fy22f[t];

fx11f[t_] = −σ11xf[t]/σ11f[t] * Fy11f[t];
fx12f[t_] = −σ12xf[t]/σ12f[t] * Fy12f[t];
fx21f[t_] = −σ21xf[t]/σ21f[t] * Fy21f[t];
fx22f[t_] = −σ22xf[t]/σ22f[t] * Fy22f[t];


fy1f[t_] = −σ1yf[t]/σ1f[t] * Y1f[t];
fy2f[t_] = −σ2yf[t]/σ2f[t] * Y2f[t];
fyf[t_] = fy1f[t] + fy2f[t];
Plot[u[t], {t, 0, tmax}, PlotRange → {19.9, 20.1}]
Plot[vf, {t, 0, tmax}, PlotLabel → "Velocità Laterale", PlotRange → {0.3, −0.1}]
Plot[rf, {t, 0, tmax}, PlotLabel → "Velocità Imbardata", PlotRange → {1.1, 1}]
Plot[{180/Pi * α1f[t], 180/Pi * α2f[t]}, {t, 0, tmax}, PlotLabel → "Alfa 1 Alfa2 (deg)"]
Plot[{ω011f[t], ω012f[t], ω021f[t], ω022f[t]}, {t, 0, tmax}, PlotLabel → "Omega Ruote"]
Plot[{ωc11f, ωc12f, ωc21f, ωc22f}, {t, 0, tmax}, PlotLabel → "Omega Cerchioni"]
Plot[{σ11xf[t], σ12xf[t], σ21xf[t], σ22xf[t]}, {t, 0, tmax}, PlotLabel → "Scorrimenti Longitudinali Ruote"]
Plot[{σ11yf[t], σ12yf[t], σ21yf[t], σ22yf[t]}, {t, 0, tmax}, PlotLabel → "Scorrimenti Laterali Ruote"]
Plot[{σ11f[t], σ12f[t], σ21f[t], σ22f[t]}, {t, 0, tmax}, PlotLabel → "Scorrimenti Ruote"]
Plot[{σ1f[t], σ2f[t]}, {t, 0, tmax}, PlotLabel->"Scorrimenti Assali (media)"]



Plot[{fx1f[t], fx2f[t]}, {t, 0, tmax}, PlotLabel → "Forze Assali (long.)"]
Plot[{fy1f[t], fy2f[t]}, {t, 0, tmax}, PlotLabel → "Forze Assali (lat.)"]
Plot[{Fy11f[t], Fy12f[t], Fy21[t], Fy22[t]}, {t, 0, tmax}, PlotLabel → "Forze Route (tot.)"]
Plot[{fx11f[t], fx12f[t], fx21f[t], fx22f[t]}, {t, 0, tmax}, PlotLabel → "Forza Ruote (long.)"]

Plot[Y1f[t], {t, 0, tmax}, PlotLabel → "Assale Anteriore"]
Plot[Y2f[t], {t, 0, tmax}, PlotLabel → "Assale Posteriore"]
Plot[fyf[t], {t, 0, tmax}, PlotLabel → "Forza laterale tot."]
R[t_] = u[t]/(rf);
S[t_] = vf/(rf);
R°[t_] = 1/R[t];
vf' = v'[t]/.solu1[[1, 1]];
β[t_] = ArcTan[vf/u[t]] * 180/Pi;
γ[t_] = ArcTan[(a1 + a2)/u[t]] * 180/Pi;
β1[t_] = ((vf + rf * a1)/u[t]) * 180/Pi;
β2[t_] = ((vf − rf * a2)/u[t]) * 180/Pi;
θf[t_] = 180/Pi * ∫ rf dt;
```

```
ay[t_] = (u[t] * rf + vf')/9.81;
ufkm[t_] = 3.6 * u[t];
Plot[ay[t], {t, t0, tmax}, PlotLabel → "ay", PlotRange → {1.45, 1.50}]
Plot[β[t], {t, t0, tmax}, PlotLabel → "βeta", PlotRange → {2.5, −0.5}]
Plot[θf[t], {t, t0, tmax}]
θf[0.1]
θf[0.5]
θf[1]
θf[tmax]
diff1[t_] = Abs[(fy2f[t]/Fz20/2/1.6002547827327125) * 100] − Abs[(fy1f[t]/Fz10/2/1.5558012353712567) * 100];

diff2[t_] = Abs[(Y2f[t]/Fz20/2/1.6002547827327125) * 100] − Abs[(Y1f[t]/Fz10/2/1.5558012353712567) * 100];

diff1[tmax]
diff2[tmax]
diff1[0.2]
diff2[0.2]
space[t_] = θf[t] * R[t]/180 * Pi;

space[0.1]
space[0.5]
space[1]
space[4]
"δ1fdeg[t_]=δ1[t]*180/Pi;
δ2fdeg[t_]=δ2[t]*180/Pi;
tsegnato=Solve[R[t]==40,t]
δ1[tsegnato]
δ2[tsegnato]"; Correttore

equazione = {α2f[t] − delta2 − a2/R[t] == 0};
uno = Solve[equazione, delta2];
Delta2 = delta2/.uno;
Kappa = Delta2/δ1[t + 5];
Plot[Kappa, {t, tinx, tmax}, PlotLabel → "sterzo1/sterzo2"]
Plot[Delta2, {t, tinx, tmax}, PlotLabel → "sterzo2"]
Table[Delta2, {t, 0, tmax, 0.1}];
corr[t_] = Corr;
corr[t];
Corr = InterpolatingPolynomial[Table[{t, Delta2}, {t, 0, tmax + 1, 0.4}], t];
cucu[t_] = Interpolation[Table[{t, Delta2}, {t, 0, tmax, 1}], t, InterpolationOrder → 1]
Plot[{Delta2, corr[t]}, {t, −delay, tmax}, PlotRange → {−0.1, 0.1}] Plots

zeta = 10;
Plot[rf, {t, t0, tmax}, PlotLabel → "vel.Imbardata", PlotRange → 1.1]
Plot[ay[t], {t, t0, tmax}, PlotLabel → "ay", PlotRange → {1.40, 1.55}]
Plot[ufkm[t], {t, t0, tmax}, PlotLabel → "Velocità avanzamento", PlotRange → {0, 100}]
Plot[β[t], {t, t0, tmax}, PlotLabel → "βeta", PlotRange → 1.5]
Plot[β1[t], {t, t0, tmax}, PlotLabel → "βeta1", PlotRange → Automatic]
Plot[β2[t], {t, t0, tmax}, PlotLabel → "βeta2", PlotRange → Automatic]
Plot[α1f[t], {t, t0, tmax}, PlotLabel → "alfa1", PlotRange → Automatic]
Plot[α2f[t], {t, t0, tmax}, PlotLabel → "alfa2", PlotRange → Automatic]
Plot[R[t], {t, t0 + 1, tmax}, PlotLabel → "Raggio", PlotRange → {13, 14}]
Plot[R°[t], {t, t0, tmax}, PlotLabel → "Raggio°", PlotRange → Automatic]
Plot[δ2[t], {t, t0, tmax}, PlotLabel → "Delta 2", PlotRange → Automatic]
Plot[fy1f[t], {t, t0, tmax}, PlotLabel → "Fy1", PlotRange → Automatic]
Plot[fy2f[t], {t, t0, tmax}, PlotLabel → "Fy2", PlotRange → Automatic]
Plot[{Abs[(fy2f[t]/Fz20/2/1.6002547827327125) * 100], Abs[fy1f[t]/Fz10/2/1.5558012353712567 * 100]}, {t, t0, tmax},
PlotLabel → "Fy %", PlotRange → Automatic]
Plot[Abs[(fy2f[t]/Fz20/2/1.6002547827327125) * 100] − Abs[(fy1f[t]/Fz10/2/1.5558012353712567) * 100], {t, t0, tmax},
PlotLabel → "diff %", PlotRange → 50]
```

```
Plot[{Abs[(Y2f[t]/Fz20/2/1.6002547827327125) * 100], Abs[Y1f[t]/Fz10/2/1.5558012353712567 * 100]}, {t, t0, tmax}, PlotLabel → "Y %",
PlotRange → Automatic]
Plot[Abs[(Y2f[t]/Fz20/2/1.6002547827327125) * 100] − Abs[(Y1f[t]/Fz10/2/1.5558012353712567) * 100], {t, t0, tmax},
PlotLabel → "diff Caratteristiche assale %", PlotRange → 50]
"Plot[Drf,{t,t0,tmax},PlotLabel→accImbardata,PlotRange→2.5]"
Plot[fyf[t], {t, t0, tmax}, PlotLabel → "Fy totale", PlotRange → Automatic]
EmitSound[Play[5 * Sin[100 * t^2], {t, 0, 0.2}]]
```

These are commands use to check pneumatic model behavior and axle's characteristic, see Chapter 6.

```
y1g[σ1g_] = d1 * Sin[c1 * ArcTan[b1 * σ1g − e1 * (b1 * σ1g − ArcTan[b1 * σ1g])]];
y2g[σ2g_] = d2 * Sin[c2 * ArcTan[b2 * σ2g − e2 * (b2 * σ2g − ArcTan[b2 * σ2g])]];

yg[σ1g_, σ2g_] = y1g[σ1g] + y2g[σ2g];


N1g[σ1g_, σ2g_] = y1g[σ1g] * a1 − y2g[σ2g] * a2;


Δfz1g[σ1g_, σ2g_] = 1/t1 * (dr1/l * (yg[σ1g, σ2g] * a2 + N1g[σ1g, σ2g]) + kϕ1/kϕt * (h − dr) * yg[σ1g, σ2g]);
Δfz2g[σ1g_, σ2g_] = 1/t2 * (dr2/l * (yg[σ1g, σ2g] * a1 − N1g[σ1g, σ2g]) + kϕ2/kϕt * (h − dr) * yg[σ1g, σ2g]);


Fz12g[σ1g_, σ2g_] = Fz10 + Δfz1g[σ1g, σ2g];
Fz11g[σ1g_, σ2g_] = Fz10 − Δfz1g[σ1g, σ2g];
Fz22g[σ1g_, σ2g_] = Fz20 + Δfz2g[σ1g, σ2g];
Fz21g[σ1g_, σ2g_] = Fz20 − Δfz2g[σ1g, σ2g];


D12g[σ1g_, σ2g_] = (A11 * Fz12g[σ1g, σ2g] + A21) * Fz12g[σ1g, σ2g];
D11g[σ1g_, σ2g_] = (A11 * Fz11g[σ1g, σ2g] + A21) * Fz11g[σ1g, σ2g];
D22g[σ1g_, σ2g_] = (A12 * Fz22g[σ1g, σ2g] + A22) * Fz22g[σ1g, σ2g];
D21g[σ1g_, σ2g_] = (A12 * Fz21g[σ1g, σ2g] + A22) * Fz21g[σ1g, σ2g];


B12g[σ1g_, σ2g_] = A31 * Sin[2 * ArcTan[Fz12g[σ1g, σ2g]/A41]]/(c1 * D12g[σ1g, σ2g]);
B11g[σ1g_, σ2g_] = A31 * Sin[2 * ArcTan[Fz11g[σ1g, σ2g]/A41]]/(c1 * D11g[σ1g, σ2g]);
B22g[σ1g_, σ2g_] = A32 * Sin[2 * ArcTan[Fz22g[σ1g, σ2g]/A42]]/(c1 * D22g[σ1g, σ2g]);
B21g[σ1g_, σ2g_] = A32 * Sin[2 * ArcTan[Fz21g[σ1g, σ2g]/A42]]/(c1 * D21g[σ1g, σ2g]);


Fy12g[σ1g_, σ2g_] = X1 * D12g[σ1g, σ2g] * Sin[c1 * ArcTan[B12g[σ1g, σ2g] * σ1g − e1 * (B12g[σ1g, σ2g] * σ1g − ArcTan[B12g[σ1g, σ2g] * σ1g])]];
Fy11g[σ1g_, σ2g_] = X2 * D11g[σ1g, σ2g] * Sin[c1 * ArcTan[B11g[σ1g, σ2g] * σ1g − e1 * (B11g[σ1g, σ2g] * σ1g − ArcTan[B11g[σ1g, σ2g] * σ1g])]];
Fy22g[σ1g_, σ2g_] = X3 * D22g[σ1g, σ2g] * Sin[c2 * ArcTan[B22g[σ1g, σ2g] * σ2g − e2 * (B22g[σ1g, σ2g] * σ2g − ArcTan[B22g[σ1g, σ2g] * σ2g])]];
Fy21g[σ1g_, σ2g_] = X4 * D21g[σ1g, σ2g] * Sin[c2 * ArcTan[B21g[σ1g, σ2g] * σ2g − e2 * (B21g[σ1g, σ2g] * σ2g − ArcTan[B21g[σ1g, σ2g] * σ2g])]];


Y1g[σ1g_, σ2g_] = (Fy12g[σ1g, σ2g] + Fy11g[σ1g, σ2g]);
Y2g[σ1g_, σ2g_] = (Fy22g[σ1g, σ2g] + Fy21g[σ1g, σ2g]);



diff1[σ1g_, σ2g_] = (Fz12g[σ1g, σ2g] − Fz11g[σ1g, σ2g]);
diff2[σ1g_, σ2g_] = (Fz22g[σ1g, σ2g] − Fz21g[σ1g, σ2g]);
diff3[σ1g_, σ2g_] = (Fy12g[σ1g, σ2g] − Fy11g[σ1g, σ2g]);
diff4[σ1g_, σ2g_] = (Fy22g[σ1g, σ2g] − Fy21g[σ1g, σ2g]);

Plot3D[{Fz11g[σ1g, σ2g], Fz12g[σ1g, σ2g], Fz21g[σ1g, σ2g], Fz22g[σ1g, σ2g]}, {σ1g, 0, σmax}, {σ2g, 0, σmax}, PlotRange → {0, 2000},
PlotLabel → "Fziy", AxesLabel → Automatic]
Plot3D[{Fz11g[σ1g, σ2g], Fz12g[σ1g, σ2g]}, {σ1g, 0, σmax}, {σ2g, 0, σmax}, PlotRange → {0, 2000}, PlotLabel → "Fz1i", AxesLabel → Automatic]
Plot3D[{Fz21g[σ1g, σ2g], Fz22g[σ1g, σ2g]}, {σ1g, 0, σmax}, {σ2g, 0, σmax}, PlotRange → {0, 2000}, PlotLabel → "Fz2i", AxesLabel → Automatic]
```

```
Plot3D[{Fy21g[σ1g, σ2g], Fy22g[σ1g, σ2g]}, {σ1g, 0, σmax}, {σ2g, 0, σmax}, PlotRange → {0, 2000}, PlotLabel → "Fy2i", AxesLabel → Automatic]
Plot3D[{Fz21g[σ1g, σ2g]}, {σ1g, 0, σmax}, {σ2g, 0, σmax}, PlotRange → {0, 2000}, PlotLabel → "Fy21", AxesLabel → Automatic]
Plot3D[{Fy22g[σ1g, σ2g]}, {σ1g, 0, σmax}, {σ2g, 0, σmax}, PlotRange → {0, 2000}, PlotLabel → "Fy22", AxesLabel → Automatic]
Plot3D[{Fy11g[σ1g, σ2g], Fy12g[σ1g, σ2g]}, {σ1g, 0, σmax}, {σ2g, 0, σmax}, PlotRange → {0, 2000}, PlotLabel → "Fy1i", AxesLabel → Automatic]
Plot3D[{Fy11g[σ1g, σ2g]}, {σ1g, 0, σmax}, {σ2g, 0, σmax}, PlotRange → {0, 2000}, PlotLabel → "Fy11", AxesLabel → Automatic]
Plot3D[{Fy12g[σ1g, σ2g]}, {σ1g, 0, σmax}, {σ2g, 0, σmax}, PlotRange → {0, 2000}, PlotLabel → "Fy12", AxesLabel → Automatic]
Plot3D[{diff3[σ1g, σ2g], diff4[σ1g, σ2g]}, {σ1g, 0, σmax}, {σ2g, 0, σmax}, PlotRange → {0, 2000}, PlotLabel → "DiffFyi", AxesLabel → Automatic]
Plot3D[{diff1[σ1g, σ2g], diff2[σ1g, σ2g]}, {σ1g, 0, σmax}, {σ2g, 0, σmax}, PlotRange → {0, 2000}, PlotLabel → "DiffZetai", AxesLabel → Automatic]


Plot3D[{Y1g[σ1g, σ2g], Y2g[σ1g, σ2g]}, {σ1g, 0, σmax}, {σ2g, 0, σmax}, PlotRange → Automatic, PlotLabel → "FYi", AxesLabel → Automatic]
Plot3D[{Y1g[σ1g, σ2g]/Fz101/2, Y2g[σ1g, σ2g]/Fz201/2}, {σ1g, 0, σmax}, {σ2g, 0, σmax}, PlotRange → Automatic,
PlotLabel → "Carratteristiche Assali", AxesLabel → Automatic] MaxValue[Y1g[σ1g, σ2g]/Fz101/2, {σ2g ≥ 0, σ2g < σmax, 0 < σ1g, σ1g ≤ σmax}, {σ
Print["SigmaconiperY1/Fz10Max"]
ArgMax[Y1g[σ1g, σ2g]/Fz101/2, {σ2g ≥ 0, σ2g < σmax, 0 < σ1g, σ1g ≤ σmax}, {σ1g, σ2g}]
Print["Y2/Fz20Max"]
MaxValue[Y2g[σ1g, σ2g]/Fz201/2, {σ1g ≥ 0, σ1g < σmax, 0 < σ2g, σ2g ≤ σmax}, {σ1g, σ2g}]
Print["SigmaconiperY2/Fz20Max"]
ArgMax[Y2g[σ1g, σ2g]/Fz201/2, {σ1g ≥ 0, σ1g < σmax, 0 < σ2g, σ2g ≤ σmax}, {σ1g, σ2g}]
Print["Y1Max"]
MaxValue[Y1g[σ1g, σ2g], {σ2g ≥ 0, σ2g < σmax, 0 < σ1g, σ1g ≤ σmax}, {σ1g, σ2g}]
Print["SigmaconiperY1Max"]
ArgMax[Y1g[σ1g, σ2g], {σ2g ≥ 0, σ2g < σmax, 0 < σ1g, σ1g ≤ σmax}, {σ1g, σ2g}]
Print["Y2Max"]
MaxValue[Y2g[σ1g, σ2g], {σ1g ≥ 0, σ1g < σmax, 0 < σ2g, σ2g ≤ σmax}, {σ1g, σ2g}]
Print["SigmaconiperY2Max"]
ArgMax[Y2g[σ1g, σ2g], {σ1g ≥ 0, σ1g < σmax, 0 < σ2g, σ2g ≤ σmax}, {σ1g, σ2g}]
```

Appendix B: miscellaneous

Shock absorber characteristic.

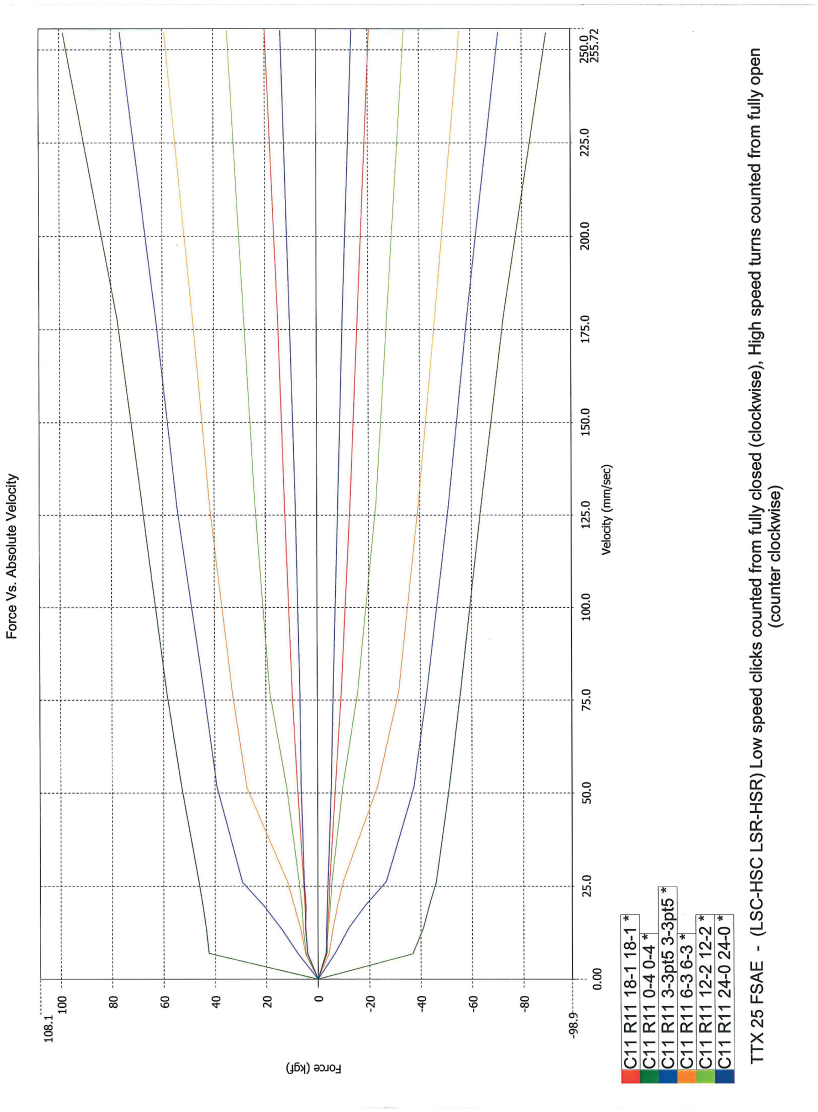

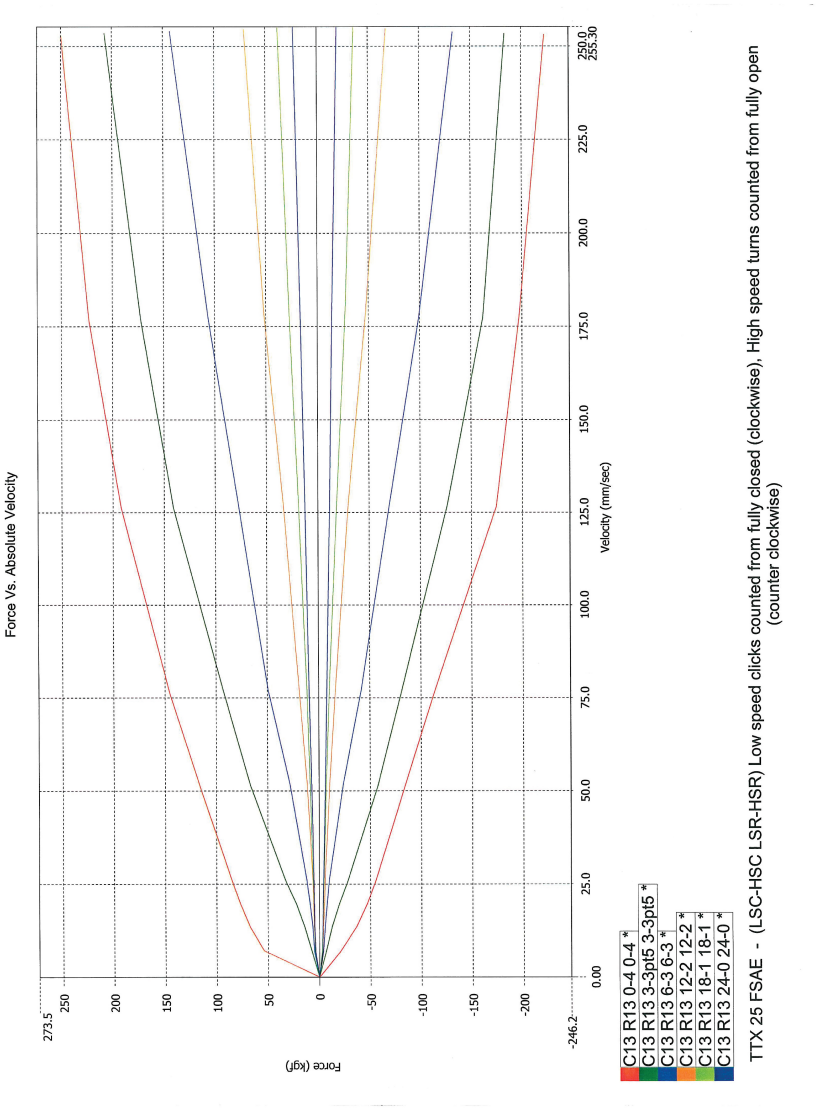
Force Vs. Absolute Velocity
Force (kgf)
273.5
250
200
150
100
50
0
-50
-100
-150
-200
-246.2
0.00
25.0
50.0
75.0
100.0
125.0
150.0
175.0
200.0
225.0
250.0
255.30
Velocity (mm/sec)
C13 R13 0-4 0-4 *
C13 R13 3-3pt5 3-3pt5 *
C13 R13 6-3 6-3 *
C13 R13 12-2 12-2 *
C13 R13 18-1 18-1 *
C13 R13 24-0 24-0 *
TTX 25 FSAE - (LSC-HSC LSR-HSR) Low speed clicks counted from fully closed (clockwise), High speed turns counted from fully open (counter clockwise)

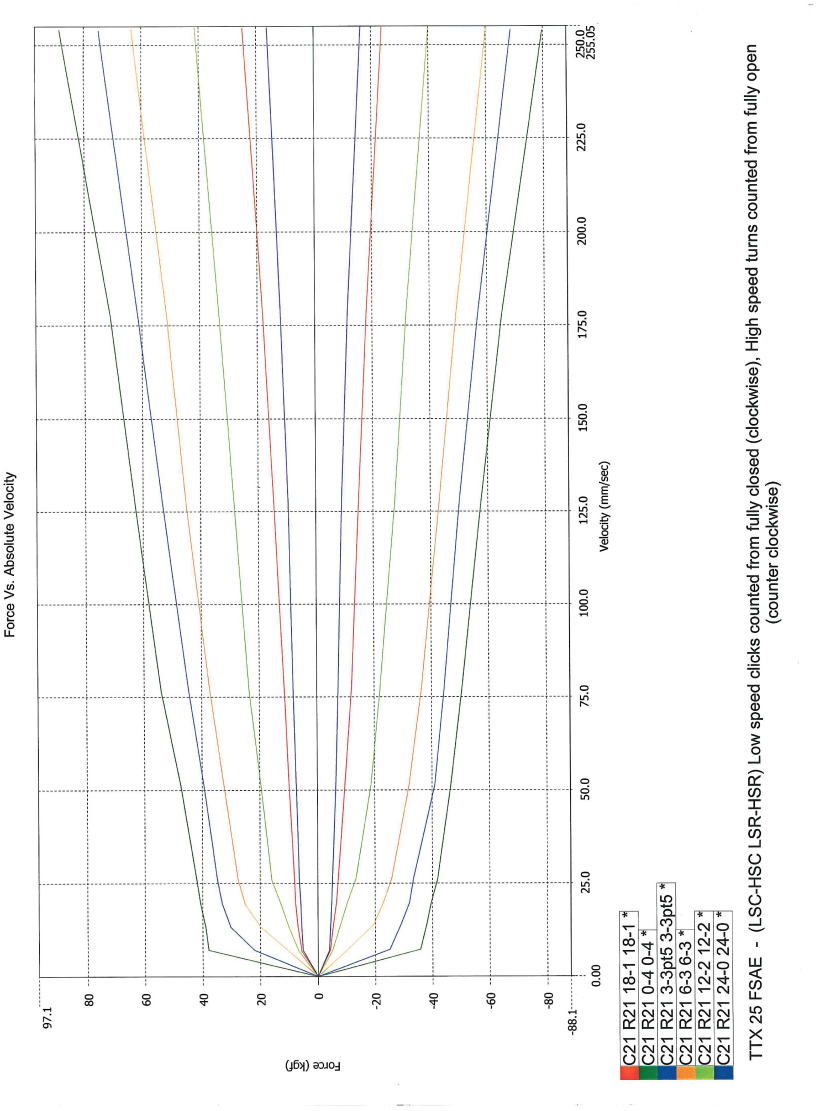
Force Vs. Absolute Velocity
Force (kgf)
97.1
80
60
40
20
0
-20
-40
-60
-80
-88.1
Velocity (mm/sec)
0.00
25.0
50.0
75.0
100.0
125.0
150.0
175.0
200.0
225.0
250.0
255.05
C21 R21 18-1 18-1 *
C21 R21 0-4 0-4 *
C21 R21 3-3pt5 3-3pt5 *
C21 R21 6-3 6-3 *
C21 R21 12-2 12-2 *
C21 R21 24-0 24-0 *
TTX 25 FSAE - (LSC-HSC LSR-HSR) Low speed clicks counted from fully closed (clockwise), High speed turns counted from fully open (counter clockwise)

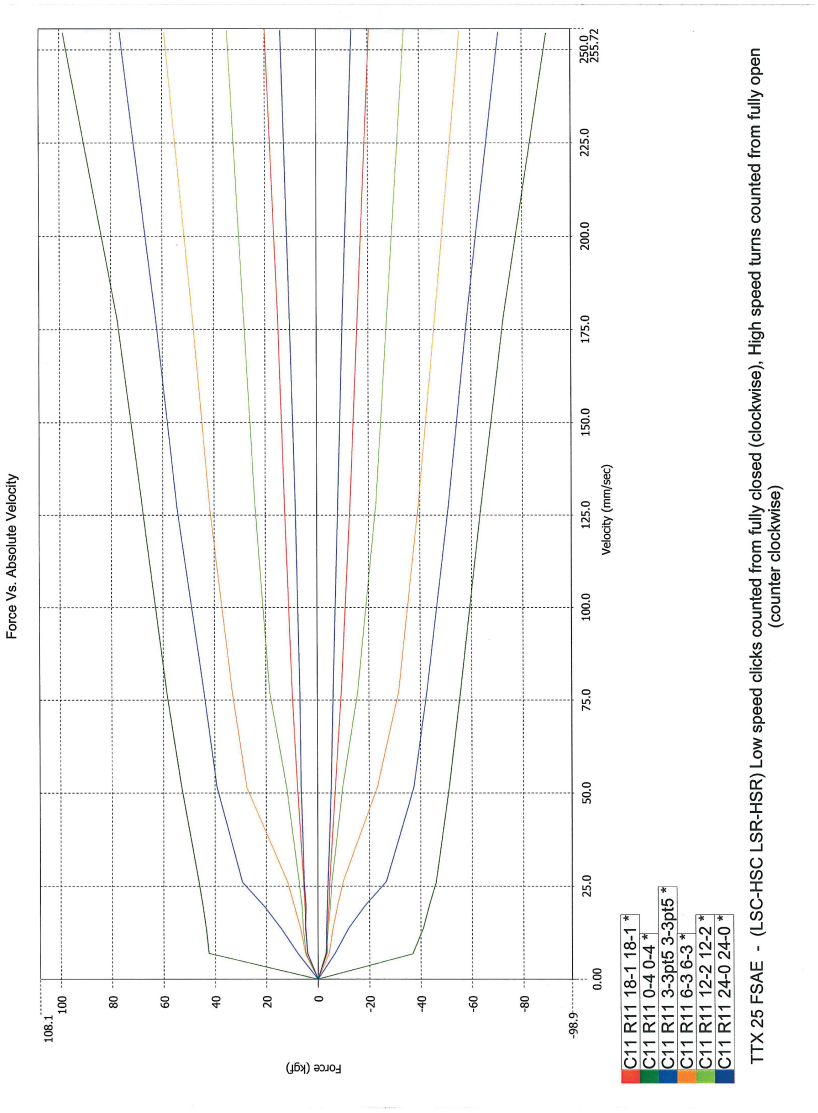
Force Vs. Absolute Velocity
Force (kgf)
108.1
100
80
60
40
20
0
-20
-40
-60
-80
-98.9
0.00
25.0
50.0
75.0
100.0
125.0
150.0
175.0
200.0
225.0
250.0
255.72
Velocity (mm/sec)
C11 R11 18-1 18-1 *
C11 R11 0-4 0-4 *
C11 R11 3-3pt5 3-3pt5 *
C11 R11 6-3 6-3 *
C11 R11 12-2 12-2 *
C11 R11 24-0 24-0 *
TTX 25 FSAE - (LSC-HSC LSR-HSR) Low speed clicks counted from fully closed (clockwise), High speed turns counted from fully open (counter clockwise)

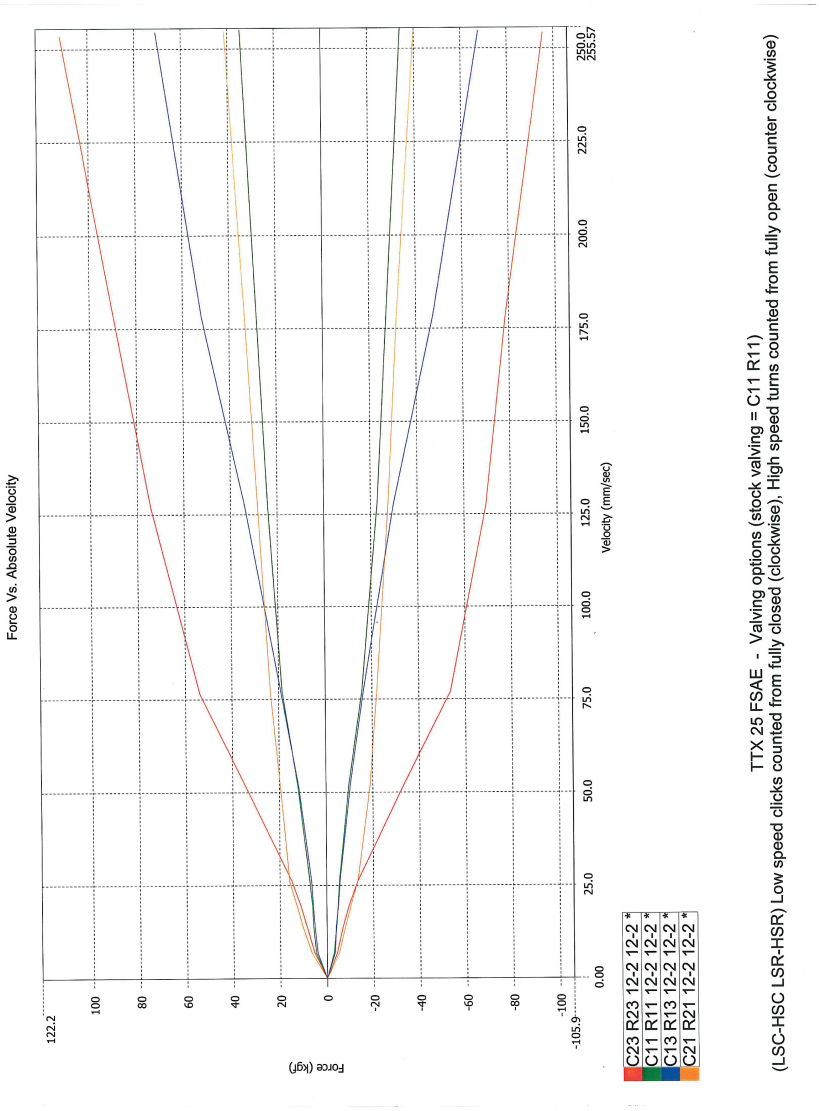

Below bushe's technical sheet.

BOCCOLE ITALIA Srl

MU BOCCOLA AUTOLUBRIFICANTE CON BASE IN ACCIAIO
SELF-LUBRICATING BUSHING WITH STEEL BASE

LEAD FREE

INTRODUZIONE DEL MATERIALE
INTRODUCTION OF MATERIAL

L'articolo è formato da un'armatura in acciaio a basso tenore di carbonio di alta qualità con strato di bronzo poroso sinterizzato intermedio e superficie rivestita dal composto di PTFE e fibra, che ne rende l'utilizzo più pulito e conforme alle esigenze ambientali. Il prodotto viene utilizzato nell'industria automobilistica, delle macchine per la lavorazione dei prodotti alimentari, delle bevande, del tabacco, ecc...

This item is based on high quality low-carbon steel backing with sintered porous bronze in it's interlayer and the compound of PTFE e fibre on it's surface which make the using more clear e environmental. Now it's applied for auto industrial, food machinery industrial, beverage machinery, tobacco machinery, as well as amarium etc...

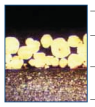

PTFE con fibra
PTFE with fibre
Bronzo poroso
Porous bronze
Armatura in acciaio
Steel backing
Strato di rivestimento
Plating layer

Struttura metallurgica
Metallurgical structure

PROPRIETÀ FISICHE E MECCANICHE
PHYSICAL AND MECHANICAL PROPERTY

Indice di performance / *Performance index*		Dati / *Data*	Indice di performance / *Performance index*		Dati / *Data*
Capacità di carico P Load capacity P	Carico statico Static load	250 N/mm²	Coefficiente di attrito Friction coef. μ	Attrito a secco Dry friction	0.08~0.20
	Carico dinamico Dynamic load	140 N/mm²		Lubrificazione ad olio Oil lubrication	0.02~0.07
Velocità lineare max. V Max line speed V	Attrito a secco Dry friction	2.5 m/s	Temperatura di lavoro Working temperature		-200°C ~ +280°C
	Lubrificazione ad olio Oil lubrication	5 m/s	Conducibilità termica Thermal conductivity		42 W/m · k
Limite valore PV PV value limit	Attrito a secco Dry friction	3.6 N/mm².m/s	Coefficiente di dilatazione lineare Coefficient of linear expansion		11 × 10⁻⁶/K
	Lubrificazione ad olio Oil lubrication	50 N/mm².m/s			

MUB BOCCOLA AUTOLUBRIFICANTE CON BASE IN BRONZO
SELF-LUBRICATING BUSHING WITH BRONZE BASE

LEAD FREE

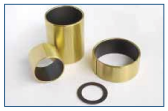

INTRODUZIONE DEL MATERIALE
INTRODUCTION OF MATERIAL

Il prodotto è formato da un rame speciale ad alta densità con uno strato di bronzo poroso sinterizzato intermedio e superficie rivestita dal composto di PTFE fibroso. Presenta buone proprietà di autolubrificazione, anti-abrasione, basso attrito, sviluppando in pieno i vantaggi del polimero multi-elemento e metallo.

It's made of high density special copper with sintered porous bronze in its interlayer and the compound of PTFE with fibre on its surface. It can offer good properties of self-lubricating, anti abrasion, low-friction, fully developing the advantages of metal and multi-element polymer. The product is applied to metallurgical industry, continuous casting and rolling mill, concrete machinery and spiral conveyers, etc.

PTFE con fibra
PTFE with fibre
Bronzo poroso
Porous bronze
Armatura in bronzo
Bronze backing

Struttura metallurgica
Metallurgical structure

PROPRIETÀ FISICHE E MECCANICHE
PHYSICAL AND MECHANICAL PROPERTY

Indice di performance / *Performance index*		Dati / *Data*	Indice di performance / *Performance index*		Dati / *Data*
Capacità di carico P Load capacity P	Carico statico Static load	250 N/mm²	Coefficiente di attrito Friction coef. μ	Attrito a secco Dry friction	0.08~0.20
	Carico dinamico Dynamic load	140 N/mm²		Lubrificazione ad olio Oil lubrication	0.02~0.07
Velocità lineare max. V Max line speed V	Attrito a secco Dry friction	2 m/s	Temperatura di lavoro Working temperature		-200°C~+280°C
	Lubrificazione ad olio Oil lubrication	5 m/s	Conducibilità termica Thermal conductivity		60 W m • k
Limite valore PV PV value limit	Attrito a secco Dry friction	3.6 N/mm².m/s	Coefficiente di dilatazione lineare Coefficient of linear expansion		18 × 10⁻⁶K
	Lubrificazione ad olio Oil lubrication	50 N/mm².m/s			

BOCCOLE ITALIA Srl

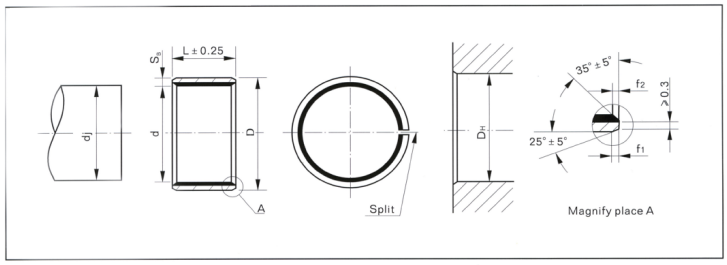

ESEMPIO D'ORDINE: *ORDERING EXAMPLE:*

Codice Prodotto Part Number	Φd	ΦD	L
MU - 0303			3
MU - 0305	3	4.5	5
MU - 0306			6
MU - 0403			3
MU - 0404	4	5.5	4
MU - 0406			6
MU - 0410			10
MU - 0505			5
MU - 0508	5	7	8
MU - 0510			10
MU - 0604			4
MU - 0606	6	8	6
MU - 0608			8
MU - 0610			10
MU - 0710	7	9	10
MU - 0806			6
MU - 0808	8	10	8
MU - 0810			10
MU - 0812			12
MU - 1008			8
MU - 1010			10
MU - 1012	10	12	12
MU - 1015			15
MU - 1020			20
MU - 1208			8
MU - 1210			10
MU - 1212	12	14	12
MU - 1215			15
MU - 1220			20
MU - 1225			25
MU - 1310	13	15	10
MU - 1320			20
MU - 1405	14	16	5
MU - 1410			10

Codice Prodotto Part Number	Φd	ΦD	L
MU - 1412			12
MU - 1415	14	16	15
MU - 1420			20
MU - 1425			25
MU - 1510			10
MU - 1512			12
MU - 1515	15	17	15
MU - 1520			20
MU - 1525			25
MU - 1610			10
MU - 1612			12
MU - 1615	16	18	15
MU - 1620			20
MU - 1625			25
MU - 1712	17	19	12
MU - 1720			20
MU - 1810			10
MU - 1815	18	20	15
MU - 1820			20
MU - 1825			25
MU - 2010			10
MU - 2015			15
MU - 2020	20	23	20
MU - 2025			25
MU - 2030			30
MU - 2215			15
MU - 2220	22	25	20
MU - 2225			25
MU - 2230			30
MU - 2415			15
MU - 2420	24	27	20
MU - 2425			25
MU - 2430			30
MU - 2515	25	28	15

BOCCOLE ITALIA Srl

Codice Prodotto Part Number	Φd	ΦD	L
MU - 2520			20
MU - 2525			25
MU - 2530	25	28	30
MU - 2540			40
MU - 2550			50
MU - 2815			15
MU - 2820	28	32	20
MU - 2825			25
MU - 2830			30
MU - 3010			10
MU - 3015			15
MU - 3020	30	34	20
MU - 3025			25
MU - 3030			30
MU - 3040			40
MU - 3220			20
MU - 3230	32	36	30
MU - 3240			40
MU - 3520			20
MU - 3530			30
MU - 3535	35	39	35
MU - 3540			40
MU - 3550			50
MU - 3720	37	41	20
MU - 4020			20
MU - 4030	40	44	30
MU - 4040			40
MU - 4050			50
MU - 4520			20
MU - 4530			30
MU - 4540	45	50	40
MU - 4545			45
MU - 4550			50
MU - 5020			20
MU - 5030			30
MU - 5040	50	55	40
MU - 5050			50
MU - 5060			60
MU - 5520			20
MU - 5525			25
MU - 5530			30
MU - 5540	55	60	40
MU - 5550			50
MU - 5555			55
MU - 5560			60
MU - 6020			20
MU - 6030			30
MU - 6040	60	65	40
MU - 6050			50
MU - 6060			60
MU - 6070			70
MU - 6530	65	70	30

Codice Prodotto Part Number	Φd	ΦD	L
MU - 6550	65	70	50
MU - 6570			70
MU - 7040			40
MU - 7050	70	75	50
MU - 7070			70
MU - 7550			50
MU - 7560	75	80	60
MU - 7580			80
MU - 8060	80	85	60
MU - 80100			100
MU - 8530			30
MU - 8560	85	90	60
MU - 85100			100
MU - 9060	90	95	60
MU - 90100			100
MU - 9560	95	100	60
MU - 95100			100
MU - 10050			50
MU - 10060	100	105	60
MU - 100115			115
MU - 10560	105	110	60
MU - 105115			115
MU - 11060	110	115	60
MU - 110115			115
MU - 11550	115	120	50
MU - 11570			70
MU - 12050			50
MU - 12060	120	125	60
MU - 120100			100
MU - 120120			120
MU - 125100	125	130	100
MU - 13060	130	135	60
MU - 130100			100
MU - 13560	135	140	60
MU - 13580			80
MU - 14060			60
MU - 140100	140	145	100
MU - 140120			120
MU - 15060			60
MU - 15080	150	155	80
MU - 150100			100
MU - 16080	160	165	80
MU - 160100			100
MU - 18080	180	185	80
MU - 180100			100
MU - 200100	200	205	100
MU - 210100	210	215	100
MU - 220100	220	225	100
MU - 250100	250	255	100
MU - 28080	280	285	80
MU - 300100	300	305	100

Appendix C: technical drawings

Only not standard parts with the exception of schock absorbers.

Part number and name	function and attributes if necessary	page number
1-toe arm insert	con. between toe arm and frame	127
2-toe arm inert two	//	128
3 -back-up insert	support for back-up bar	129
4-c. fiber pipes insert	carbon fiber- rod ends con.	130
5-frame supports	rod ends frame con.	131
6-rocker support	rocker-frame con.	132
7-shimming frame support	-	133
8-toe arm shimming	-	134
9-rocker shimming	-	135
10-roll-bar arms	regolable arm to chose roll-stiffnes	136
11-roll-bars	regolable bars to chose roll-stiffnes	137
12-roll-bars support	con. between frame and roll-bars	138
13-triangle insert: rear-low	con. between up c. pipes and up rights	139
14-triangle insert: rear-up	con. between low c. pipes and up rights	140
15-rear rocker	harmonize spring ratio and roll-bars stiffnes	141
16-triangle insert: front-low	con. between up c. pipes and uprights	142
17-triangle insert: front-up	con. between low c. pipes and uprights	143
18-rocker front	harmonize spring ratio and roll-bars stiffnes	144
19-schock absorber (no springs)	manufacturer informations	145
steering-system	not displayed because of private GreenTeam know-how	/

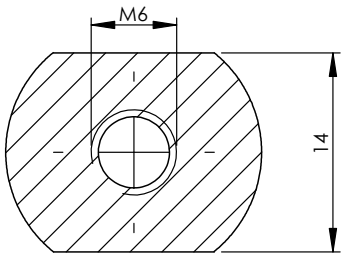

SEZIONE C-C

SEZIONE A-A

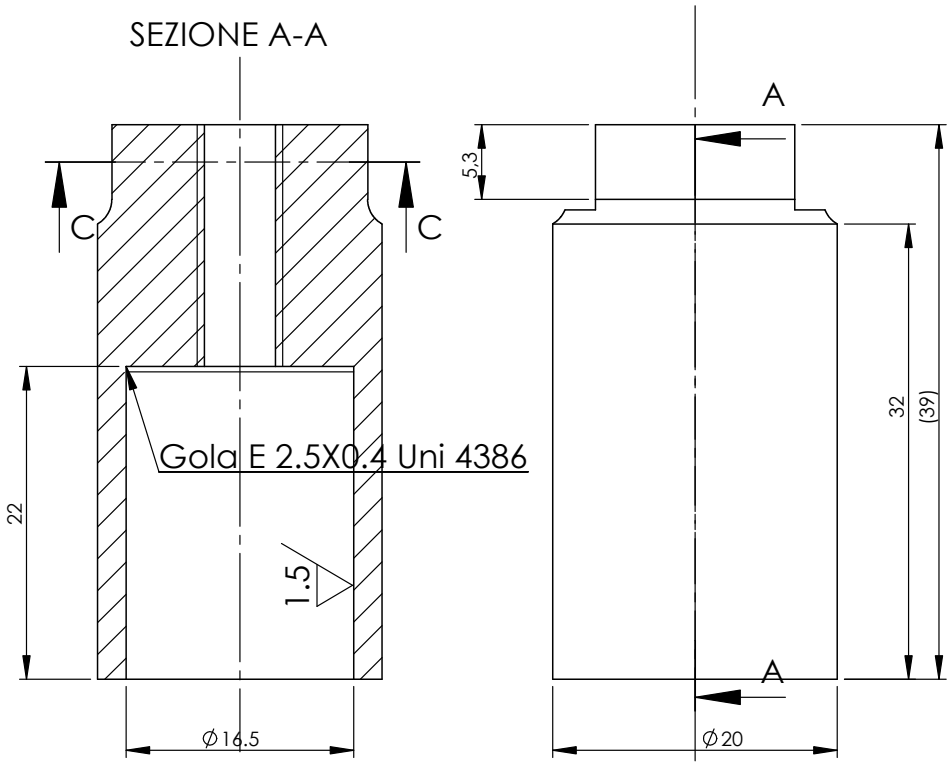

Raggi non quotati R=2.

SE NON SPECIFICATO: QUOTE IN MILLIMETRI FINITURA SUPERFICIE: TOLLERANZE: LINEARE: UNI EN 22768/2 H ANGOLARE:	FINITURA: 3 / (1.5 /)	NON SCALARE IL DISEGNO	REVISIONE
	NOME	TITOLO:	
DISEGNATO	Paolo Di Sacco	Toe arms insert	
VERIFICATO			
APPROVATO			
FATTO			
QUALITA'		MATERIALE: Al 7075	N. DISEGNO 1
			A4
			pag. 127
		SCALA:2:1	

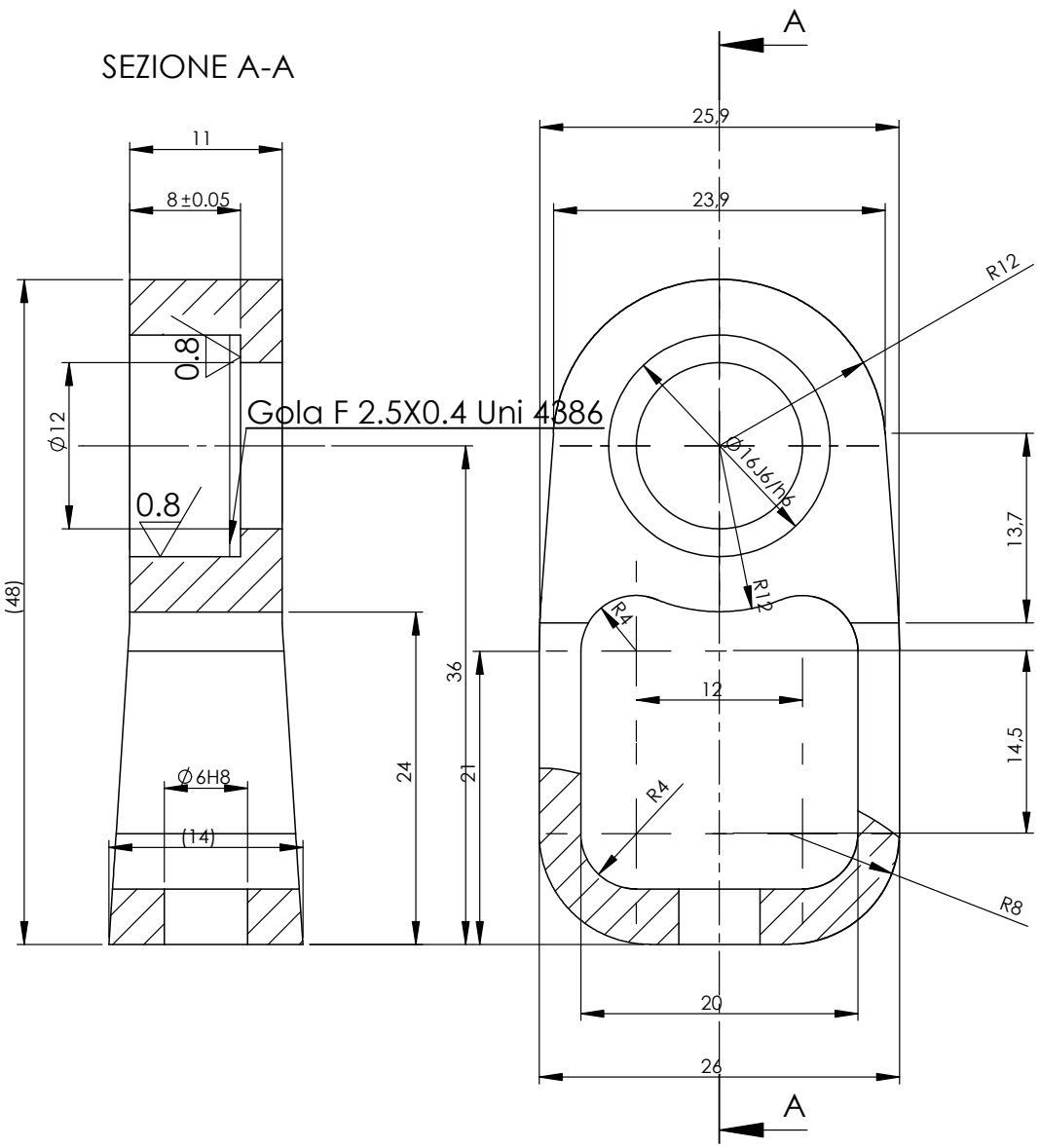

Raggi non quotati R=1.

SE NON SPECIFICATO: QUOTE IN MILLIMETRI FINITURA SUPERFICIE: TOLLERANZE: LINEARE: UNI EN 22768/2 H ANGOLARE:	FINITURA: 2.4 / (0.8 /)	NON SCALARE IL DISEGNO	REVISIONE
	NOME	TITOLO:	
DISEGNATO	Paolo Di Sacco	Toe arm insert 2	
VERIFICATO			
APPROVATO			
FATTO			
QUALITA'		MATERIALE: Al 7075	N. DISEGNO 2
			A4
		SCALA:2:1	FOGLIO 1 DI 1

SEZIONE A-A

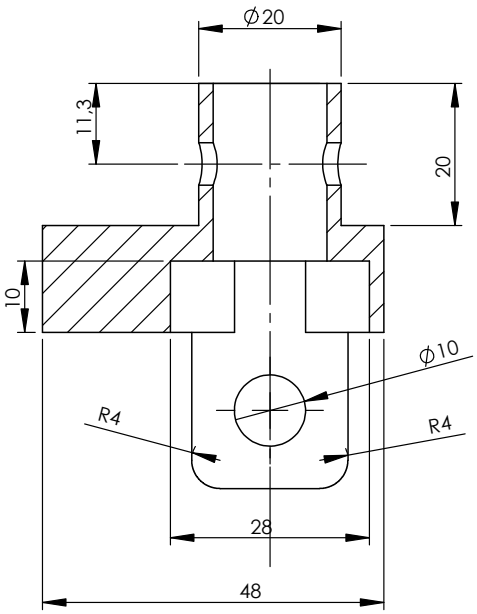

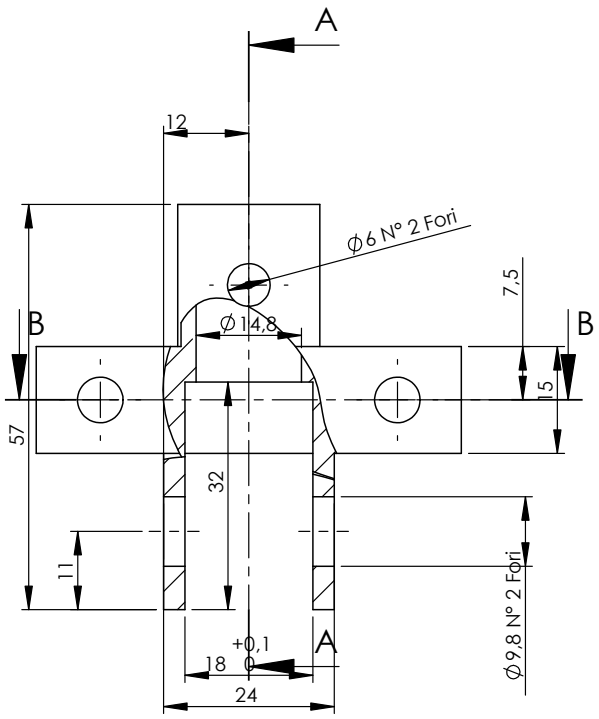

SEZIONE B-B

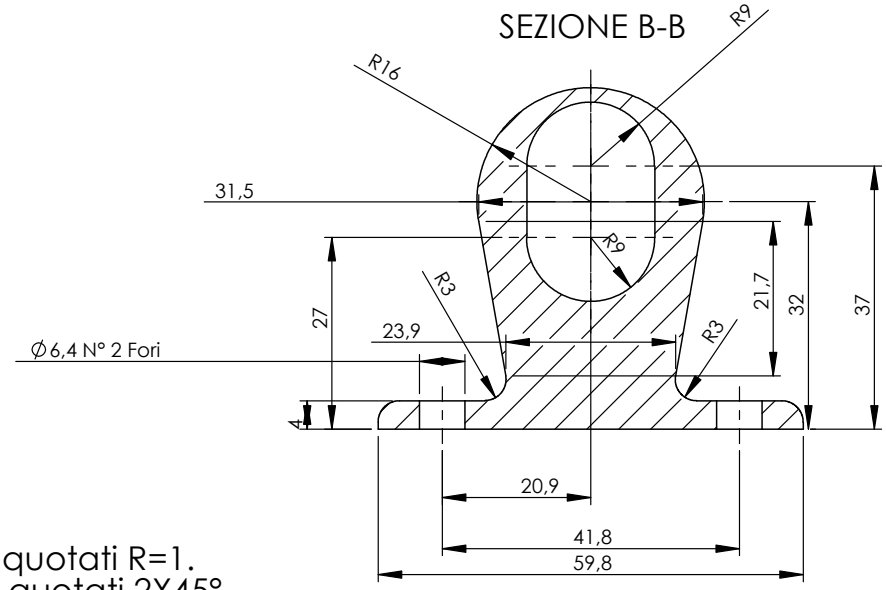

Raggi non quotati R=1.
Smussi non quotati 2X45°

SE NON SPECIFICATO: QUOTE IN MILLIMETRI FINITURA SUPERFICIE: TOLLERANZE: LINEARE: UNI EN 22768/2 H ANGOLARE:	FINITURA: 2.4	SBAVATURA E INTERRUZIONE DEI BORDI NETTI	NON SCALARE IL DISEGNO / REVISIONE
NOME			TITOLO: Back-up support
DISEGNATO	Paolo Di Sacco		
VERIFICATO			
APPROVATO			
FATTO			
QUALITA'		MATERIALE: Al 7075	N. DISEGNO 3 — A4
			SCALA:1:1 — FOGLIO 1 DI 1

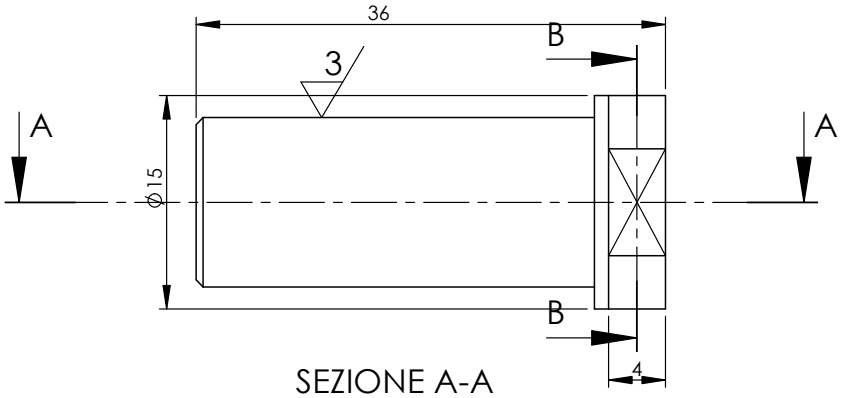

SEZIONE B-B

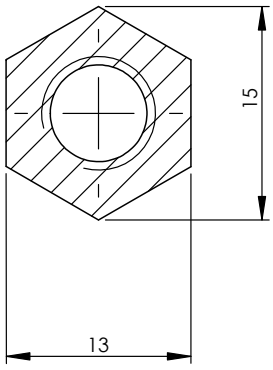

SEZIONE A-A

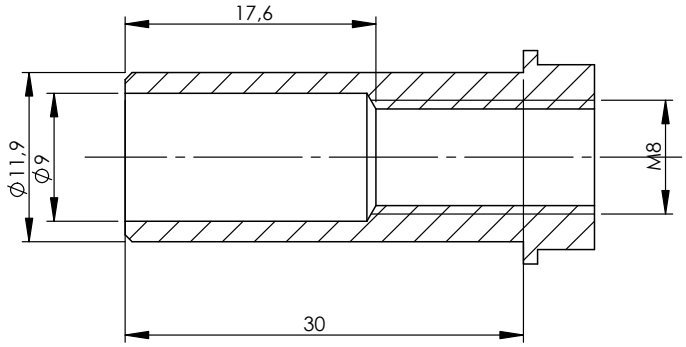

Raggi non quotati R=0.5.
Smussi non quotati 0.5X45°.

SE NON SPECIFICATO: QUOTE IN MILLIMETRI FINITURA SUPERFICIE: TOLLERANZE: LINEARE: UNI EN 22768/2 H ANGOLARE:	FINITURA: 3 ( )	SBAVATURA E INTERRUZIONE DEI BORDI NETTI	NON SCALARE IL DISEGNO / REVISIONE
NOME			TITOLO:
DISEGNATO	Paolo Di Sacco		Carbon fiber pipes insert
VERIFICATO			
APPROVATO			
FATTO			
QUALITA'		MATERIALE: Al 7075	N. DISEGNO 4 — A4
			pag. 130
		SCALA:2:1	FOGLIO 1 DI 1

SEZIONE C-C

SEZIONE A-A

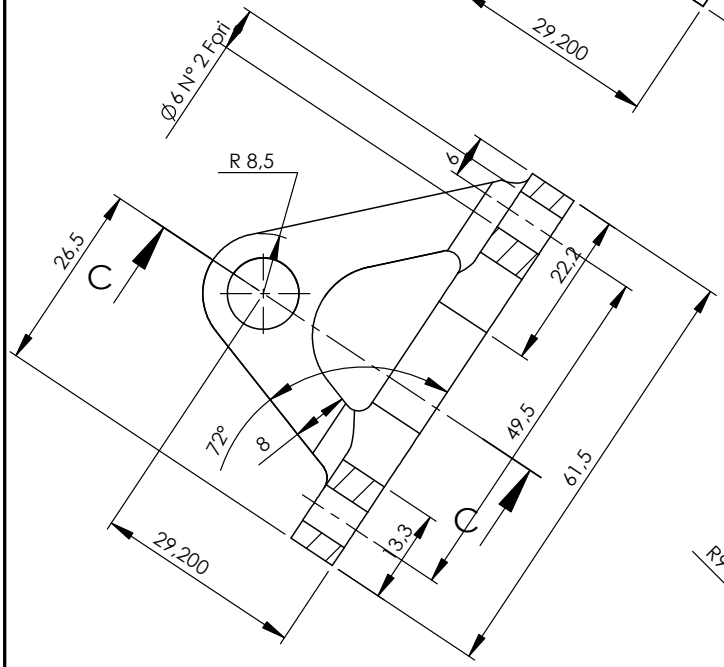

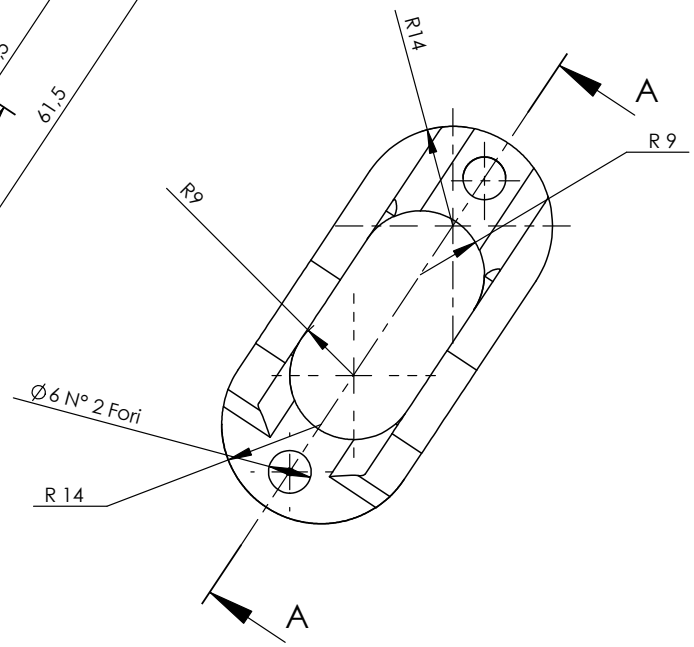

Raggi non quotati R=1.5 .
Smussi non quotati 1X45°.

SE NON SPECIFICATO: QUOTE IN MILLIMETRI FINITURA SUPERFICIE: TOLLERANZE: LINEARE: UNI EN 22768/2 H ANGOLARE:	FINITURA: $\sqrt{4.8}$ ($\sqrt{1.2}$)	SBAVATURA E INTERRUZIONE DEI BORDI NETTI	NON SCALARE IL DISEGNO / REVISIONE

	NOME				TITOLO:
DISEGNATO	Paolo Di Sacco				Frame support
VERIFICATO					
APPROVATO					
FATTO					
QUALITA'		MATERIALE:	N. DISEGNO		A4
		Al 7075	5		pag. 131
			SCALA:1:1	FOGLIO 1 DI 1	

SEZIONE C-C

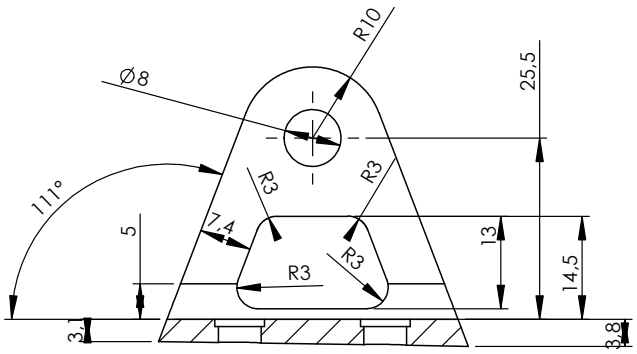

SEZIONE D-D

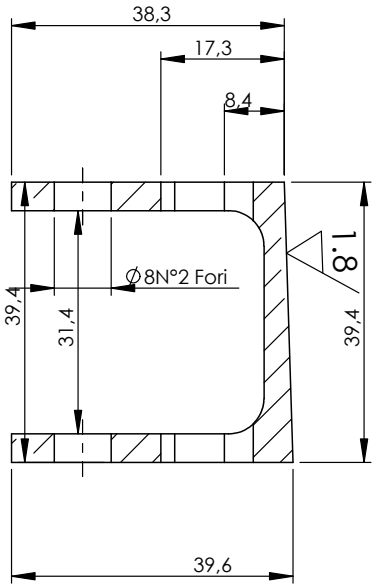

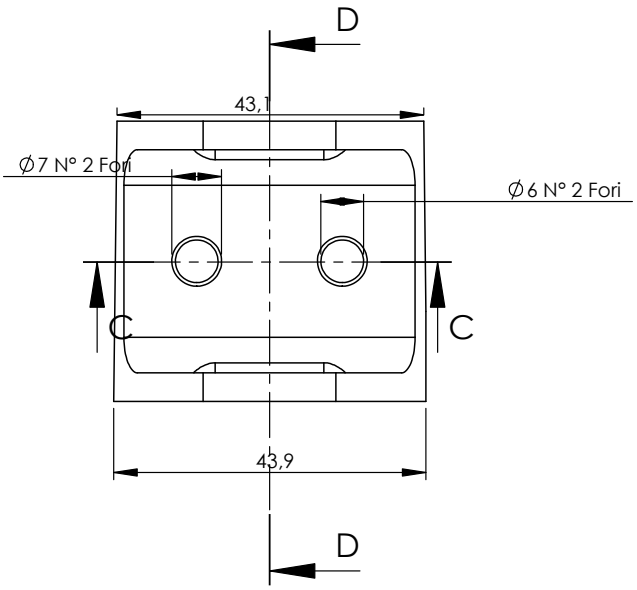

Raggi non quotati R=2 .
Smussi non quotati 1X45° .

SE NON SPECIFICATO: QUOTE IN MILLIMETRI FINITURA SUPERFICIE: TOLLERANZE: LINEARE: UNI EN 22768/2 H ANGOLARE:	FINITURA: 2.4 / (1.8 /)	SBAVATURA E INTERRUZIONE DEI BORDI NETTI	NON SCALARE IL DISEGNO / REVISIONE
NOME			TITOLO:
DISEGNATO	Paolo Di Sacco		Rocker support
VERIFICATO			
APPROVATO			
FATTO			
QUALITA'		MATERIALE: Al 7075	N. DISEGNO 6 / A4
			SCALA:1:1 / FOGLIO 1 DI 1

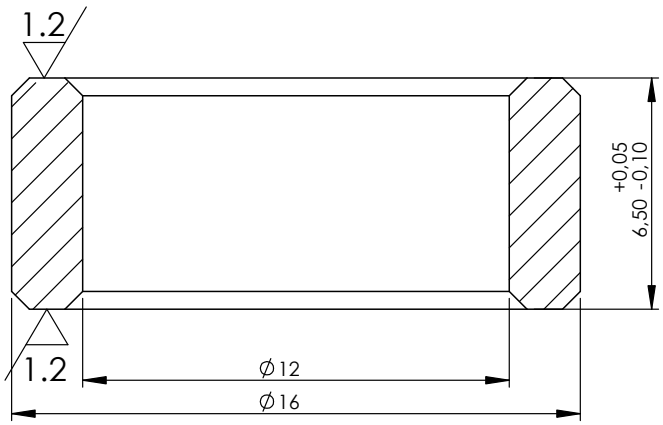

Smussi non quotati 0.5X45° .

SE NON SPECIFICATO: QUOTE IN MILLIMETRI FINITURA SUPERFICIE: TOLLERANZE: LINEARE: UNI EN 22768/2 H ANGOLARE:	FINITURA: (1.2)	SBAVATURA E INTERRUZIONE DEI BORDI NETTI	NON SCALARE IL DISEGNO / REVISIONE
NOME			TITOLO:
DISEGNATO	Paolo Di Sacco		Shimming frame support
VERIFICATO			
APPROVATO			
FATTO			
QUALITA'		MATERIALE: Al 7075	N. DISEGNO 7 — A4
			SCALA:5:1 — FOGLIO 1 DI 1

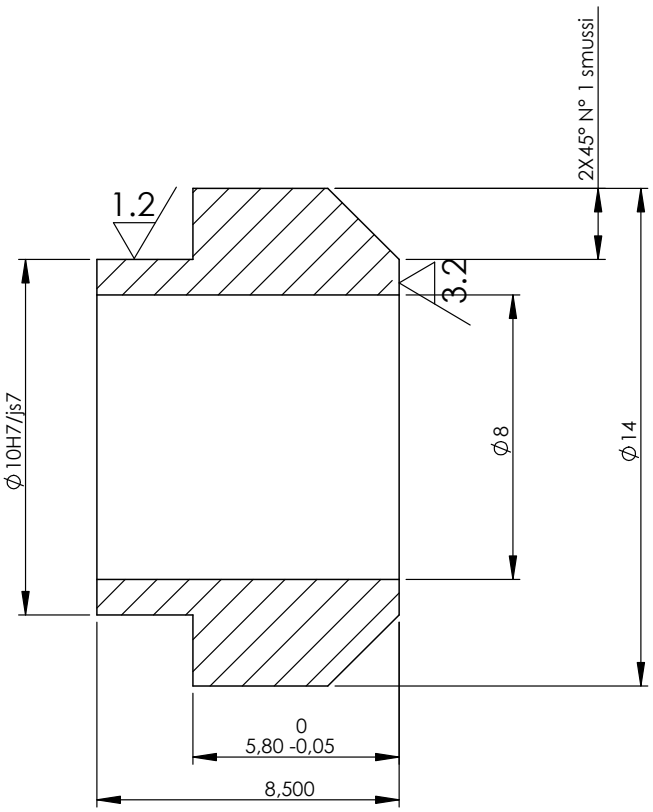

Smussi non quotati 2X45° .

Raccordi non quotati R=0.5 .

SE NON SPECIFICATO: QUOTE IN MILLIMETRI FINITURA SUPERFICIE: TOLLERANZE: LINEARE: UNI EN 22768/2 H ANGOLARE:	FINITURA: (1.2 , 3.2)	SBAVATURA E INTERRUZIONE DEI BORDI NETTI	NON SCALARE IL DISEGNO / REVISIONE
NOME			TITOLO:
DISEGNATO	Paolo Di Sacco		Toe arm shimming
VERIFICATO			
APPROVATO			
FATTO			
QUALITA'		MATERIALE: Al 7075	N. DISEGNO 8
			A4
			pag. 134
		SCALA:5:1	FOGLIO 1 DI 1

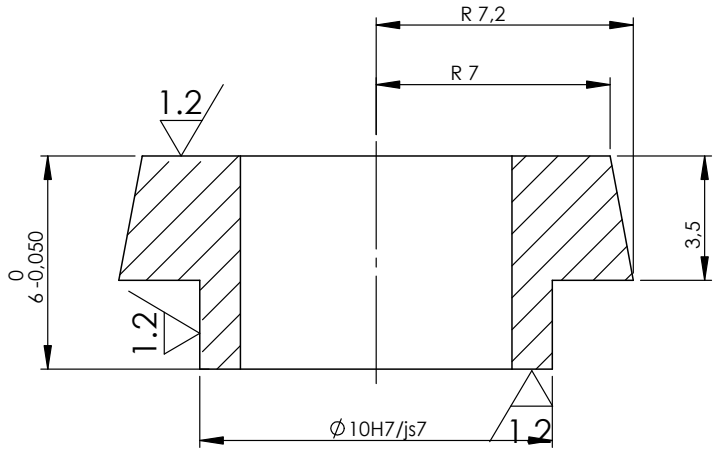

Raccordi non quotati R=0.5 .

SE NON SPECIFICATO: QUOTE IN MILLIMETRI FINITURA SUPERFICIE: TOLLERANZE: LINEARE: UNI EN 22768/2 H ANGOLARE:	FINITURA: 1.2 ( )	SBAVATURA E INTERRUZIONE DEI BORDI NETTI	NON SCALARE IL DISEGNO / REVISIONE
NOME			TITOLO: Rocker shimming
DISEGNATO	Paolo Di Sacco		
VERIFICATO			
APPROVATO			
FATTO			
QUALITA'		MATERIALE: Al 7075	N. DISEGNO 9 / A4
			pag. 135
		SCALA:5:1	FOGLIO 1 DI 1

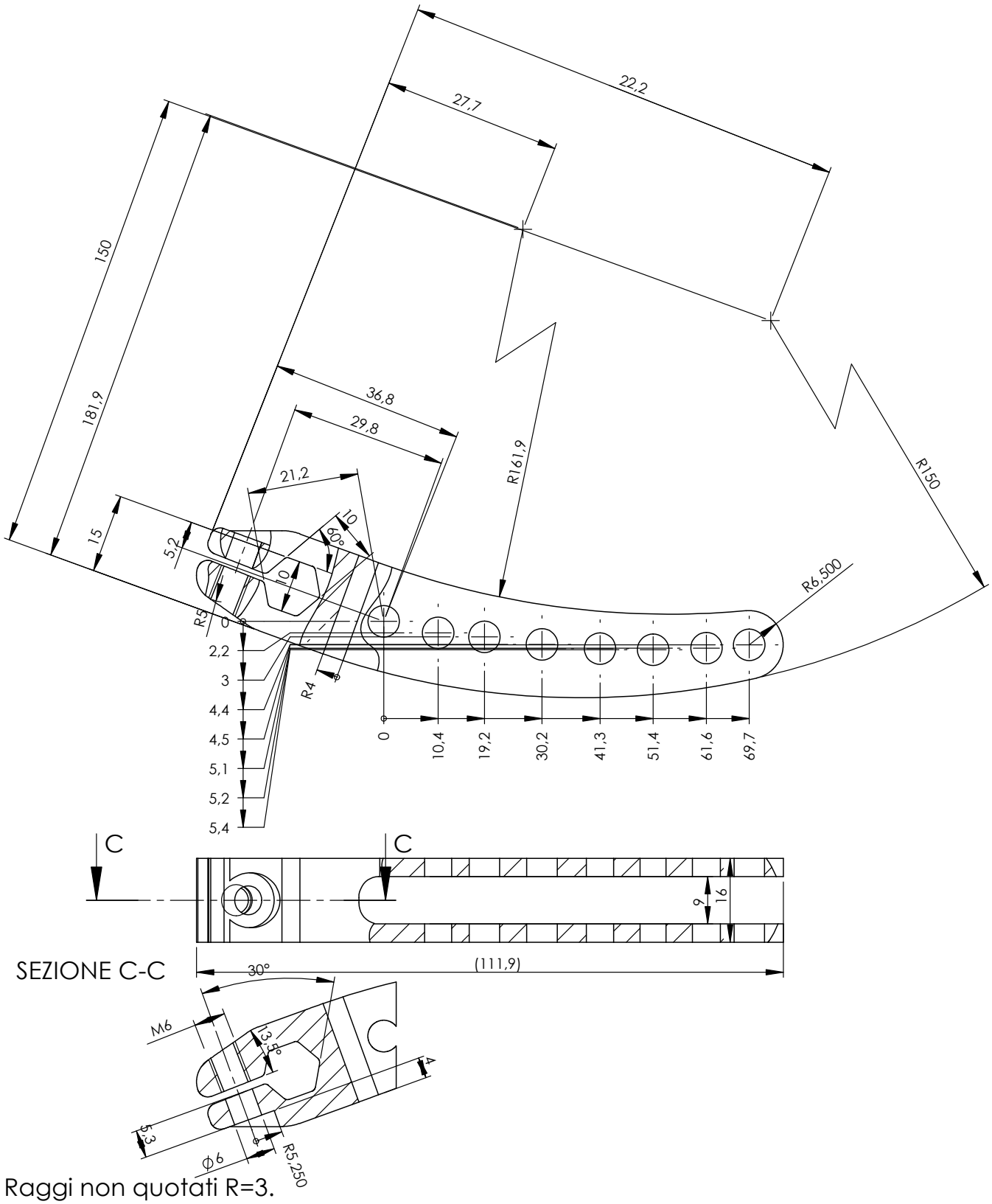

Raggi non quotati R=3.

SE NON SPECIFICATO: QUOTE IN MILLIMETRI FINITURA SUPERFICIE: TOLLERANZE: LINEARE: UNI EN 22768/2 H ANGOLARE:	FINITURA: 1.2	SBAVATURA E INTERRUZIONE DEI BORDI NETTI	NON SCALARE IL DISEGNO / REVISIONE

	NOME	TITOLO:
DISEGNATO	Paolo Di Sacco	Roll-bar arm
VERIFICATO		
APPROVATO		
FATTO		
QUALITA'	MATERIALE: Al 7075/C40	N. DISEGNO 10

A4

SCALA:1:2 | FOGLIO 1 DI 1

SEZIONE A-A
SCALA 1 : 2

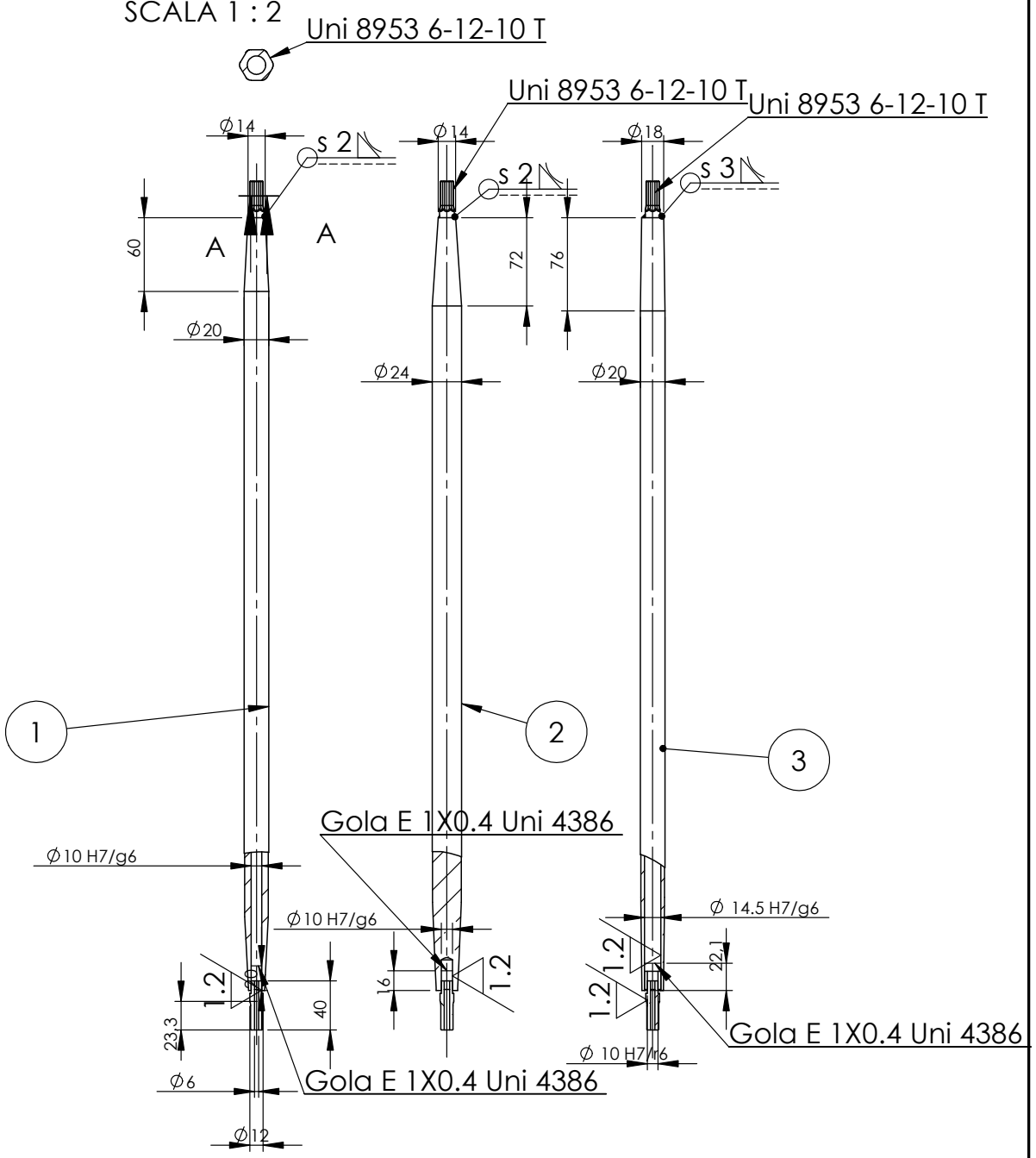

Smussi non quotati 0.5X45°.
Raccordi non quotati R=0.5 .

Lunghezza barre complessiva 630 mm
barra 1 rigida barra 2 morbida barra 3 intermedia.(1=C 40, 2=Al 3003, 3= C40.)

SE NON SPECIFICATO: QUOTE IN MILLIMETRI FINITURA SUPERFICIE: TOLLERANZE: LINEARE: UNI EN 22768/2 H ANGOLARE:	FINITURA: 2.4 / 1.2 ( )	SBAVATURA E INTERRUZIONE DEI BORDI NETTI	NON SCALARE IL DISEGNO / REVISIONE
NOME			TITOLO:
DISEGNATO: Paolo Di Sacco			Roll-bars
VERIFICATO			
APPROVATO			
FATTO			
QUALITA'	MATERIALE: Al 7075/C40		N. DISEGNO: 11 — A4
SCALA:1:10	FOGLIO 1 DI 1		

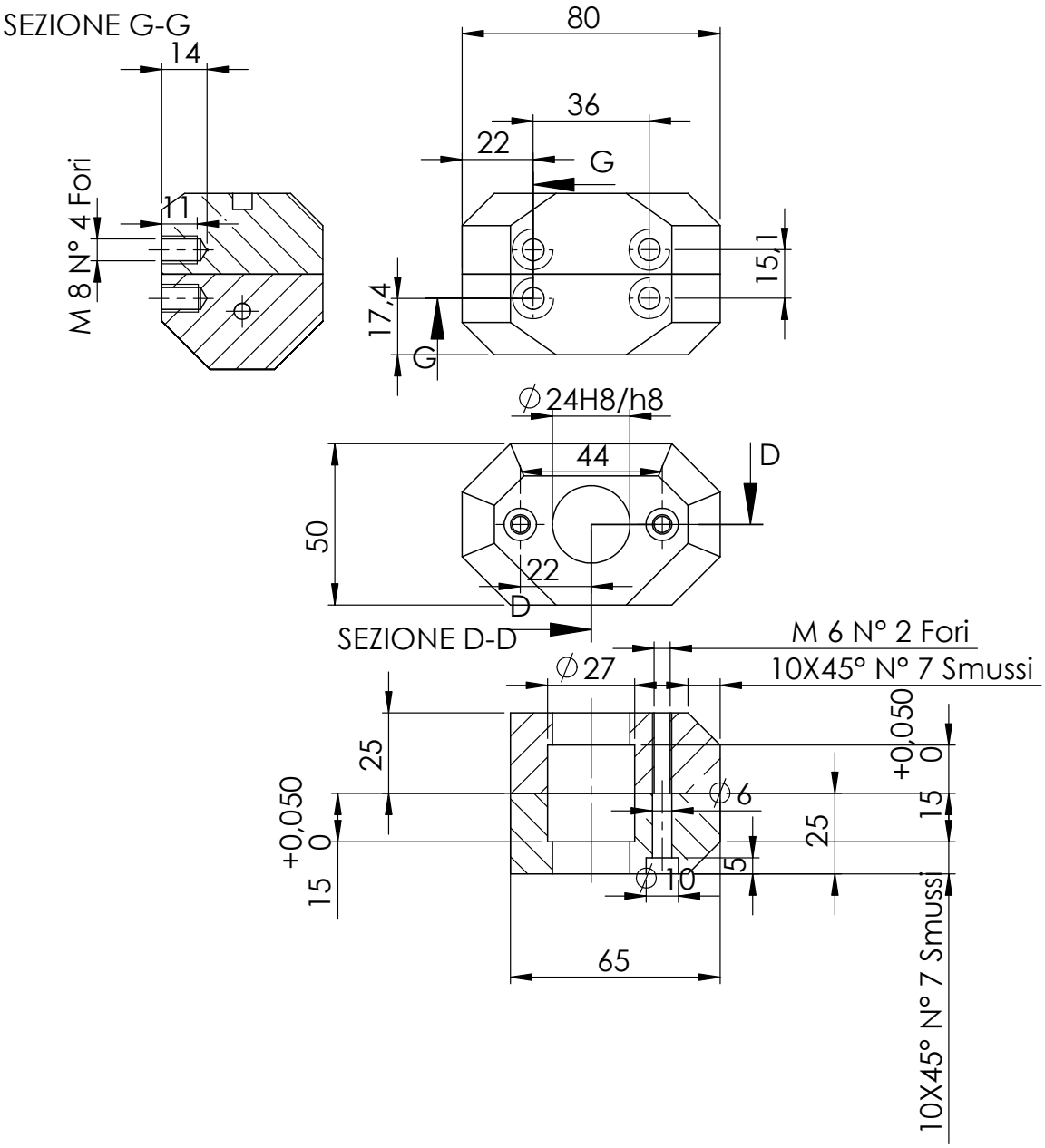

SE NON SPECIFICATO: QUOTE IN MILLIMETRI FINITURA SUPERFICIE: TOLLERANZE: LINEARE: UNI EN 22768/2 H ANGOLARE:	FINITURA: 2.4	SBAVATURA E INTERRUZIONE DEI BORDI NETTI	NON SCALARE IL DISEGNO / REVISIONE
NOME			TITOLO:
DISEGNATO	Paolo Di Sacco		Roll-bars supports
VERIFICATO			
APPROVATO			
FATTO			
QUALITA'		MATERIALE: Al 7075	N. DISEGNO 12 / A4
			SCALA:1:2 / FOGLIO 1 DI 1

SEZIONE D-D

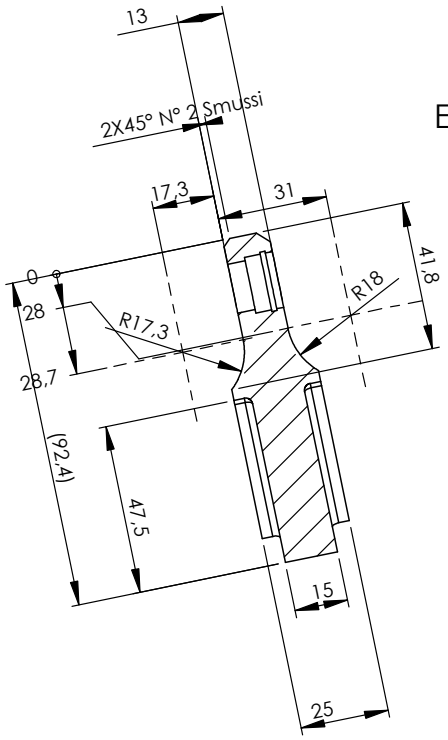

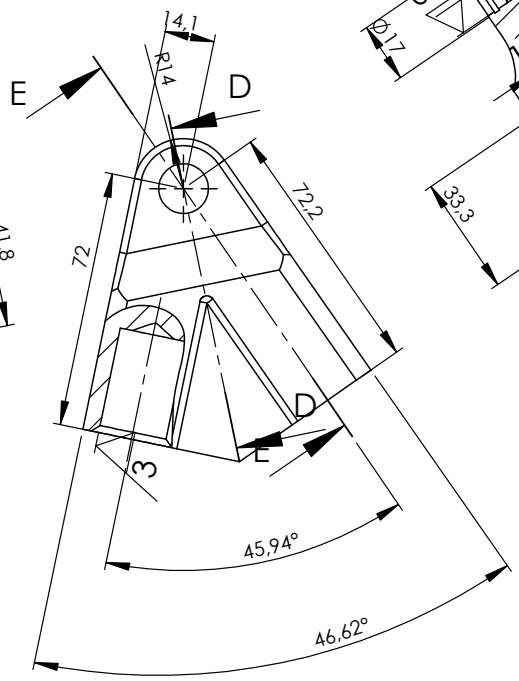

SEZIONE E-E

Gola E 0.2X0.6 Uni 4386

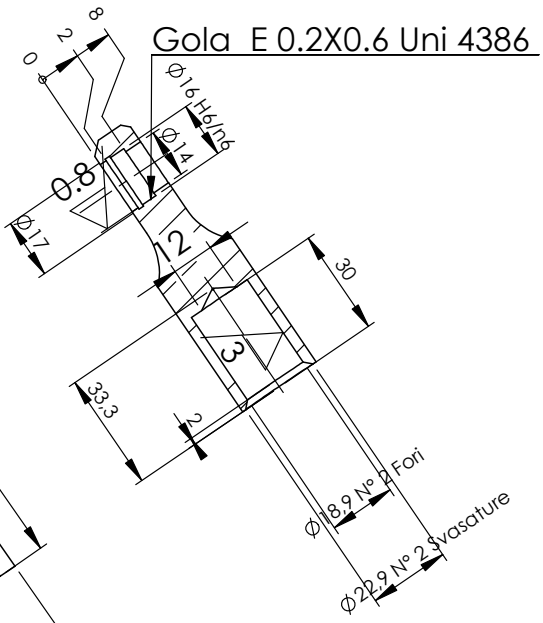

Smussi non quotati 4X45°.
Raccordi non quotati R=3.

SE NON SPECIFICATO: QUOTE IN MILLIMETRI FINITURA SUPERFICIE: TOLLERANZE: LINEARE: UNI EN 22768/2 H ANGOLARE:	FINITURA: 2.4 / (0.8 / , 3 /)			SBAVATURA E INTERRUZIONE DEI BORDI NETTI	NON SCALARE IL DISEGNO	REVISIONE
	NOME				TITOLO:	
DISEGNATO	Paolo Di Sacco				Triangle insert: rear-low	
VERIFICATO						
APPROVATO						
FATTO						
QUALITA'		MATERIALE:			N. DISEGNO	A4
		Al 7075			13	pag. 139
					SCALA:1:2	FOGLIO 1 DI 1

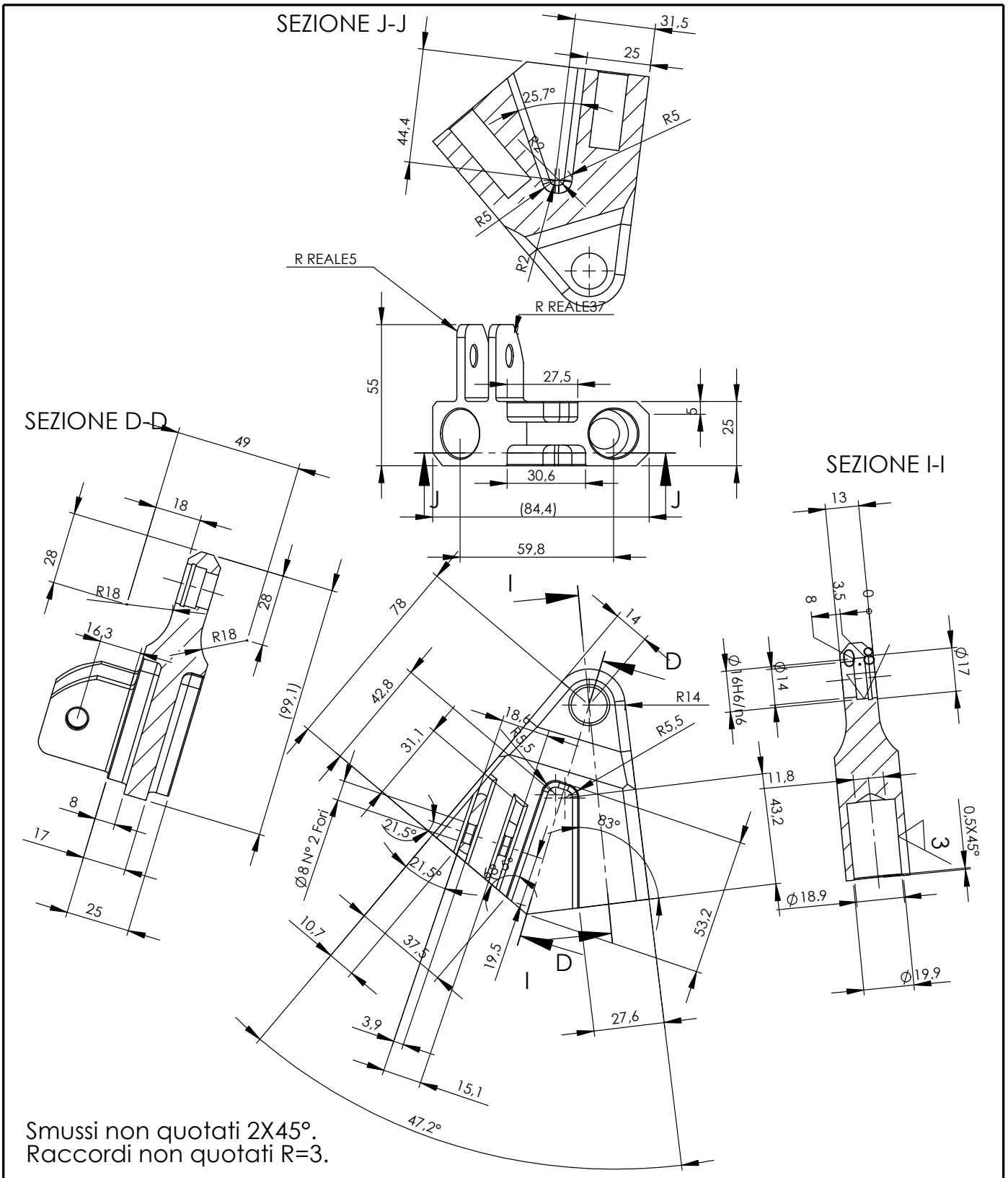

Smussi non quotati 2X45°.
Raccordi non quotati R=3.

SE NON SPECIFICATO: QUOTE IN MILLIMETRI FINITURA SUPERFICIE: TOLLERANZE: LINEARE: UNI EN 22768/2 H ANGOLARE:	FINITURA: 2.4 / 3 / 0.8 / (,)	SBAVATURA E INTERRUZIONE DEI BORDI NETTI	NON SCALARE IL DISEGNO / REVISIONE
NOME			TITOLO:
DISEGNATO: Paolo Di Sacco			Triangle insert: rear-up
VERIFICATO			
APPROVATO			
FATTO			
QUALITA'	MATERIALE: Al 7075	N. DISEGNO 14	A4
			pag. 140
		SCALA:1:2	FOGLIO 1 DI 1

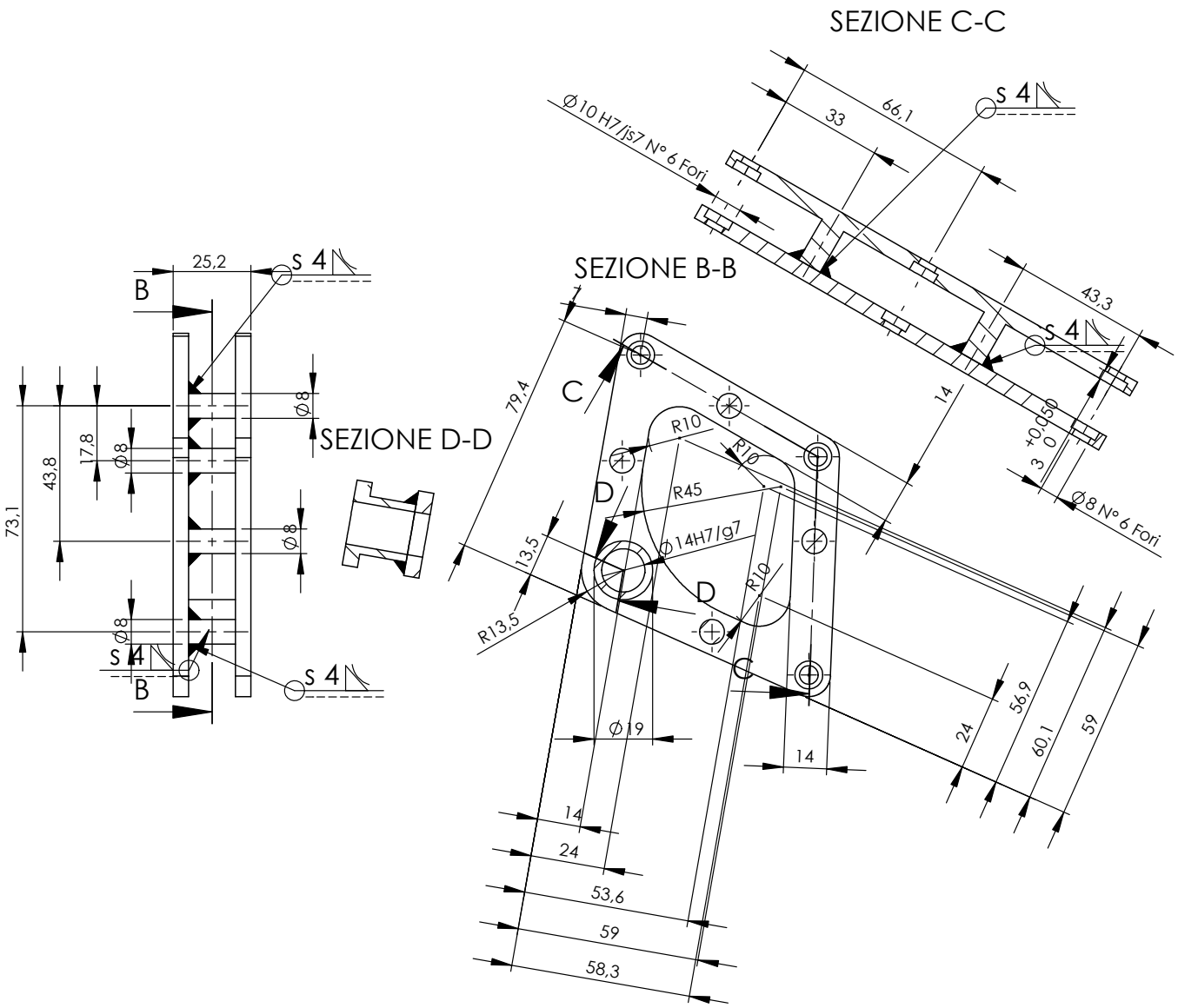

Raggi non quotati R=7.

SE NON SPECIFICATO: QUOTE IN MILLIMETRI FINITURA SUPERFICIE: TOLLERANZE: LINEARE: UNI EN 22768/2 H ANGOLARE:	FINITURA: 1.2	SBAVATURA E INTERRUZIONE DEI BORDI NETTI	NON SCALARE IL DISEGNO / REVISIONE
NOME			TITOLO:
DISEGNATO: Paolo Di Sacco			Rear rocker
VERIFICATO			
APPROVATO			
FATTO			
QUALITA'	MATERIALE: Al 7075		N. DISEGNO: 15
SCALA:1:1	FOGLIO 1 DI 1		A4

SEZIONE B-B

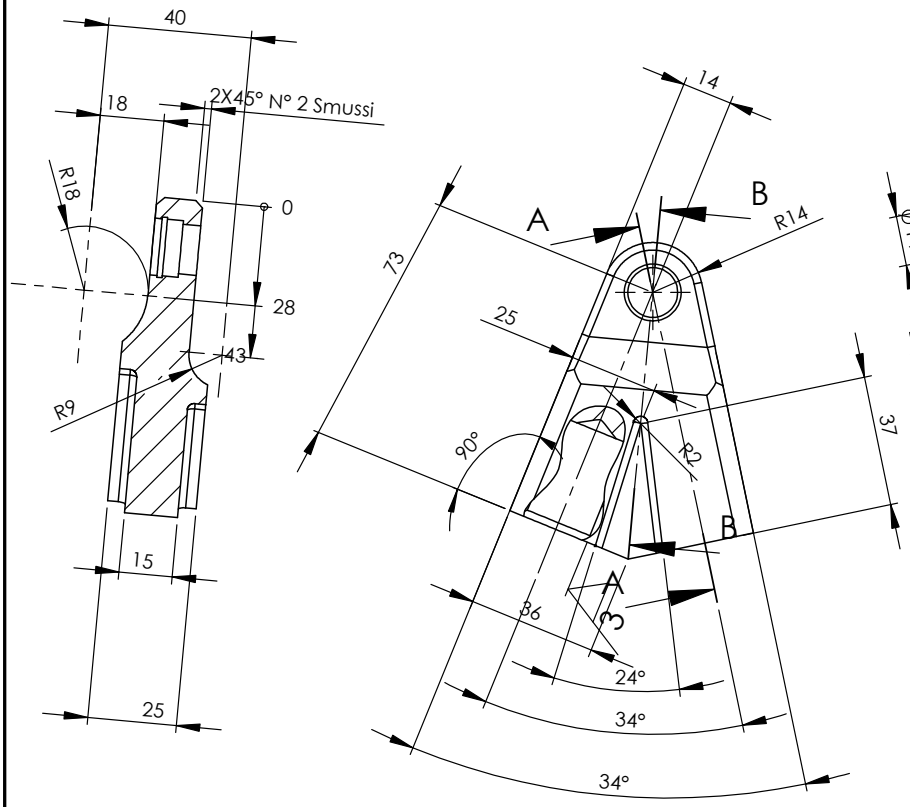

SEZIONE A-A

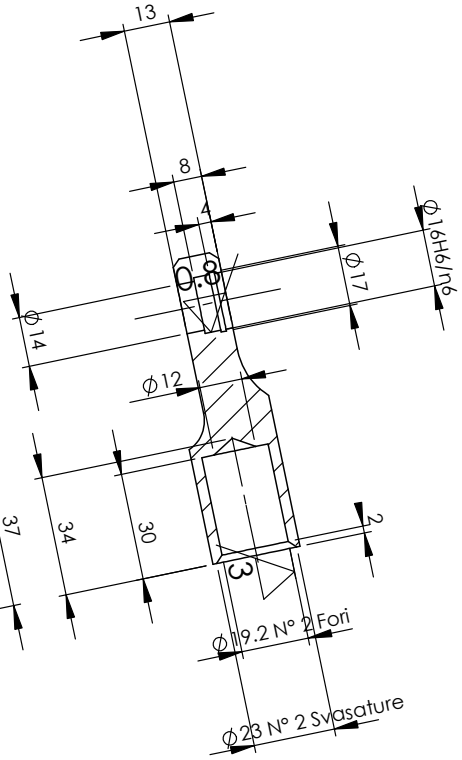

Smussi non quotati 4X45° .
Raccordi non quotati R=2 .

SE NON SPECIFICATO: QUOTE IN MILLIMETRI FINITURA SUPERFICIE: TOLLERANZE: LINEARE: UNI EN 22768/2 H ANGOLARE:	FINITURA: 2.4 / (0.8 / , 3 /)	SBAVATURA E INTERRUZIONE DEI BORDI NETTI	NON SCALARE IL DISEGNO / REVISIONE
NOME			TITOLO:
DISEGNATO	Paolo Di Sacco		Triangle insert front-low
VERIFICATO			
APPROVATO			
FATTO			
QUALITA'		MATERIALE: Al 7075	N. DISEGNO 16
			A4
		SCALA:1:1	FOGLIO 1 DI 1

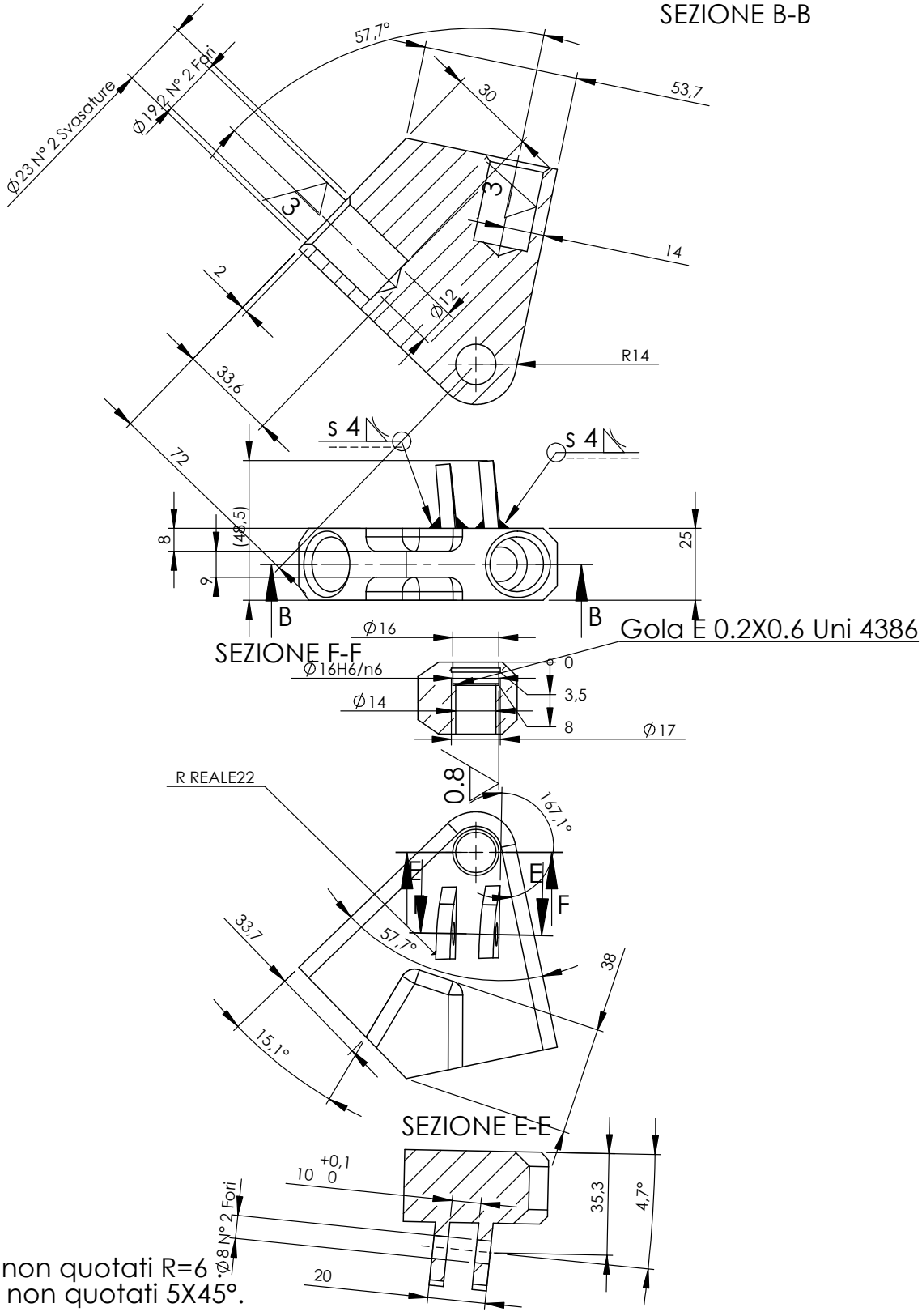

Raggi non quotati R=6 .
Smussi non quotati 5X45°.

SE NON SPECIFICATO: QUOTE IN MILLIMETRI FINITURA SUPERFICIE: TOLLERANZE: LINEARE: UNI EN 22768/2 H ANGOLARE:	FINITURA: 2.4 / (3 / , 0.8 /)	SBAVATURA E INTERRUZIONE DEI BORDI NETTI	NON SCALARE IL DISEGNO / REVISIONE
NOME			TITOLO:
DISEGNATO: Paolo Di Sacco			Triangle insert: front-up
VERIFICATO			
APPROVATO			
FATTO			
QUALITA'	MATERIALE: Al 7075		N. DISEGNO: 17
			SCALA:1:2 / FOGLIO 1 DI 1

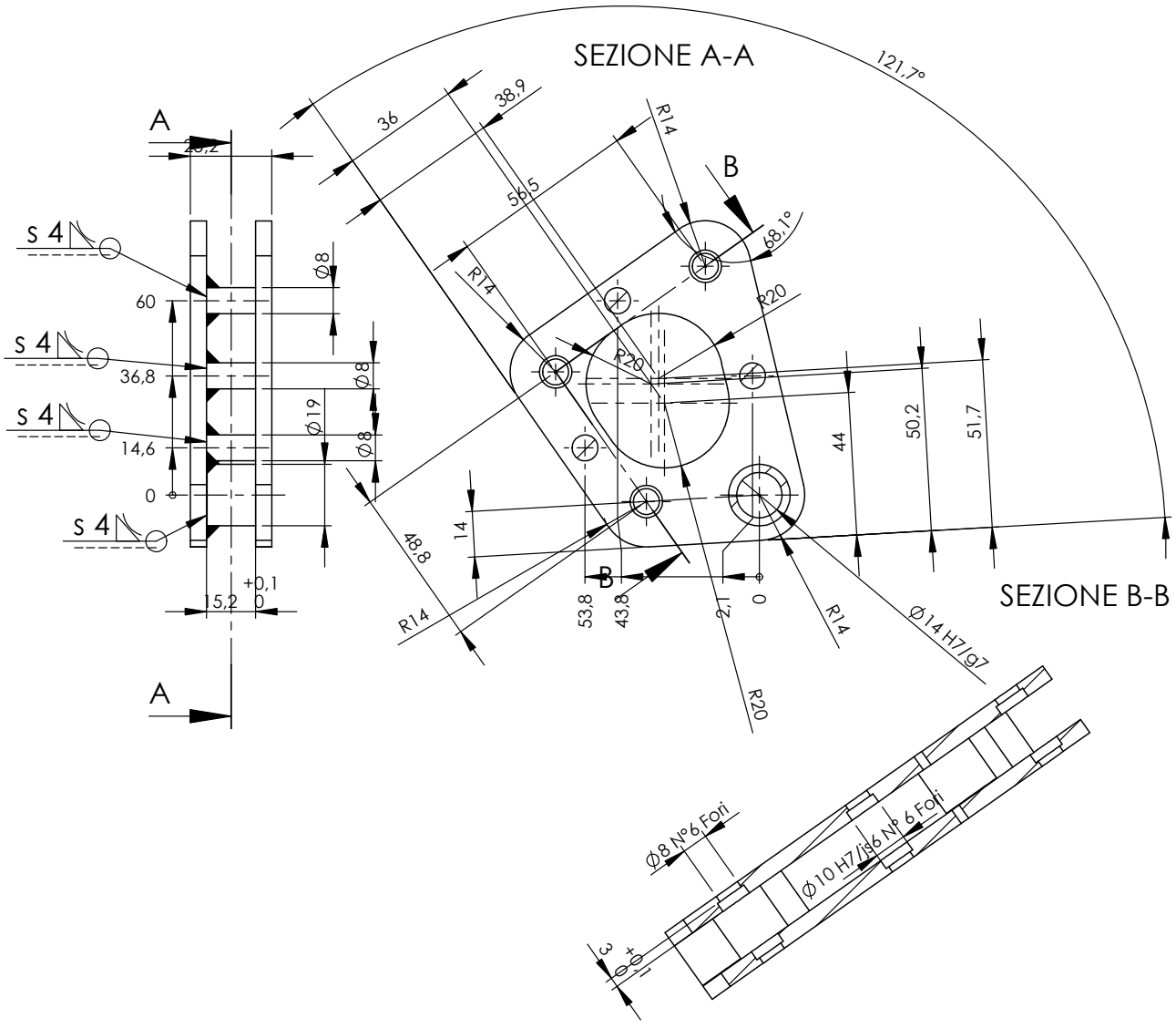

SE NON SPECIFICATO: QUOTE IN MILLIMETRI FINITURA SUPERFICIE: TOLLERANZE: LINEARE: UNI EN 22768/2 H ANGOLARE:	FINITURA: 1.2		SBAVATURA E INTERRUZIONE DEI BORDI NETTI	NON SCALARE IL DISEGNO	REVISIONE	
	NOME			TITOLO:		
DISEGNATO	Paolo Di Sacco			Front rocker		
VERIFICATO						
APPROVATO						
FATTO						
QUALITA'		MATERIALE:		N. DISEGNO	A4	
		Al 7075		18	pag. 144	
				SCALA:1:2	FOGLIO 1 DI 1	

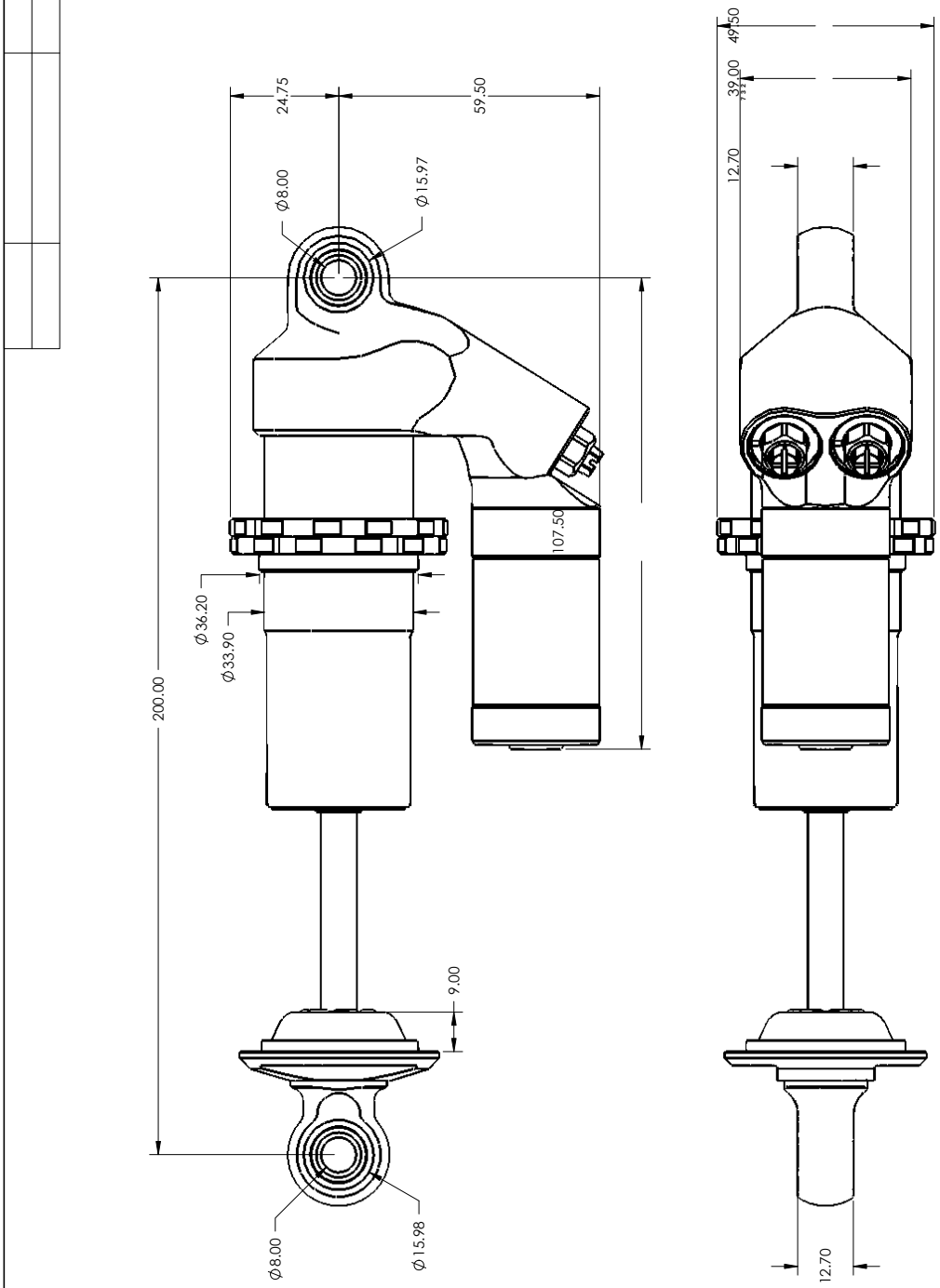
24.75
59.50
Ø8.00
Ø15.97
107.50
Ø36.20
Ø33.90
200.00
9.00
Ø8.00
Ø15.98
49.50
39.00
12.70
12.70

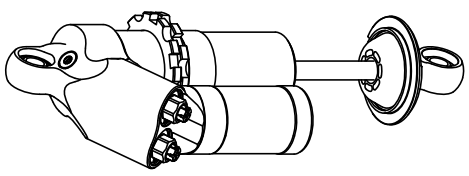

Bibliography

[1] Robert D. Adams, J. Comyn, and William Charles Wake. *Structural Adhesive Joints in Engineering*. Springer, October 1997.

[2] Pierangelo Andreini. *Manuale dell'ingegnere meccanico*. HOEPLI EDITORE, 2002.

[3] Marco Beghini. *Lezioni ed esercitazioni di tecnica delle costruzioni meccaniche*. Il Campano, 2013.

[4] D.A. Bigwood and A.D. Crocombe. Elastic analysis and engineering design formulae for bonded joints. *International Journal of Adhesion and Adhesives*, 9(4):229–242, October 1989.

[5] Mario Conserva, Franco Bonollo, and Giancarlo Donzelli. *Alluminio. Manuale degli impieghi*. Edimet, 2005.

[6] Vincenzo D'Agostino. *Fondamenti di meccanica applicata alle macchine*. Maggioli Editore, 2013.

[7] Wolfgang Fleischmann. *Loctite worldwide design handbook: 1996-97*. Loctite, Rocky Hill, Conn., 1995.

[8] Francesco Giusti and Marco Santochi. *Tecnologia meccanica e studi di fabbricazione*. CEA, 2000.

[9] H.L. Groth and P. Nordlund. Shape optimization of bonded joints. *International Journal of Adhesion and Adhesives*, 11(4):204–212, October 1991.

[10] Massimo Guiggiani. *Dinamica del veicolo*. Citta' Studi, [S.l.], 2007.

[11] Robert C Juvinall and Kurt M Marshek. *Fondamenti della progettazione dei componenti delle macchine*. ETS, Pisa, 1993.

[12] William F Milliken and Douglas L , Milliken. *Race car vehicle dynamics*. SAE International, Warrendale, PA, U.S.A., 1995.

[13] Lorenzo Morello and Giancarlo Genta. *L'autotelaio*. Levrotto & Bella, 2007.

[14] H. B Pacejka and Society of Automotive Engineers. *Tire and vehicle dynamics*. SAE International, [Warrendale, PA], 2006.

[15] Barsali Barsotti Rosa. *Disegno di macchine*. San Marco Litotipo, 1993.

[16] Ahmed A Shabana. *Computational dynamics*. Wiley, New York [u.a., 1994.

[17] Ahmed A. Shabana. *Dynamics of Multibody Systems*. Cambridge University Press, May 2005.

[18] SKF. *Catalogo generale: versione ridotta*. SKF, 1989.

[19] Carroll Smith. *Tune to win*. Aero Publishers, Fallbrook, CA, 1978.

[20] Allan Staniforth. *Competition car suspension: design, construction, tuning*. Haynes North America, Newbury Park, CA, 1999.